A pinch of silver salt to enable room temperature *rac*-lactide ring-opening polymerisation using Ti-salen complexes.

J. Koh, C. Baker, M. N. Diamantakis, N. J. Long, and C. Romain*

Department of Chemistry, Imperial College London, Molecular Sciences Research Hub, White City Campus, 82 Wood Lane, W12 0BZ, London, UK

Data available on data repository at: https://doi.org/10.14469/hpc/14821

Table of Content

General methods and reagents:

All synthetic manipulations were carried out under inert atmosphere (i.e. dry nitrogen) using a MBraun UNILab glovebox or standard Schlenk techniques. Solvents including tetrahydrofuran (THF), dichloromethane (DCM), toluene, and pentane were obtained from Inert PureSolv MD5 solvent purification system and stored over 3Å molecular sieves overnight prior to use. Deuterated solvents including CD_2Cl_2 and C_6D_6 were stored over 3Å molecular sieves overnight prior to use.

The salen pro-ligands were synthesised following standard literature procedures using 3,5-di-*tert*-butylsalicylaldehyde and the corresponding diamine.[1] The (S,S)-(+)-1,2-diaminocyclohexane was purchased from Fluorochem (purity 98%). The Ti-salen complexes **1-3** were synthesised following standard literature procedures using $Ti(O^iPr)_4$ and the corresponding salen pro-ligands.[1-2]

rac-lactide (*rac*-LA) was purchased from Sigma-Aldrich, recrystallised from dry toluene (targeting $[rac\text{-LA}]_0$ ~1M at 90 °C) and sublimed once under reduced pressure.

Silver (tetrakis[3,5-bis(trifluoromethyl)phenyl]borate) was prepared as a diethyl ether adduct including 2 equivalents of Et_2O per Ag^+ (1 equiv.) but will simply be referred to as $[Ag][B(Ar^{CF3})_4]$ for clarity. $[Ag][B(Ar^{CF3})_4]$ was synthesised via salt metathesis using $[Na][B(Ar^{CF3})_4]$ and $[Ag][NO_3]$ in Et_2O as previously reported using a modified method.[3]

Silver (tetrakis[3,5-bis(trifluoromethyl)phenyl]borate) was also prepared as an acetonitrile adduct including 2 equivalents of CH_3CN per Ag^+ (1 equiv.) and will be referred to as $[Ag][B(Ar^{CF3})_4].2CH_3CN$. It was similarly prepared via salt metathesis using $[Na][B(Ar^{CF3})_4]$ and $[Ag][NO_3]$ using CH_3CN as previously reported by others.[4]

Silver (tetrakis[perfluoro *tert*-butoxy]aluminate $[Ag][Al(OR^F)_4]$ with $R^F = C(CF_3)_3$ was purchased from Ionic Liquid Technologies (IoLiTec) and used as received (assay >99% by NMR, lot W002x108.4-KI-0019).

Silver triflate [Ag][OTf] ≥ 99.95 % trace metals basis was purchased from Sigma-Aldrich and used as received.

Silver hexafluoroantimonate $[Ag][SbF_6]$ (99%) was purchased from ThermoFisher and used as received (white powder).

All other reagents were obtained from commercial sources (Sigma-Aldrich, Fluorochem, TCI) and used as received.

Characterisation techniques:

NMR spectra were recorded on Bruker AV400 at 298 K (400MHz) unless specified. All chemical shifts were determined using residual signals of the deuterated solvents and were calibrated vs $SiMe_4$.

Gel permeation chromatography (GPC) was performed using Agilient 1260 Infinity II Multi-Detector GPC System fitted with a set of two Agilient PLgel 5µm MIXED-C columns (300 x 7.5 mm) and one MIXED-C precolumn (15 x 7.5 mm), calibrated using a polystyrene standard with $CHCl_3$ as eluent at a 1 mL min^{-1} flow rate at 40°C. Polymer samples were dissolved in HPLC grade $CHCl_3$ and filtered at 0.22 µm prior to analysis.

MALDI conditions: MALDI-ToF spectrometry measurements were performed on Shimadzu MALDI 8030 spectrometer with MALDI Solutions Data Acquisition software using positive ionisation. Polymers were dissolved in THF and complexes/salts (1:1 equiv) dissolved in DCM at a concentration of 10 mg ml^{-1}. 1,8,9-Trihydroxyanthracene was used as a matrix (10 mg ml^{-1} in THF/DCM). No cationizing agent was used due to the presence of silver in all samples. The solutions of complex/polymer and matrix were mixed in ratios of 1/2 and 1/4 (v/v), respectively. The mixed solution was spotted on a stainless steel MALDI plate and left to dry for a couple of hours. The spectra were recorded using linear mode.

General polymerisation procedures:

For reactions at room temperature (using silver salts other than AgOTf):
In a glovebox, *rac*-LA (1.0 mmol, 0.1441g) was dissolved in DCM (1ml). The solution was then transferred to a separate vial containing the corresponding titanium complex (0.01 mmol) and allowed to dissolve. Once dissolved, the solution was then transferred to a vial containing the appropriate silver salt (0.01 mmol). 100 µl aliquots were taken at fixed intervals and quenched in 300 µl of pentane, precipitating the polymer and any remaining *rac*-LA to halt polymerization. The pentane was then allowed to evaporate under air and $CDCl_3$ added to the vial for NMR spectroscopy analysis.

For reactions at room temperature using AgOTf:
In a glovebox, to solution of *rac*-LA in DCM (144 mg, 1 mmol, 1.0 M, 100 equiv.) in a PTFE screw-capped vial, stock solutions of catalyst/DCM (6.6 mg, 10 µmol, 1 eq) and AgOTf/toluene (2.6 mg, 10 µmol, 1 eq) were added. DCM was added prior to the stock solutions, so the overall final concentration was [LA] = 1.0 M with DCM/toluene ~ 9:1 (v/v). The vial was capped and stirred at room temperature in the glovebox. An aliquot was taken by taking 100 µL of solution and quenching in 300 µL hexane.

Synthesis of complex 1 -3
The Ti-salen complexes **1-3** were synthesised following standard literature procedures using $Ti(O^iPr)_4$ (1 equiv.) and the corresponding salen pro-ligands H_2L (1 equiv.).[1-2]

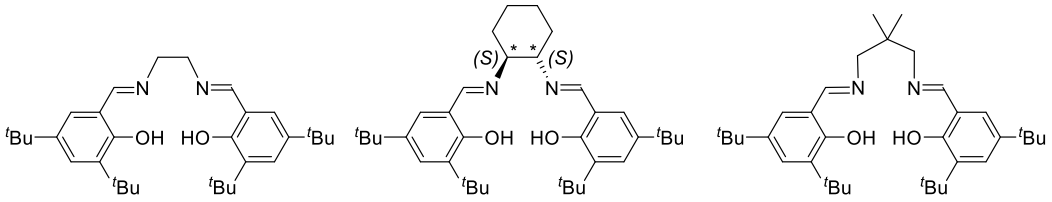

$H_2\mathbf{L^1}$ $H_2(\mathbf{S,S})\text{-}\mathbf{L^2}$ $H_2\mathbf{L^3}$

and

$H_2\mathbf{L^2}$ = *rac-trans*-$H_2\mathbf{L^2}$
[i.e. *rac* mixture of $H_2(\mathbf{S,S})\text{-}\mathbf{L^2}$ and $H_2(\mathbf{R,R})\text{-}\mathbf{L^2}$]

*Synthesis of **1** (using $H_2\mathbf{L^1}$)*: Yield: 50.8% (0.474g), ^{1}H NMR (400 Mhz, C_6D_6, δ (ppm): 7.77 (d, 2H, *H*C=N), 7.59 (s, 2H, Ar*H*), 7.13 (d, 2H, Ar*H*), 4.39 (hep, 2H, OC*H*$(CH_3)_2$), 3.31 (s, 4H, CH_2), 1.83 (s, 18H, C(CH_3)$_3$), 1.36 (s, 18H, C(CH_3)$_3$), 0.92 (d, 12H, OCH(CH_3)$_2$). EA: Expected: C, 69.49; H, 9.21; N, 4.27. Found: C, 69.95; H, 9.39; N, 4.16.

*Synthesis of **2** (using $H_2\mathbf{L^2}$):* Yield: 46.0% (0.475g). ^{1}H NMR (400 Mhz, C_6D_6, δ (ppm)): 7.95 (d, 1H, *H*C=N), 7.91 (d, 1H, *H*C=N), 7.81 (d, 1H, Ar*H*), 7.74 (d, 1H, Ar*H*), 7.35 (d, 1H, Ar*H*), 7.20 (d, 1H, Ar*H*), 4.97 (hep, 1H, OC*H*$(CH_3)_2$), 4.81 (hep, 1H, OC*H*$(CH_3)_2$), 4.43 (t, 1H, NC*H*CH_2), 2.13 (t, 1H, NC*H*CH_2), 1.89, 1.72 (2s, 18H, C(CH_3)$_3$), 1.89-1.36 (m, 8H, CH_2), 1.40, 1.36 (2s, 18H, C(CH_3)$_3$), 1.20-1.09 (m, 12H, OCH(CH_3)$_2$) EA: Expected: C, 70.96; H, 9.36; N, 3.94. Found: C, 71.21; H, 9.73; N, 3.89.

Synthesis of **(S,S)-2** *(using $H_2(\mathbf{S,S})\text{-}\mathbf{L^2}$)*: Yield: 60.6 % (0.197 mg).

*Synthesis of **3***: Yield: 72.8% (0.168g) ^{1}H NMR (400 Mhz, C_6D_6, δ (ppm)): 7.71 (d, 1H, Ar-***H***), 7.65 (s, 1H, *H*C=N), 7.59 (d, 1H, Ar-*H*), 7.54 (s, 1H, *H*C=N), 7.14 (d, 1H, Ar-*H*), 7.12 (d, 1H, Ar-*H*), 5.12 (hep, 1H, OC*H*$(CH_3)_2$), 4.83 (d, 1H, NCH_2), 4.68 (hep, 1H, OC*H*$(CH_3)_2$), 3.73 (d, 1H, NCH_2), 2.84, 2.74 (dd, 2H, NCH_2), 1.77 (s, 9H, C(CH_3)$_3$), 1.43 (dd, 6H, OCH(CH_3)$_2$), 1.39, 1.37, 1.35 (3s, 27H, C(CH_3)$_3$), 1.08 (dd, 6H, OCH(CH_3)$_2$), 0.78, 0.38 (2s, 6H, N-CH_2C(CH_3)$_2$). EA: Expected: C, 70.47; H, 9.52; N, 4.01. Found: C, 70.44; H, 9.77; N, 3.99.

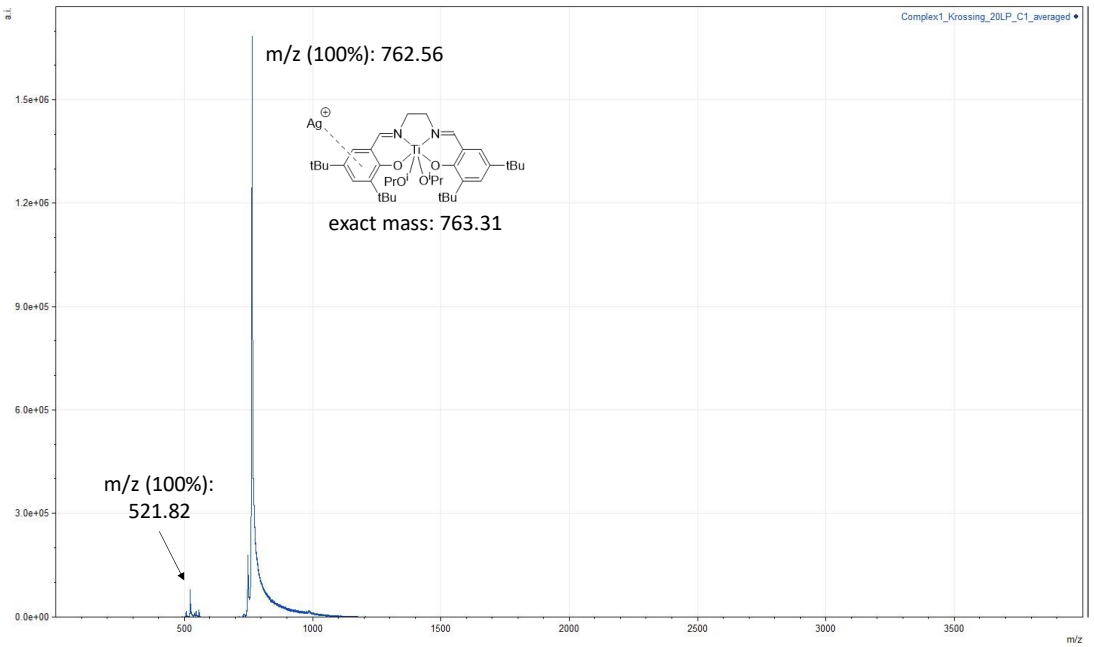

Figure S1: MALDI-ToF spectrum for **1** in the presence of [Ag][Al(OR^F)$_4$] showing formation of a silver adduct between **1** and Ag cation (m/z for [**1**+Ag]$^+$: calc. = 763.31, found = 762.56).

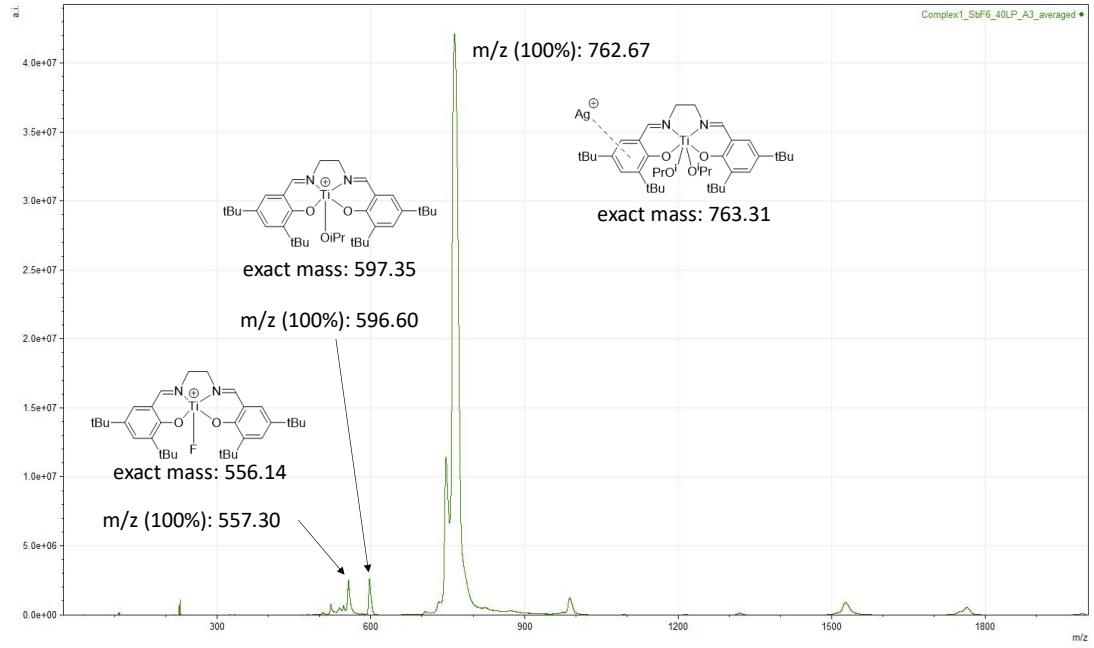

Figure S2: MALDI-ToF spectrum for **1** in the presence of [Ag][SbF$_6$] showing formation of a silver adduct between **1** and Ag cation (m/z for [**1**+Ag]$^+$: calc. = 763.31, found = 762.67).

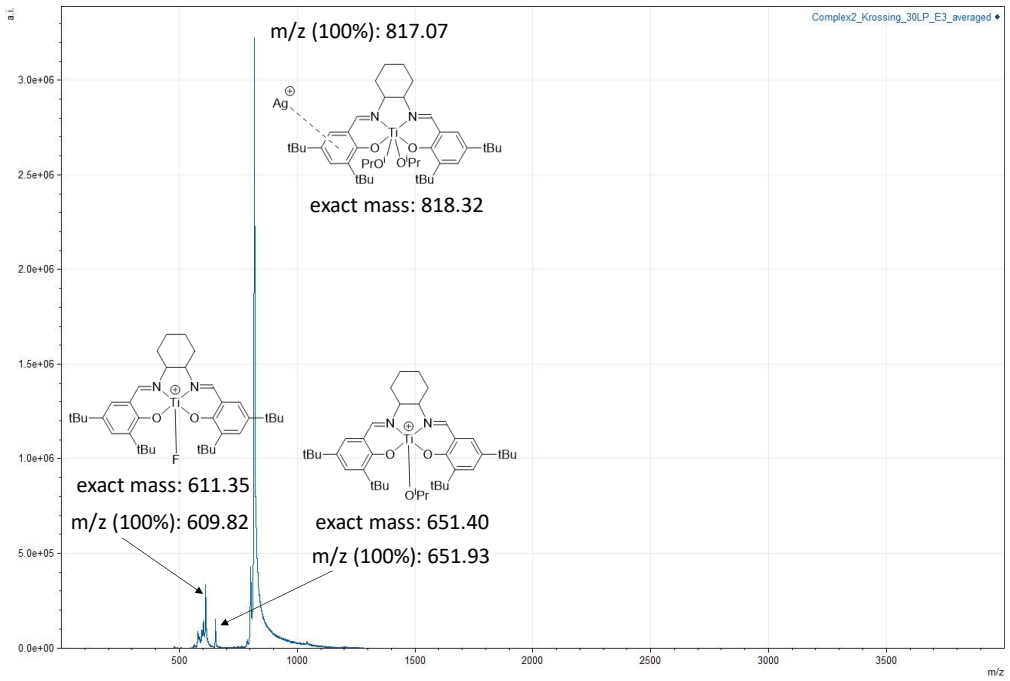

Figure S3: MALDI-ToF spectrum for **2** in the presence of [Ag][Al(OR^F)$_4$] showing formation of a silver adduct between **2** and Ag cation ((m/z for [**2**+Ag]$^+$: calc. = 818.32, found = 817.07).

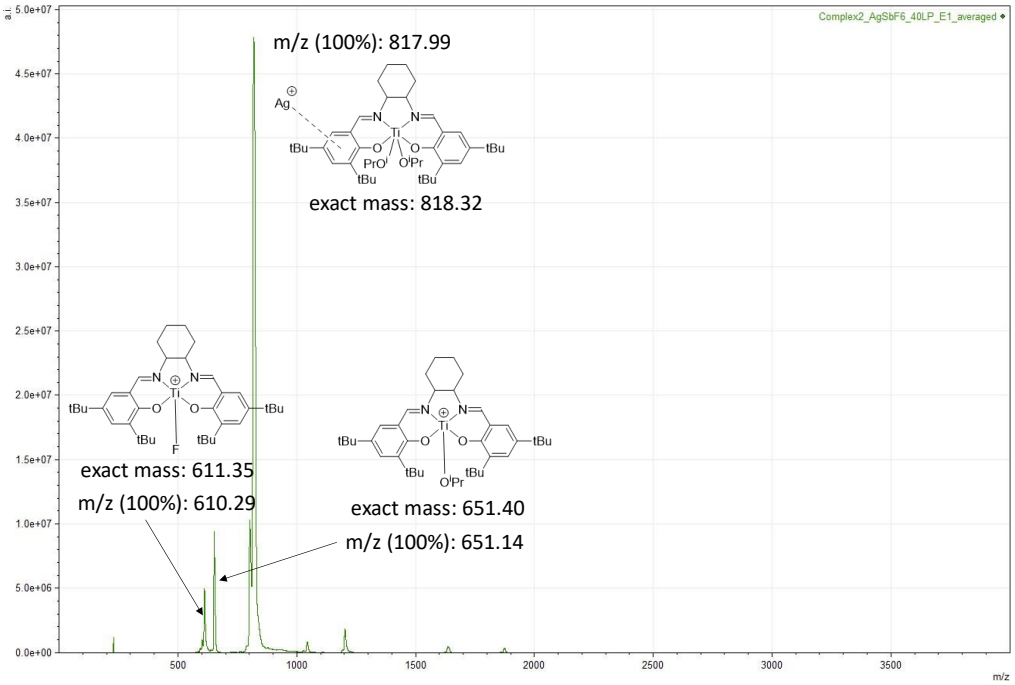

Figure S4: MALDI-ToF spectrum for **2** in the presence of [Ag][SbF$_6$] showing formation of a silver adduct between **2** and Ag cation (m/z for [**2**+Ag]$^+$: calc. = 818.32, found = 817.99).

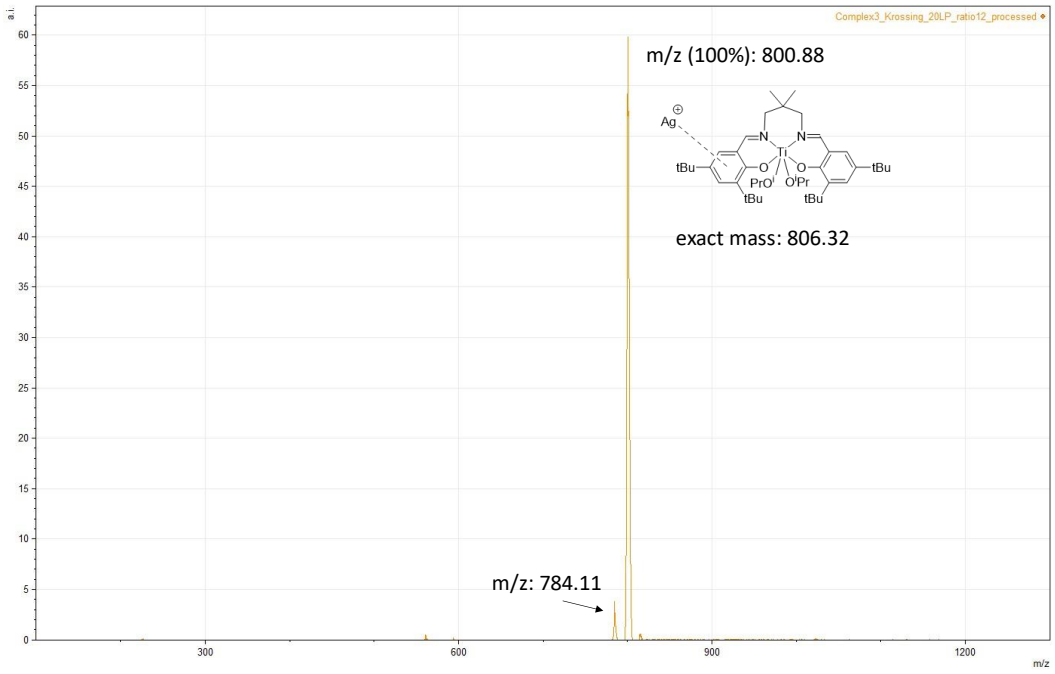

Figure S5: MALDI-ToF spectrum for **3** in the presence of [Ag][Al(OR^F)$_4$] showing formation of a silver adduct between 3 and Ag cation (m/z for [**3**+Ag]$^+$: calc. = 806.32, found = 800.87).

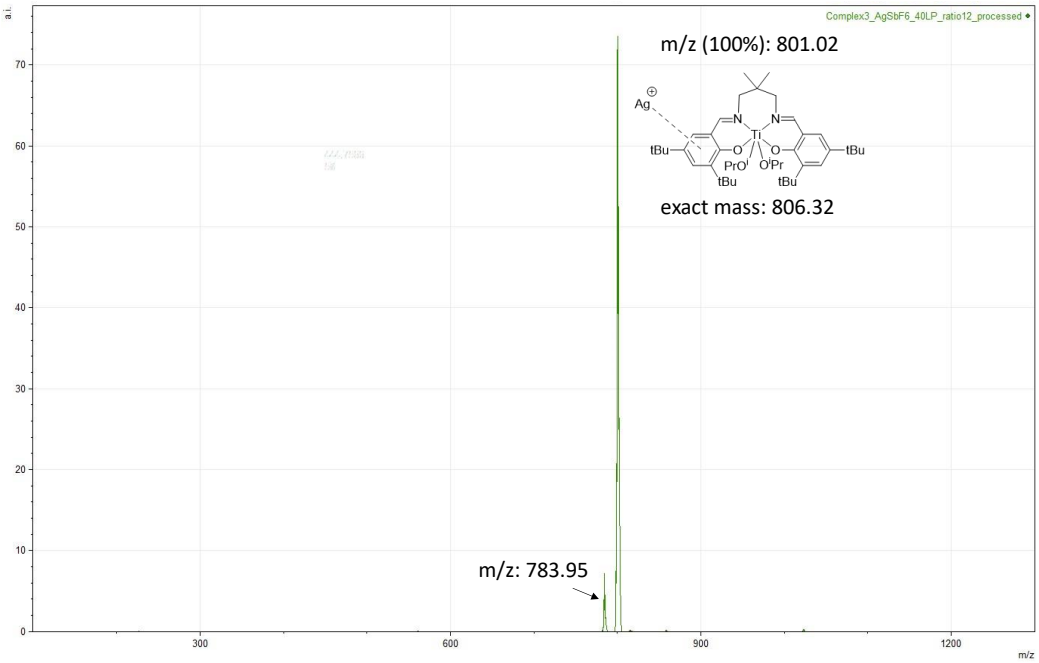

Figure S6: MALDI-ToF spectrum for **3** in the presence of [Ag][SbF$_6$] showing formation of a silver adduct between **3** and Ag cation (m/z for [**3**+Ag]$^+$: calc. = 806.32, found = 801.02).

➢ ^{1}H NMR spectra of complexes 1-3

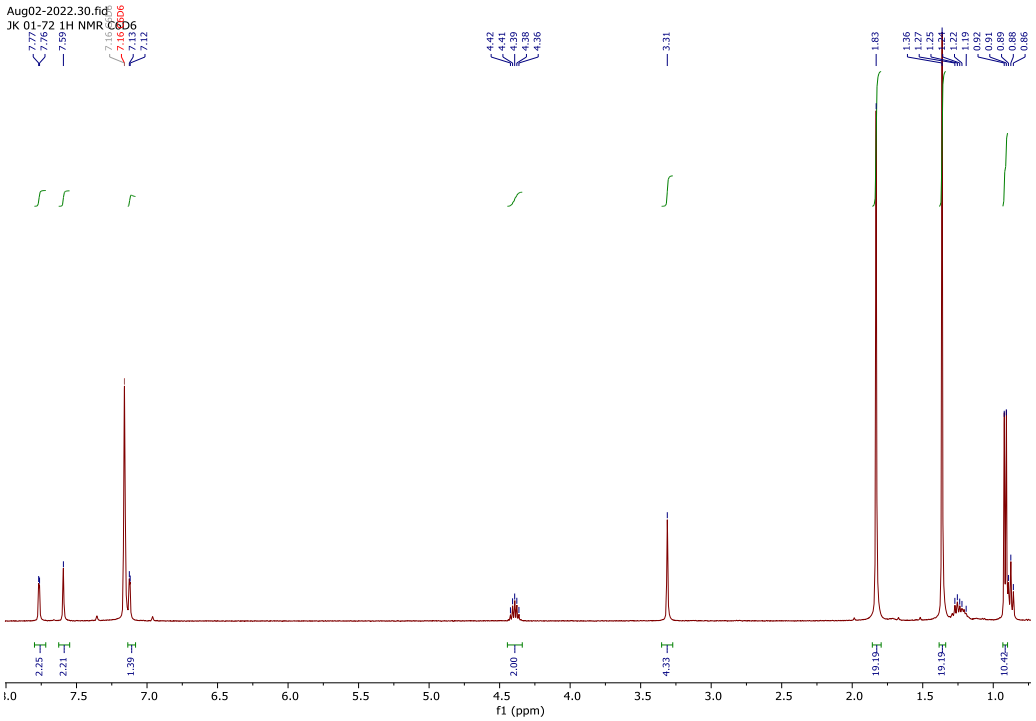

Figure S7: ^{1}H NMR spectrum of **1** in C_6D_6

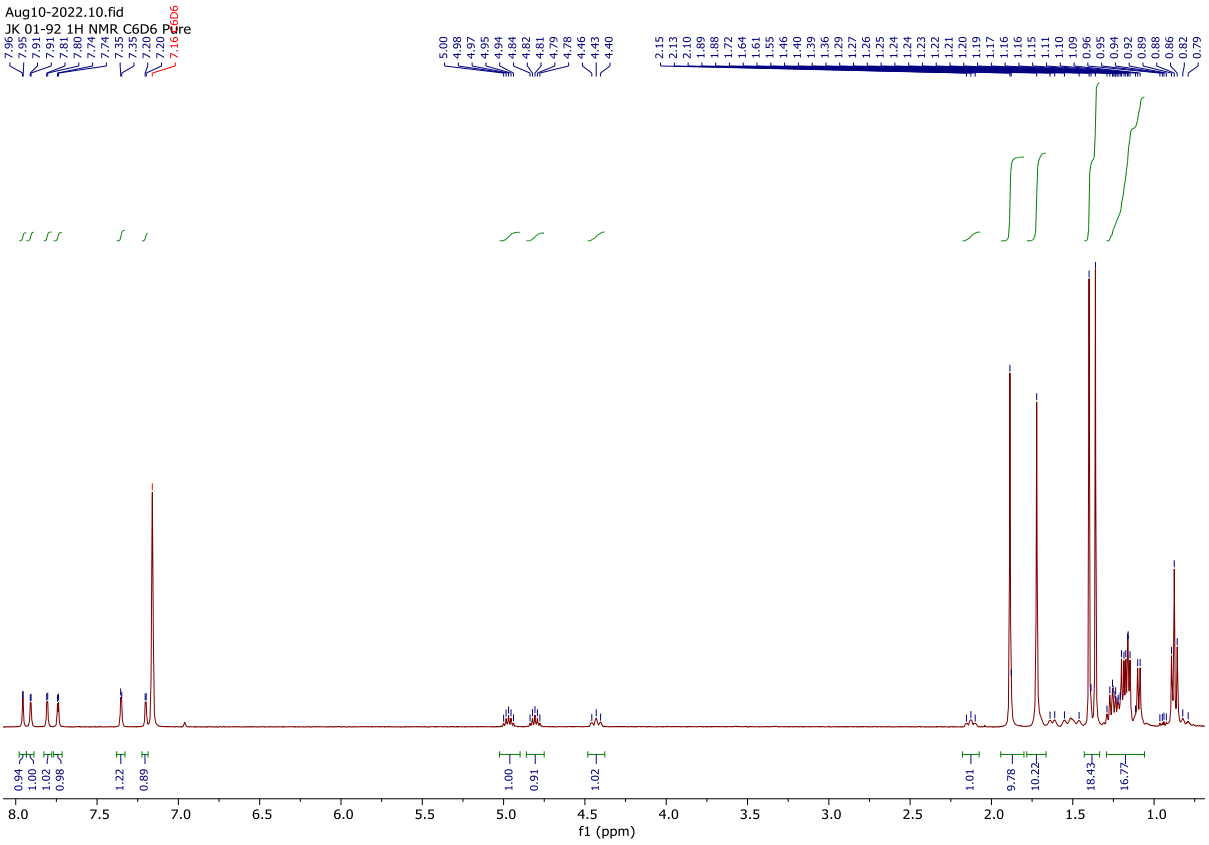

Figure S8: ^{1}H NMR spectrum of **2** in C_6D_6

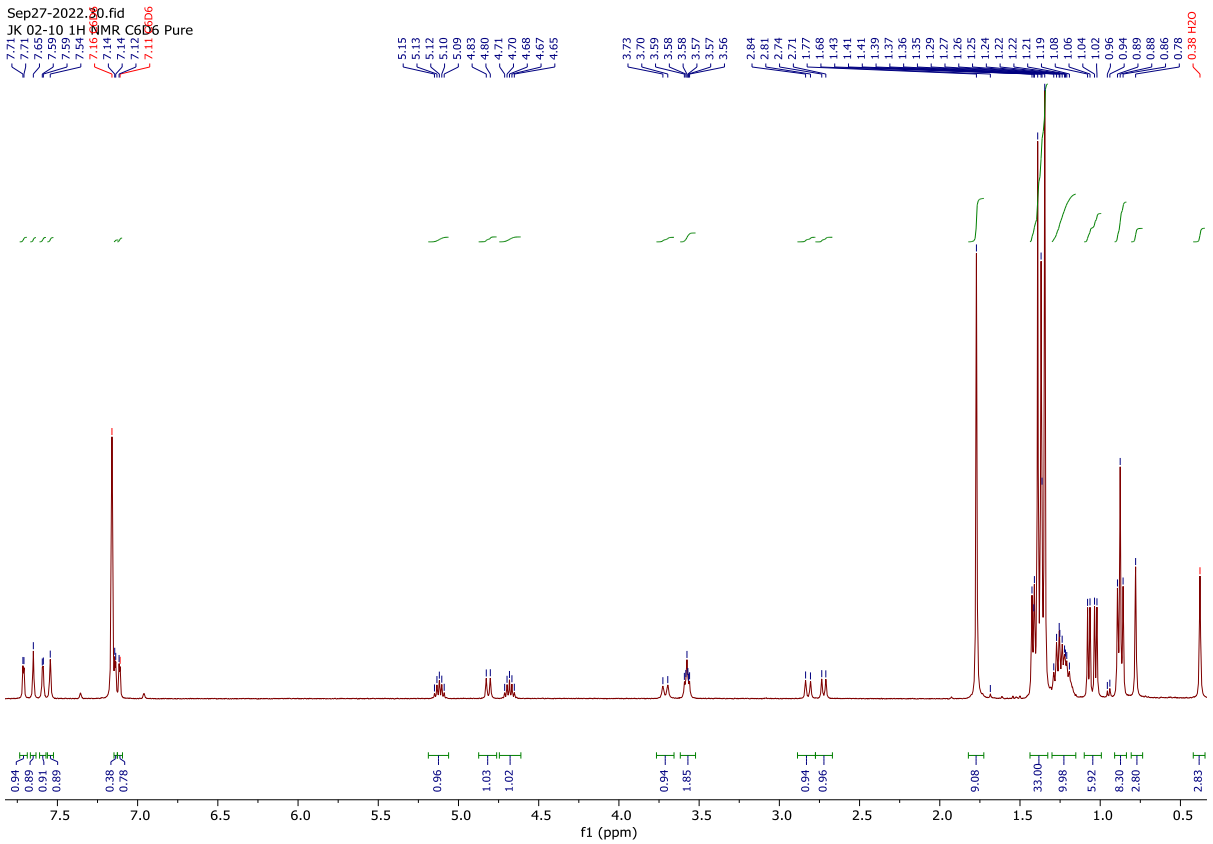

Figure S9: ^{1}H NMR spectrum of **3** in C_6D_6.

➢ **NMR spectra for [Ag][B(Ar^{CF3})$_4$]**

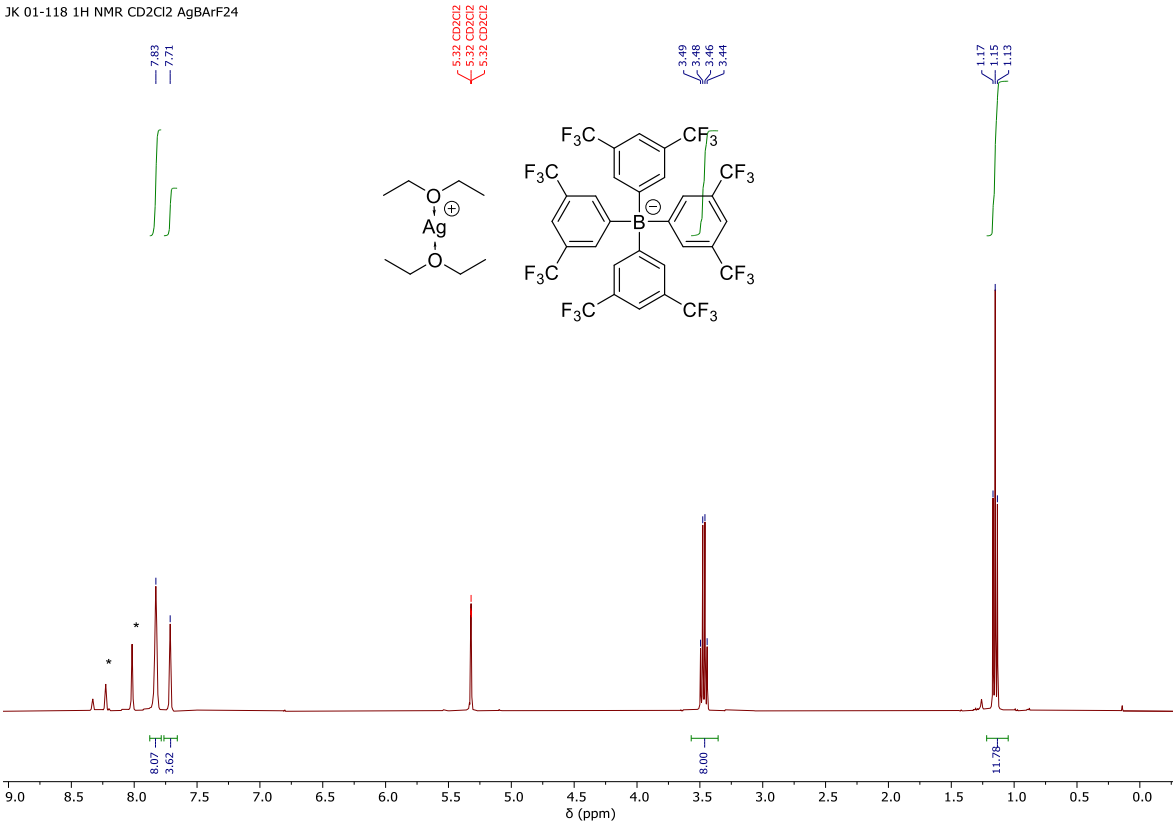

Figure S10: ^{1}H NMR spectrum (CD_2Cl_2) of [Ag][B(Ar^{CF3})$_4$] with 2 equiv. of Et_2O per silver cation (1 equiv.),[5] δ_{1H} (ppm): 7.83 (s, 8H, Ar-*H*), 7.71 (s, 4H. Ar-H), 3.48 (q, 8H, OC*H*$_2$CH$_3$), 1.15 (t, 12H, OCH$_2$C*H*$_3$), signals demoted * are attributed to decomposition product B(Ar^{CF3})$_3$ (δ_{1H} (ppm): 8.03ppm, 8.23ppm)[6]

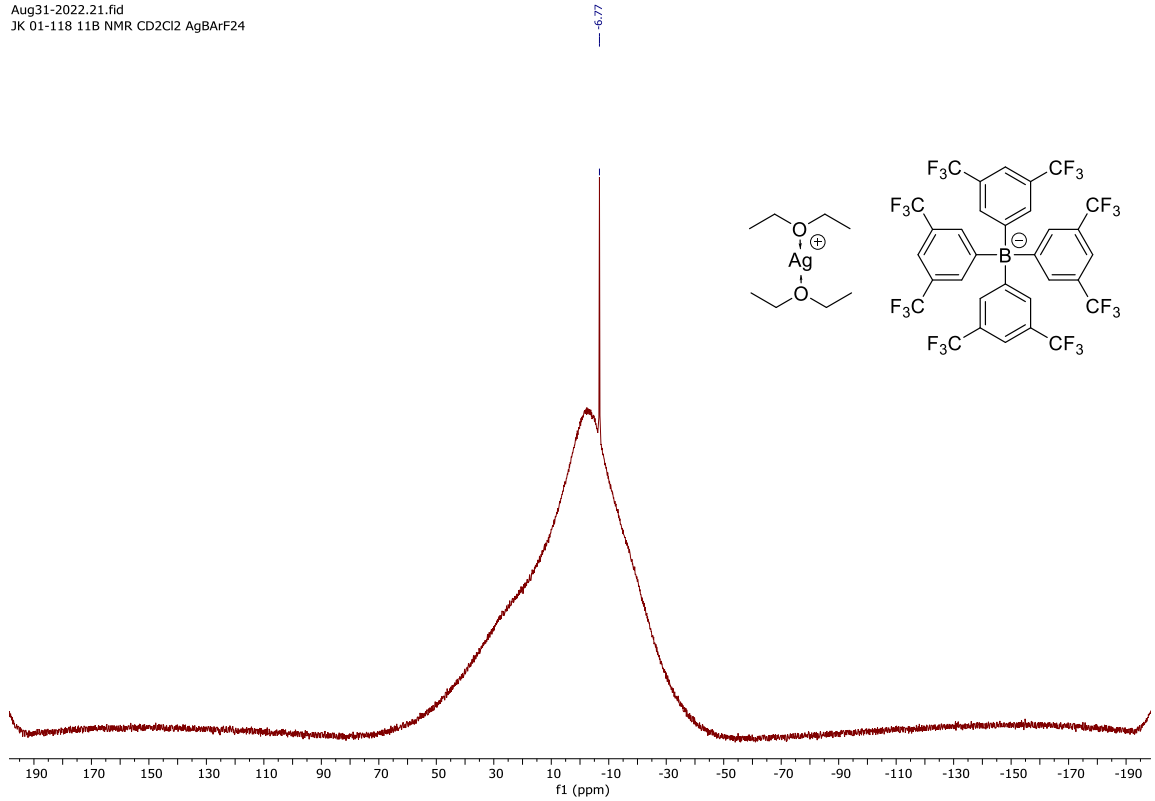

Figure S11: ^{11}B NMR spectrum (CD_2Cl_2) of [Ag][B(Ar^{CF3})$_4$] with 2 equiv. of Et_2O per silver cation (1 equiv.), δ_{11B} = - 6.77 ppm.

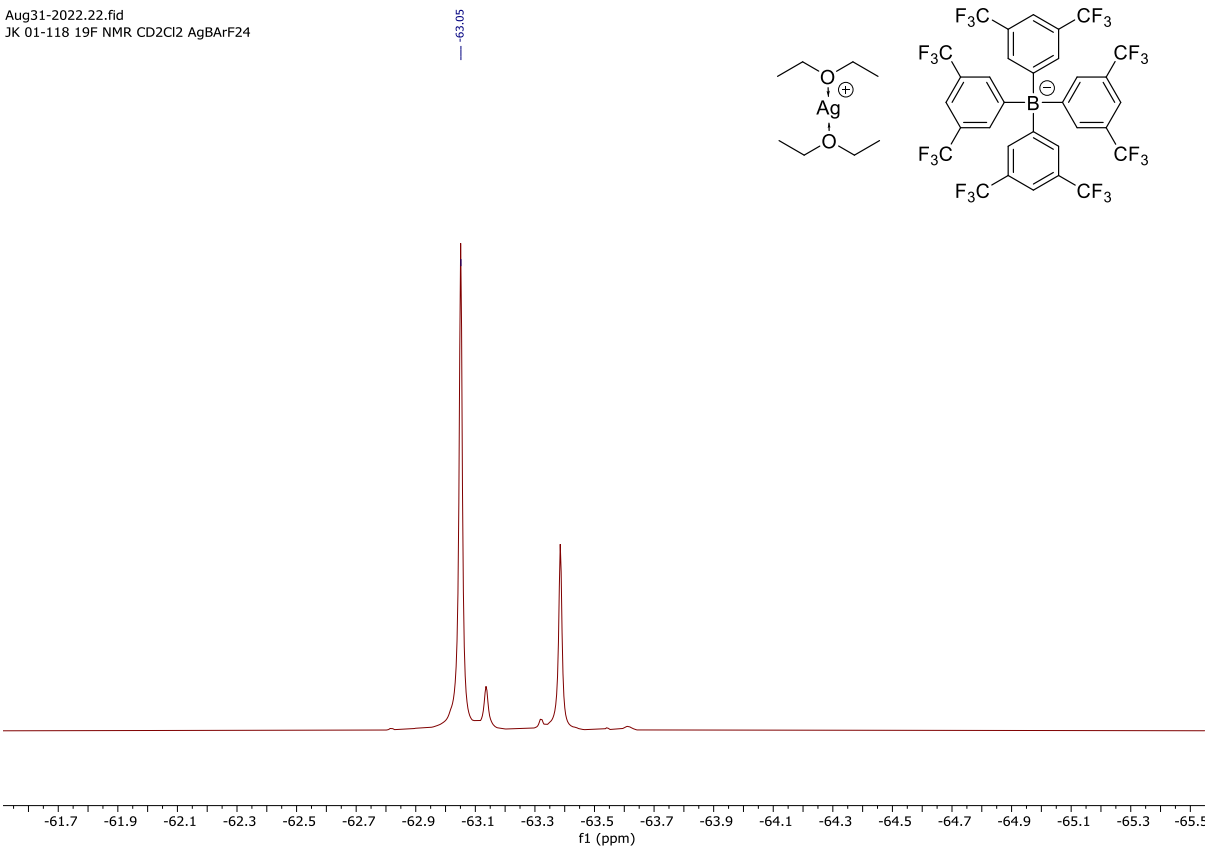

Figure S12: ^{19}F NMR spectrum (CD_2Cl_2) of [Ag][$B(Ar^{CF3})_4$] with 2 equiv. of Et_2O per silver cation (1 equiv.), δ_{19F} = -63.05 ppm

➢ **NMR spectra for [Ag][B(Ar^{CF3})$_4$].2CH$_3$CN**

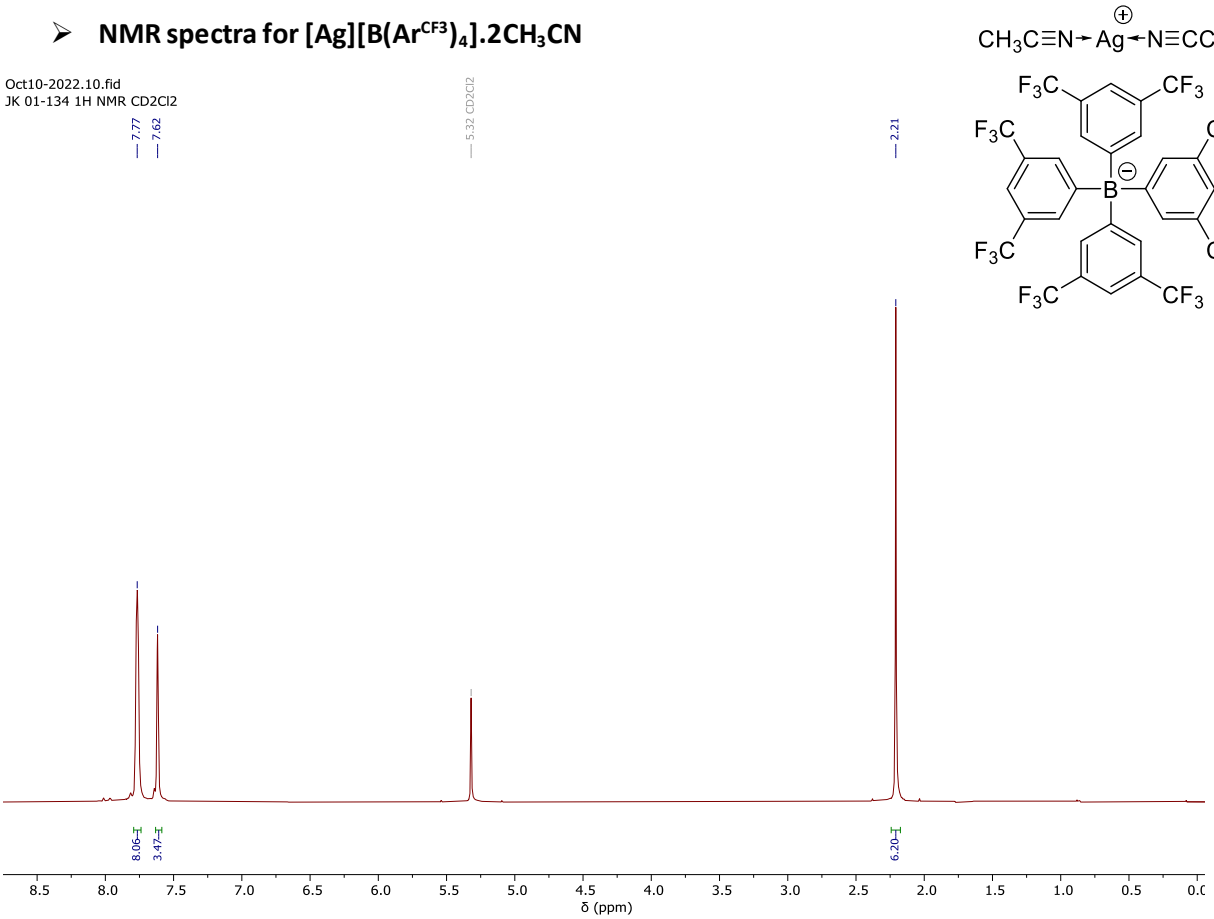

Figure S13: ^{1}H NMR spectrum (CD_2Cl_2) of [Ag][B(Ar^{CF3})$_4$] with 2 equiv. of CH_3CN per silver cation (1 equiv.), δ_{1H} (ppm) = 7.77 (s, 8H, Ar-H), 7.62 (s, 4H, Ar-H), 2.21 (s, 6H, CH_3CN).

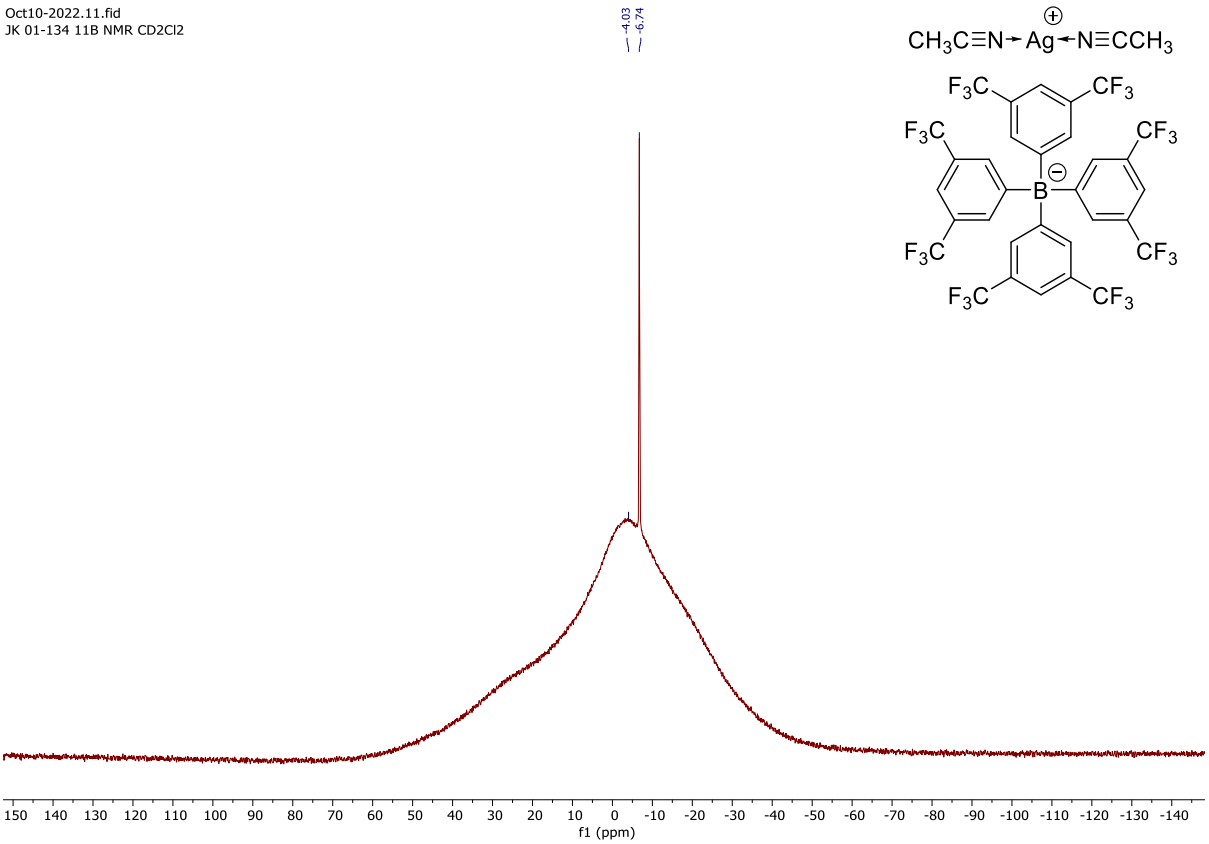

Figure S14: ^{11}B NMR spectrum (CD_2Cl_2) of [Ag][B(Ar^{CF3})$_4$] with 2 equiv. of CH_3CN per silver cation (1 equiv.), δ_{11B} = -6.74 ppm

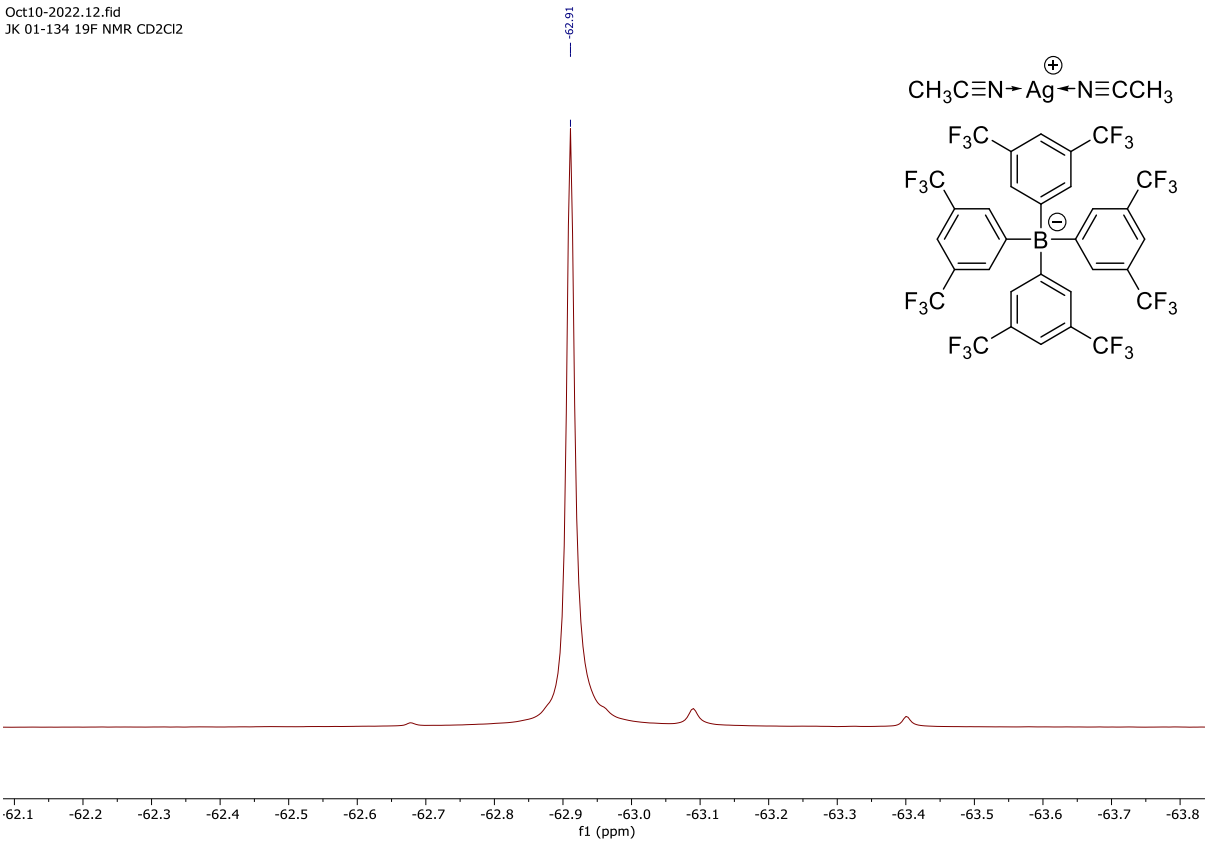

Figure S15: ^{19}F NMR spectrum (CD_2Cl_2) of [Ag][B(Ar^{CF3})$_4$] with 2 equiv. of CH_3CN per silver cation (1 equiv.), δ_{19F} = -62.91 ppm

➢ **NMR spectra for [Ag][Al(OR^F)$_4$] with R^F = C(CF$_3$)$_3$** (as received from IoLiTec)

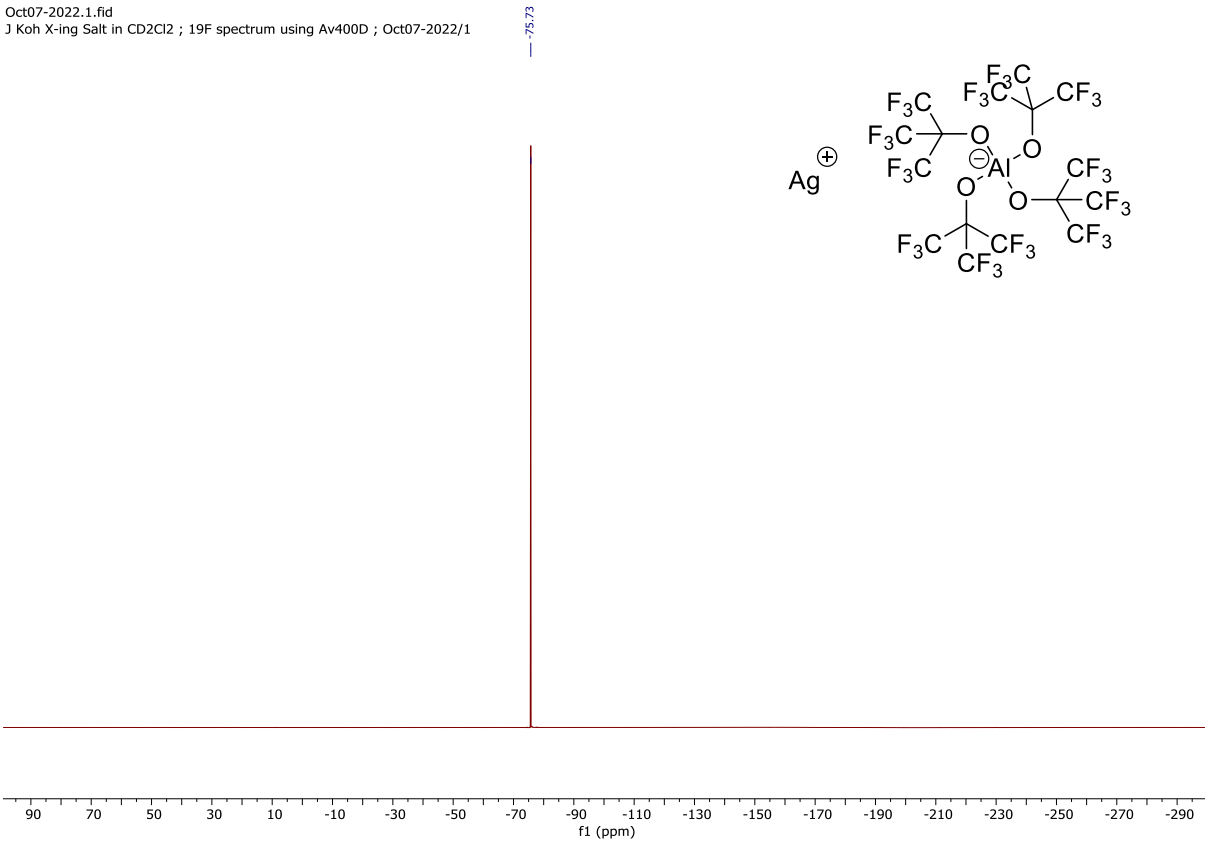

Figure S16: ^{19}F NMR spectrum (CD_2Cl_2) of [Ag][Al(OR^F)$_4$], δ_{19F} = -75.73 ppm.

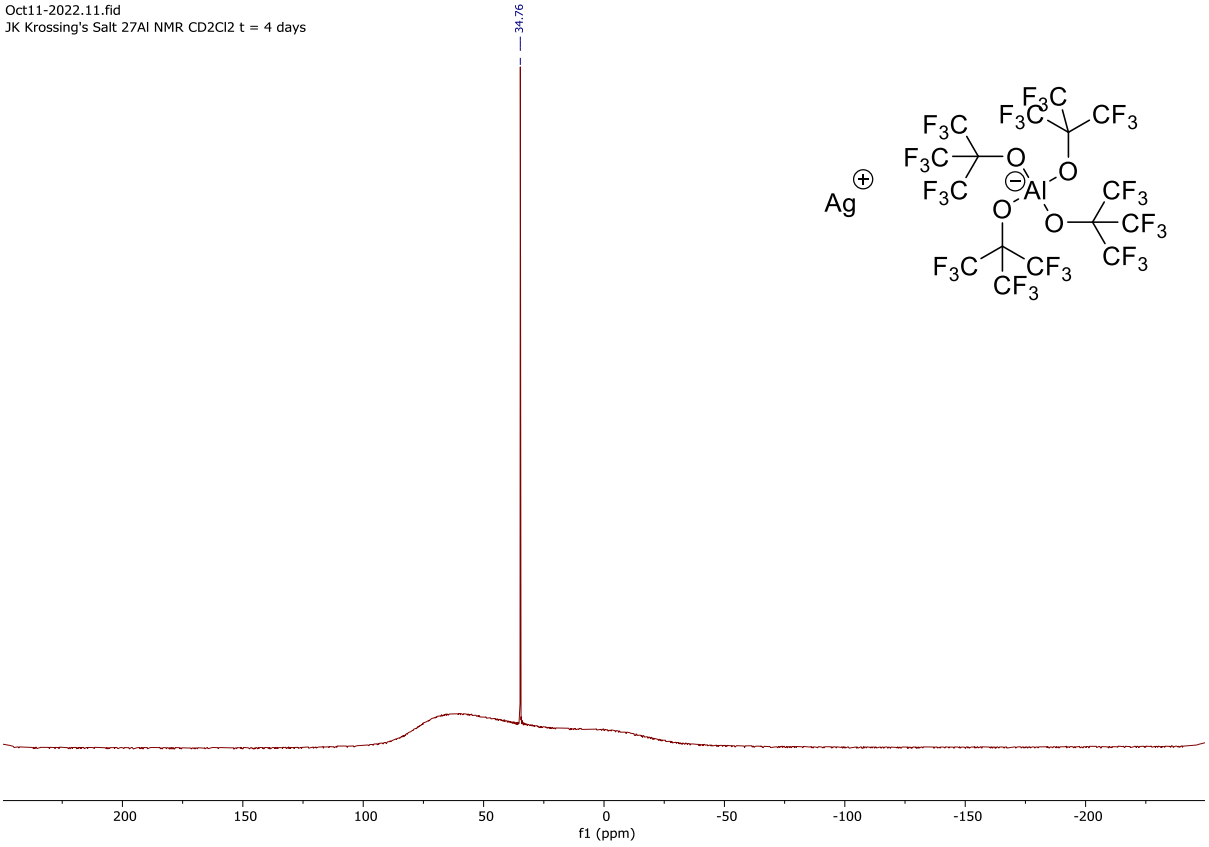

Figure S17: ^{27}Al NMR spectrum (CD_2Cl_2) of [Ag][Al(OR^F)$_4$], δ_{27Al} = -34.76 ppm.

➢ Data for *rac*-LA ROP initiated by **1** in the presence of [Ag][OTf]

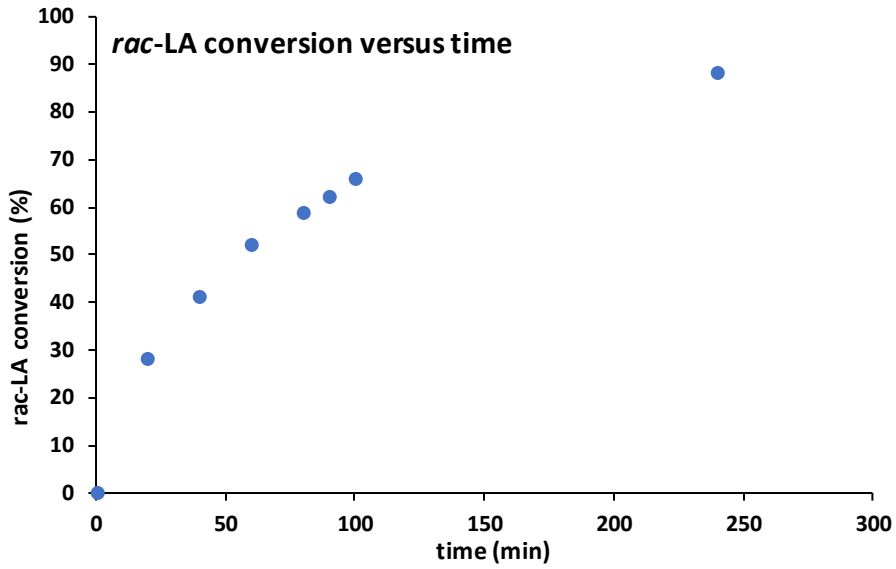

Figure S18: *rac*-LA conversion versus time for polymerisation initiated by **1** + AgOTf (Table 1, Entry 1).

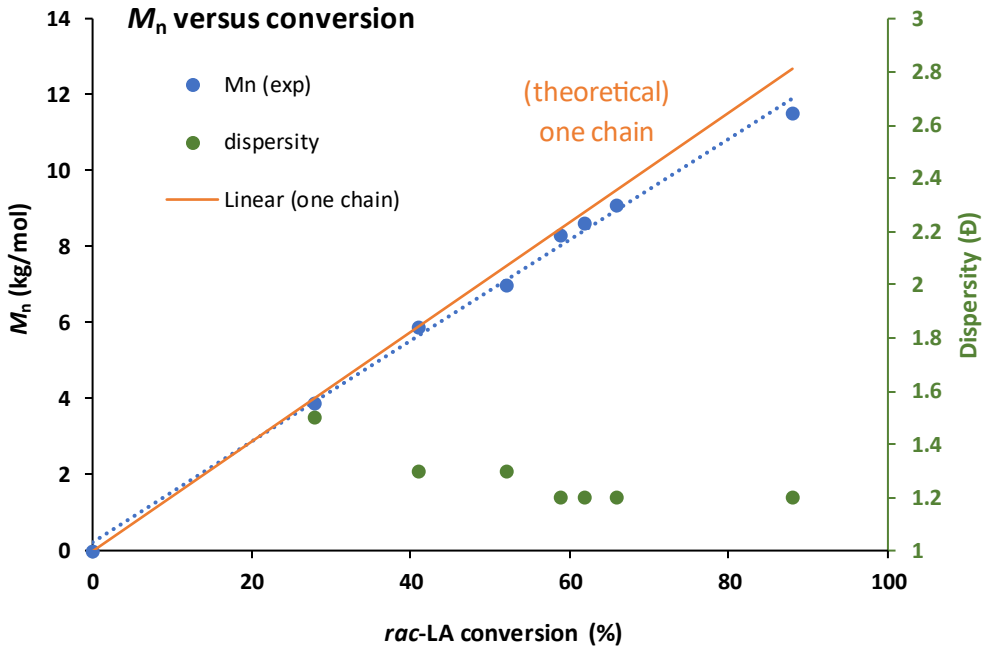

Figure S19: M_n (•) and dispersity (•) versus *rac*-LA conversion for polymerisation initiated by **1** + [Ag][OTf] showing good match with one chain per **1** (plain orange line), (Table 1, Entry 1)

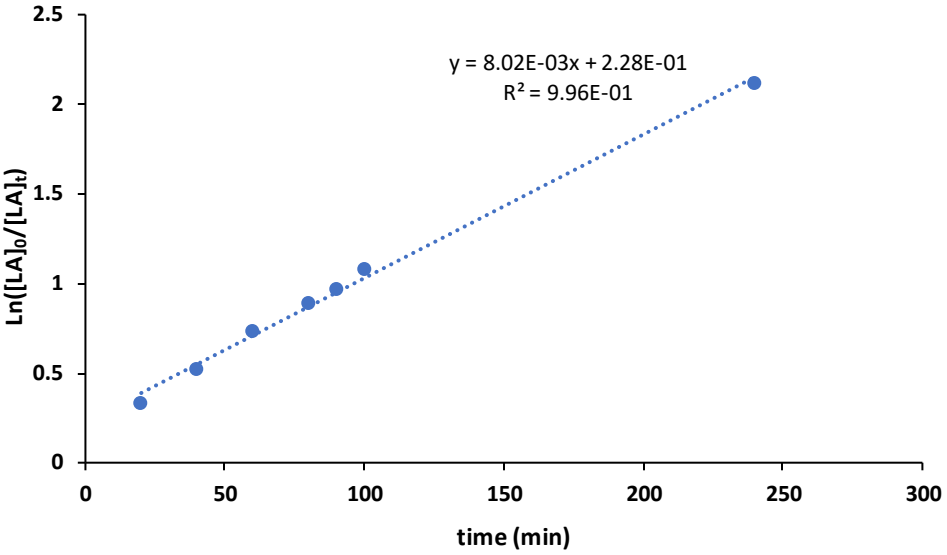

Figure S20: ln([*rac*-LA]$_0$ / [*rac*-LA]$_t$) vs time (min) for *rac*-LA ROP initiated by **1** + [Ag][OTf] (per Table 1, Entry 1).

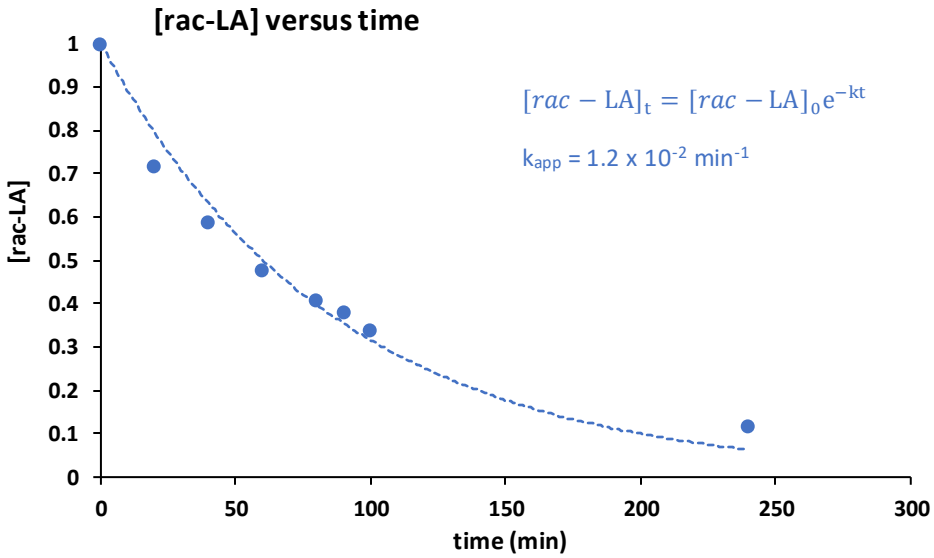

Figure S21: [*rac*-LA] versus time for reaction initiated by **1** + [Ag][OTf] (Table 1, Entry 1). (temporal least-square fit with k_{app} = 1.20 x 10^{-2} min^{-1})

➢ Data for *rac*-LA ROP initiated by **1** in the presence of [Ag][SbF_6]

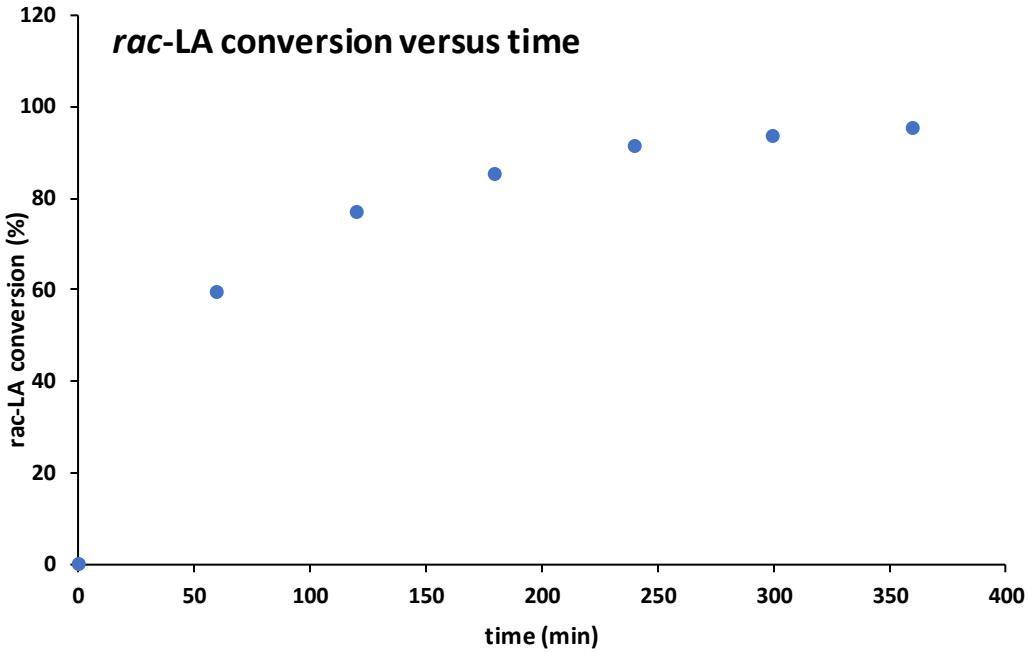

Figure S22: *rac*-LA conversion versus time for polymerisation initiated by **1** + [Ag][SbF_6] (Table 1, Entry 2).

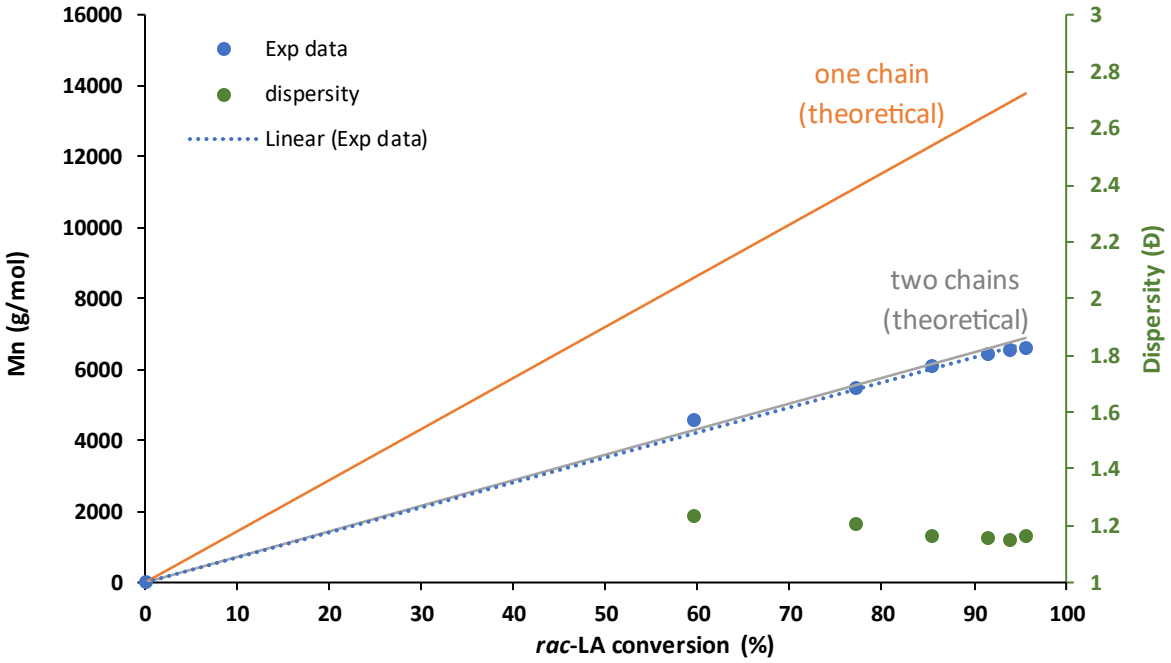

Figure S23: M_n (•) and dispersity (•) versus *rac*-LA conversion for polymerisation initiated by **1** + [Ag][SbF_6] showing good match with 2 chains per **1** (plain grey line) (Table 1, Entry 2).

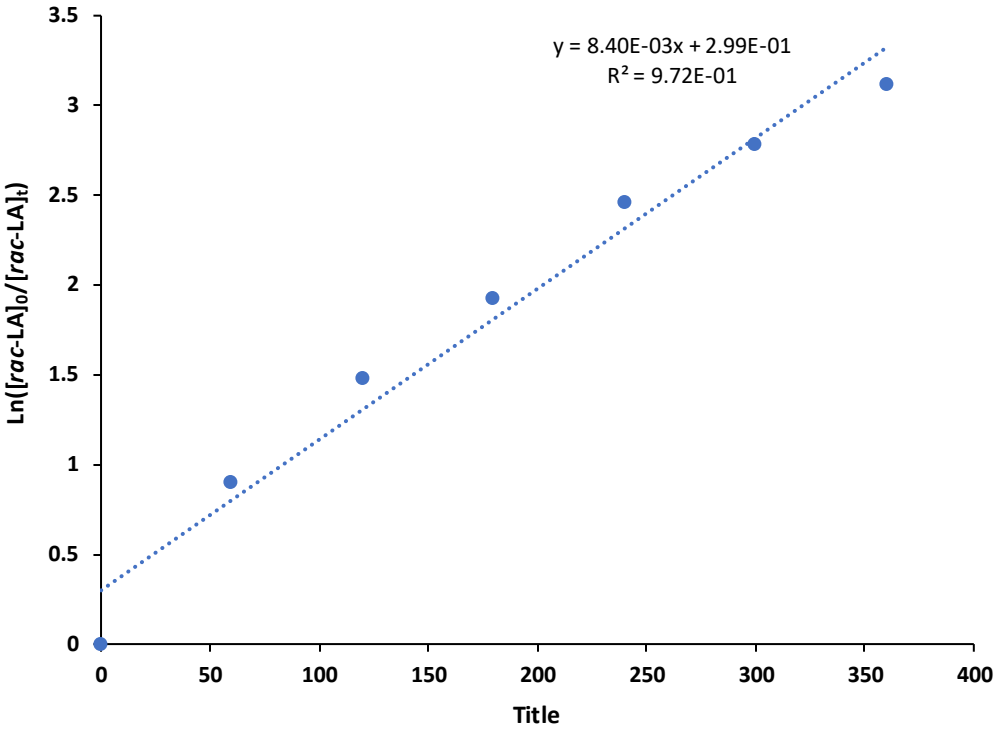

Figure S24: ln($[rac\text{-LA}]_0$ / $[rac\text{-LA}]_t$) vs time (min) for *rac*-LA ROP initiated by **1** + [Ag][SbF_6] (Table 1, Entry 2).

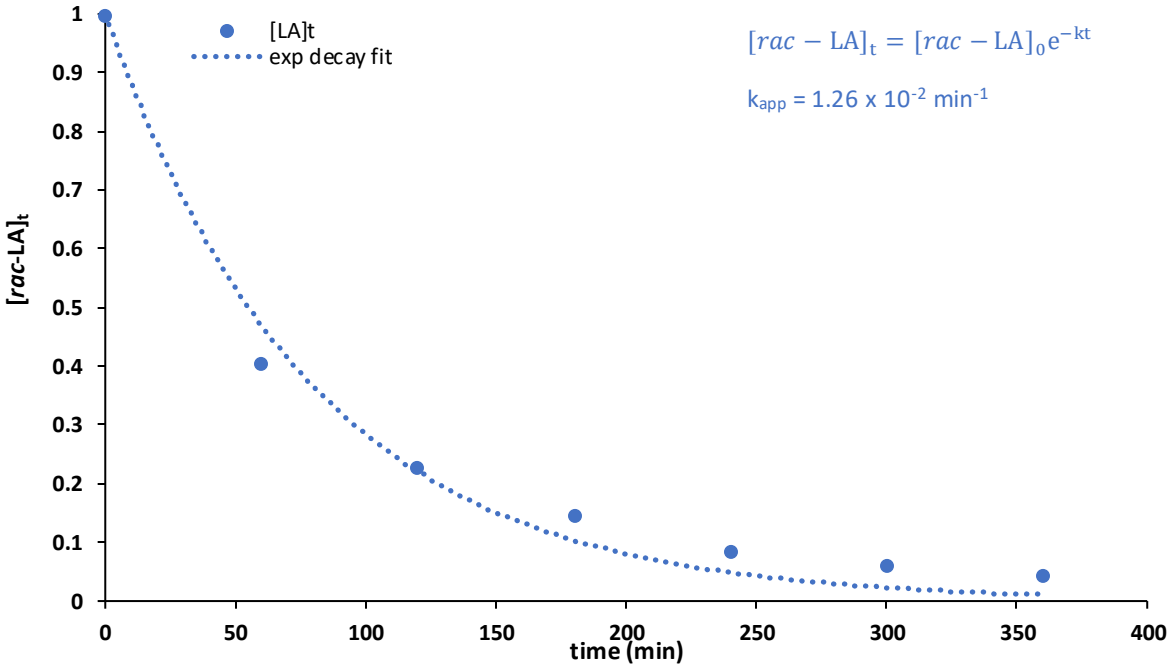

Figure S25: [*rac*-LA] versus time for reaction initiated by **1** + [Ag][SbF_6] (Table 1, Entry 2). (temporal least-square fit with k_{app} = 1.26 x 10^{-2} min^{-1})

➢ Data for *rac*-LA ROP initiated by **1** in the presence of [Ag][B(Ar^{CF3})$_4$]

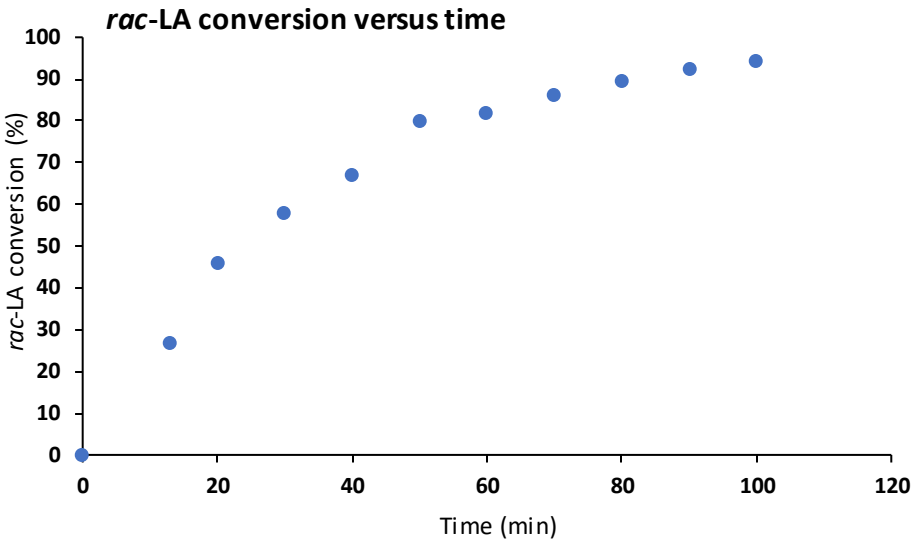

Figure S26: *rac*-LA conversion versus time for polymerisation initiated by **1** + [[Ag][B(Ar^{CF3})$_4$] (Table 1, Entry 3).

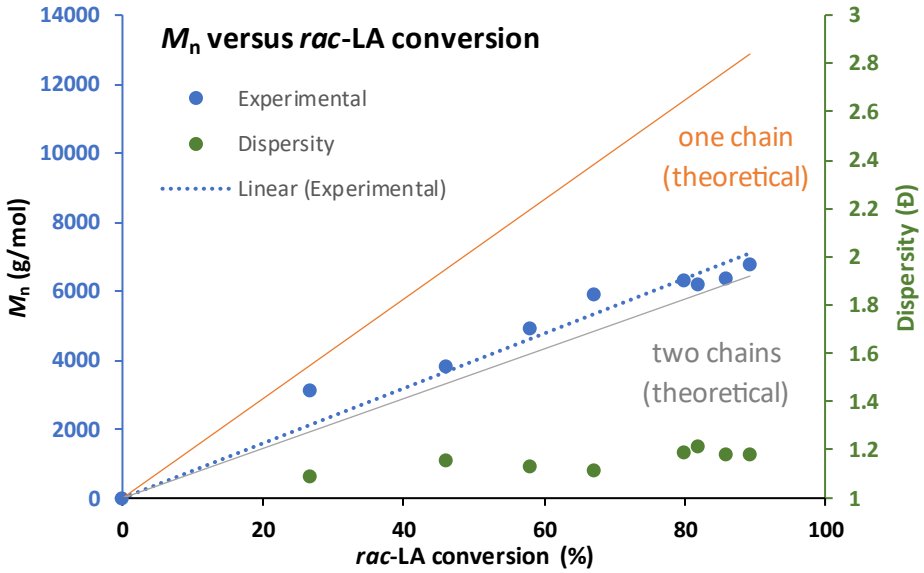

Figure S27: M_n (•) and dispersity (•) versus *rac*-LA conversion for polymerisation initiated by **1** + [Ag][B(Ar^{CF3})$_4$] showing good match with two chains per **1** (plain grey line), (Table 1, Entry 3).

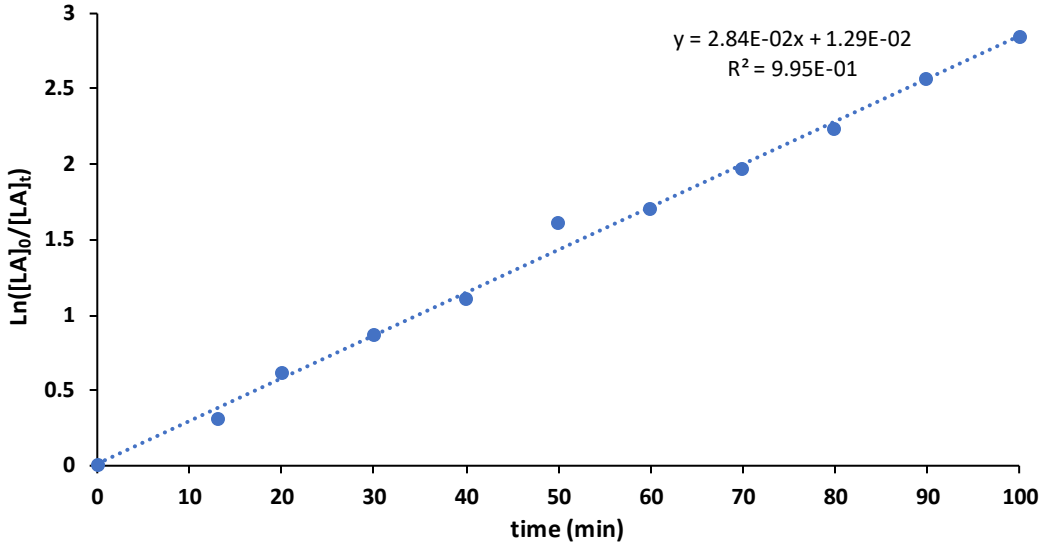

Figure S28: ln([*rac*-LA]$_0$ / [*rac*-LA]$_t$) vs time (min) for *rac*-LA ROP initiated by **1** + [Ag][B(Ar^{CF3})$_4$] (Table 1, Entry 3).

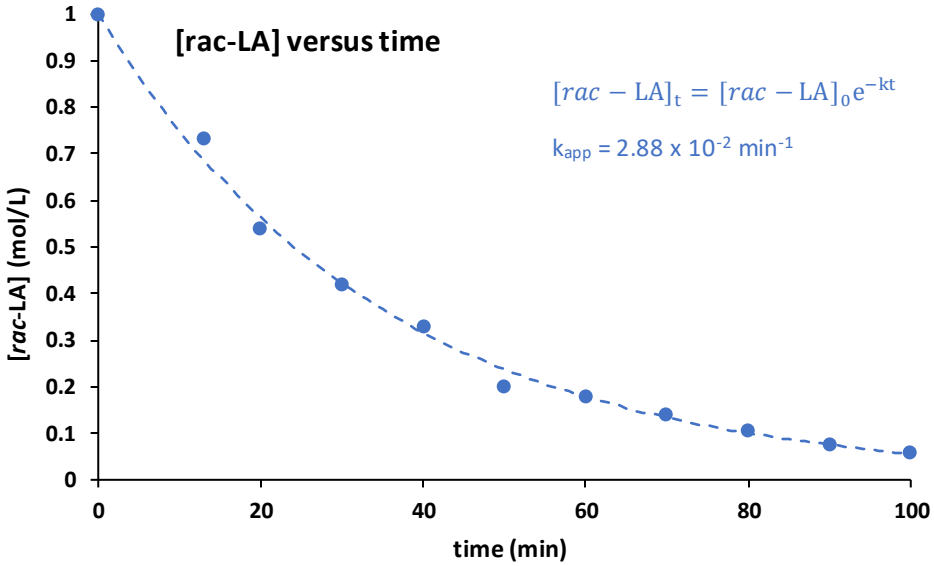

Figure S29: [*rac*-LA] versus time for reaction initiated by **1** + [Ag][B(Ar^{CF3})$_4$] (Table 1, Entry 3). (temporal least-square fit with k_{app} = 2.88 x 10^{-2} min^{-1})

➢ Data for *rac*-LA ROP initiated by **1** in the presence of [Ag][Al(OR^F)$_4$]

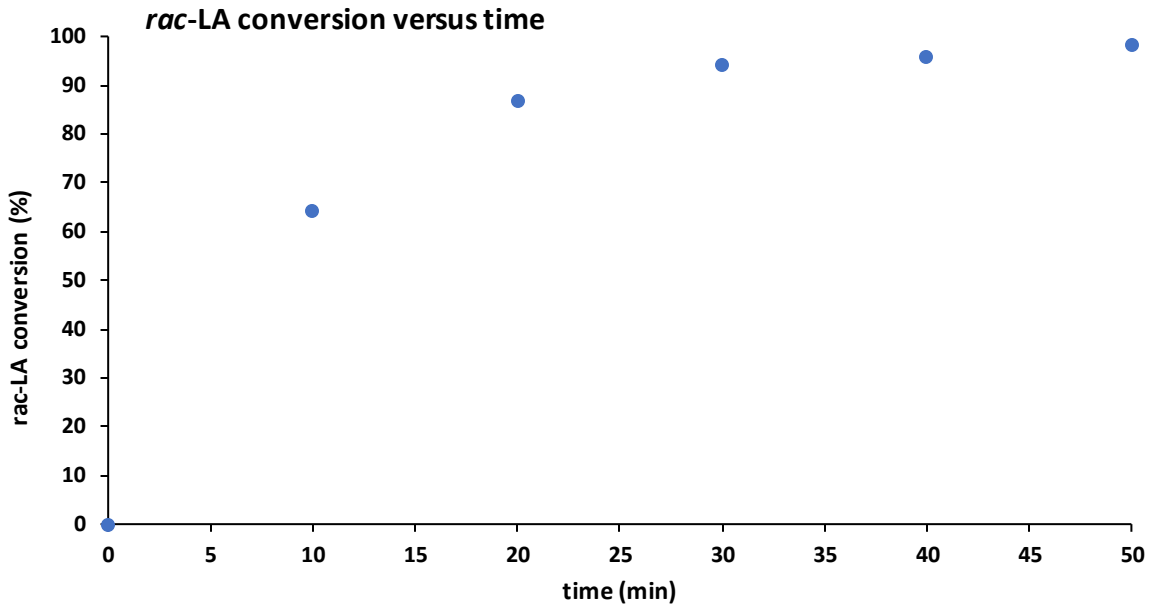

Figure S30: : *rac*-LA conversion versus time for polymerisation initiated by **1** + [Ag][Al(OR^F)$_4$] (Table 1, Entry 5).

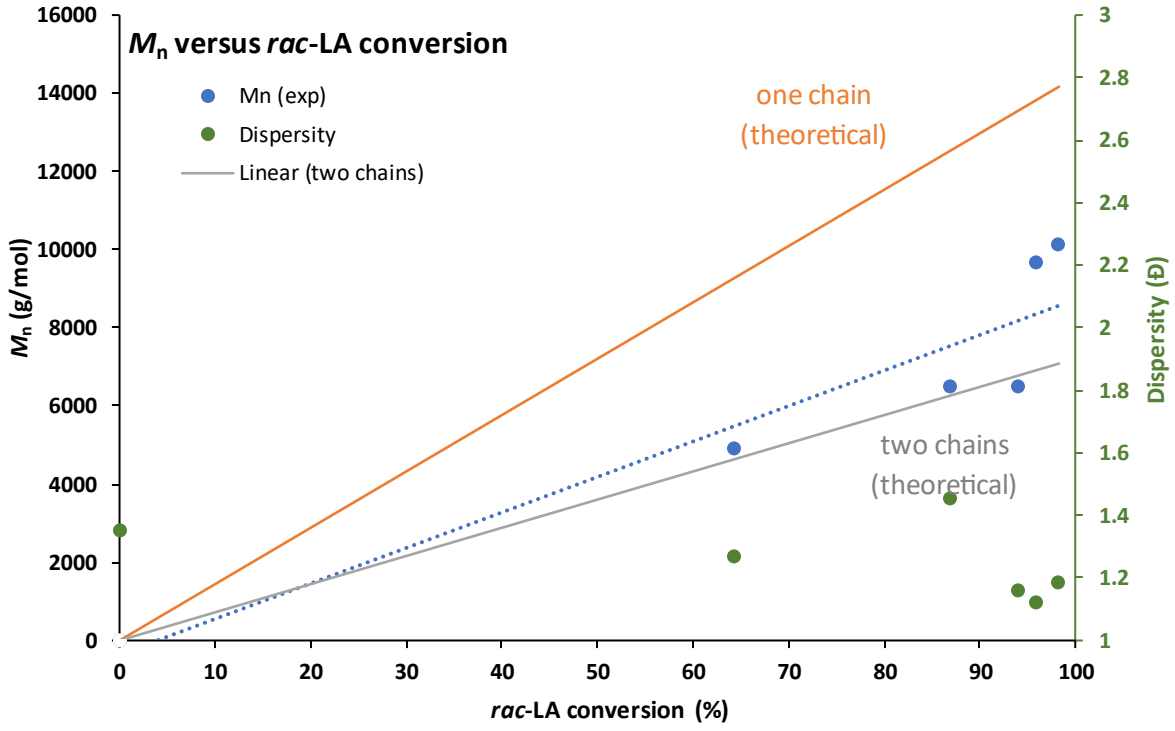

Figure S31: M_n versus *rac*-LA conversion for polymerisation initiated by **1** + [Ag][Al(OR^F)$_4$] showing good match with two chains per 1 (grey line), (Table 1, Entry 5).

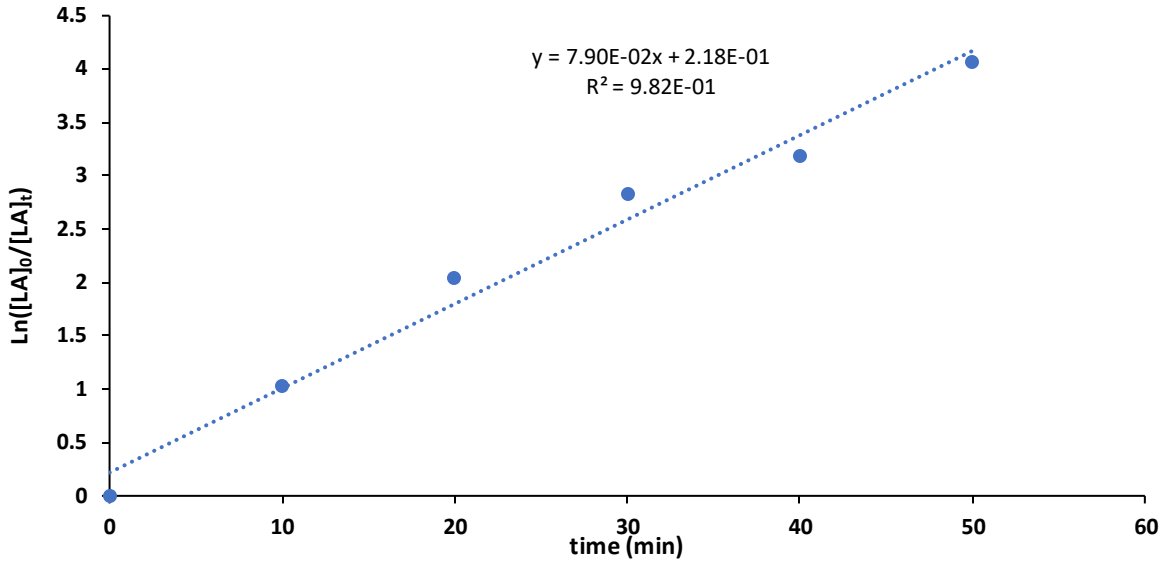

Figure S32: ln([*rac*-LA]$_0$ / [*rac*-LA]$_t$) vs time (min) for *rac*-LA ROP initiated by **1** + [Ag][Al(OR^F)$_4$] (Table 1, Entry 5).

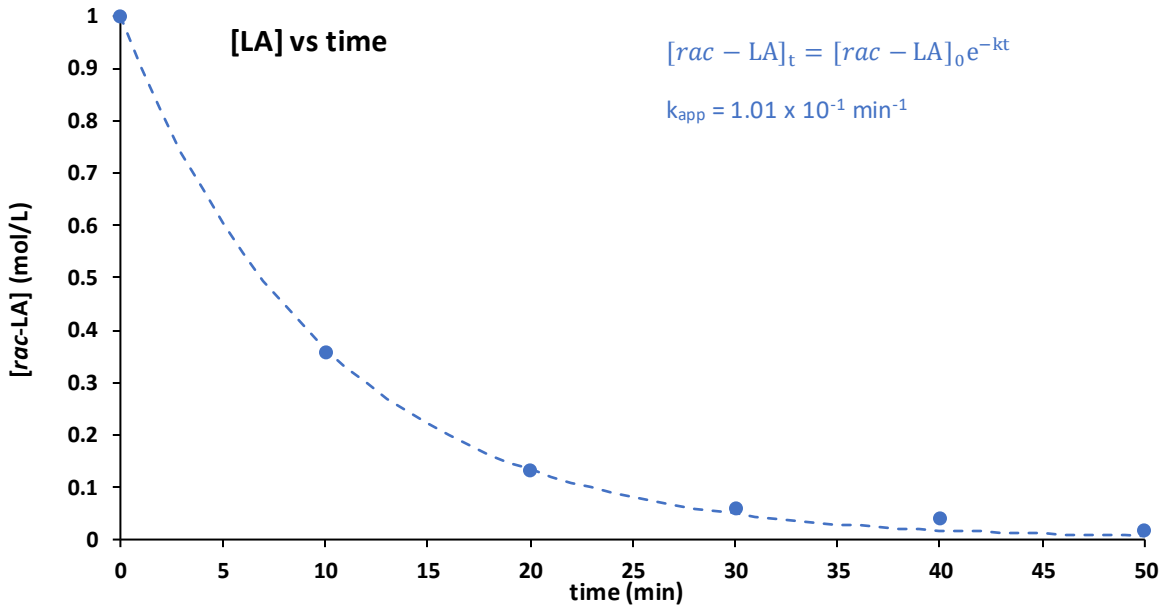

Figure S33: [*rac*-LA] versus time for reaction initiated by **1** + [Ag][Al(OR^F)$_4$] (Table 1, Entry 5). (temporal least-square fit with k_{app} = 1.01 x 10^{-1} min^{-1})

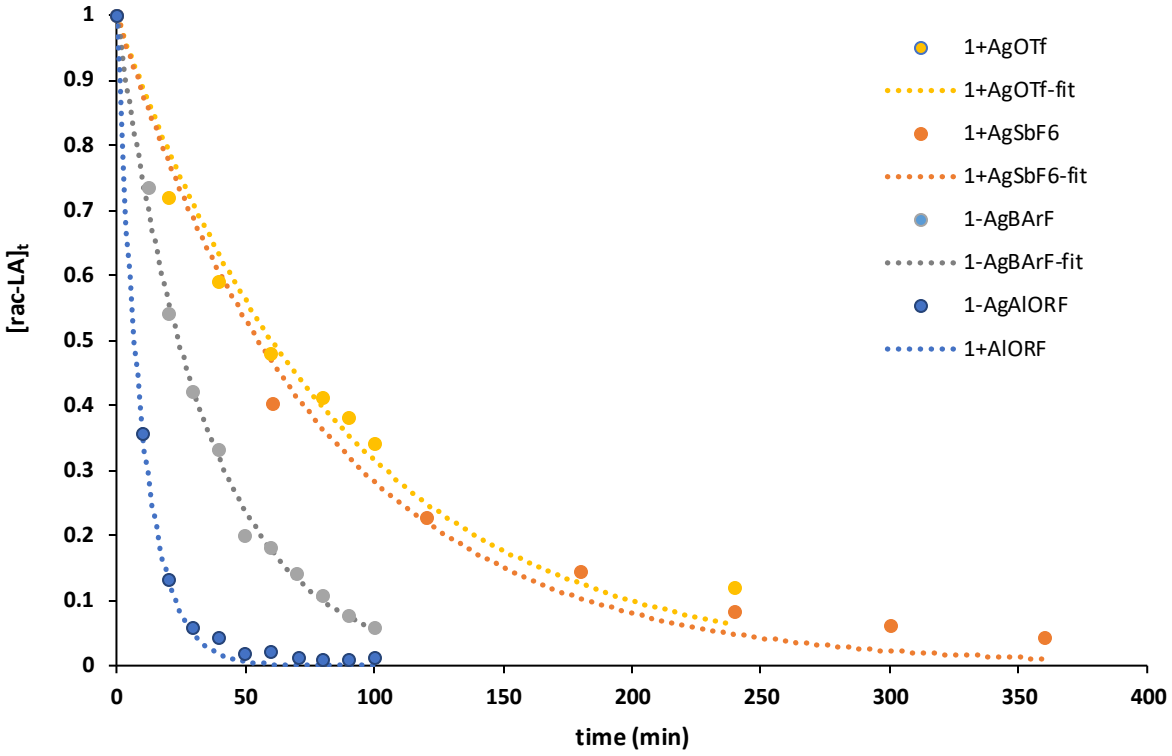

Figure S34: Overlay of [*rac*-LA]$_t$ versus time for polymerisation initiated by **1** in the presence of the different silver salts, including exponential decay fitting (dash line), as per figure legend.

Table S1: reaction rate for polymerisation initiated using **1** + the different silver salts

Complex (1 equiv.)	**Silver salt** (1 equiv.)	k_{app}[a] (min^{-1})
1	[Ag][OTf]	1.2×10^{-2}
1	[Ag][SbF_6]	1.3×10^{-2}
1	[Ag][$B(Ar^{CF3})_4$]	2.9×10^{-2}
1	[Ag][$Al(OR^F)_4$]	1.0×10^{-1}

Reaction conditions: 1/[silver salt]/[LA] = 1/1/100, [LA]0 = 1 M, dichloromethane, room temperature; a) k_{app} determined using temporal least-square fit for an exponential decay, [*rac*-LA]$_t$ = [rac-LA]$_0$.exp(-k_{app}.t), as per Figure S28.

➢ *Same Excess Experiments:*

In order to investigate for deactivation of the catalytic system (e.g. reaction of the silver salt with **1**), "*same excess*" experiments were carried out. Two reactions with different initial concentration of *rac*-LA were performed (i.e. $[rac\text{-LA}]_0$ = 1.5 M and 1.0 M) and monitored. The reaction with the higher initial concentration (i.e. $[\text{rac-LA}]_0$ = 1.5 M) will reach at some point the same concentration as the reaction with lower initial concentration $[rac\text{-LA}]_0$ = 1.0 M. At this point, in the absence of deactivation, the catalytic system which has already completed several monomer insertions should have the same activity as the reaction started at a lower concentration. Thus, a time shift of the curve should overlay if there is no deactivation. It should be noted that a slightly lower activity could also be inferred from the polymer chain growing from the metal centre hampering further monomer insertion (i.e. sort of product inhibition).

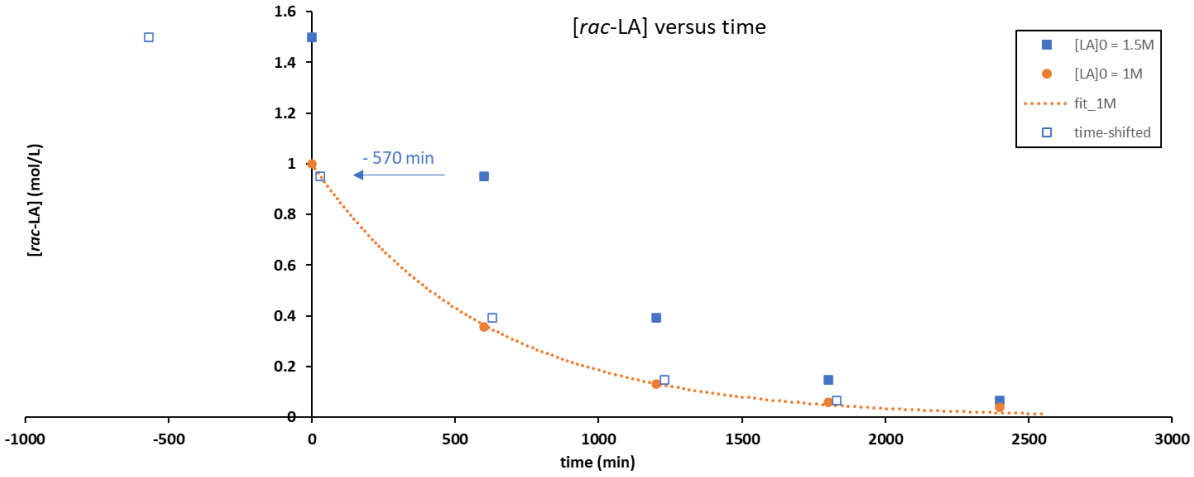

Figure S35: *rac*-LA polymerisation initiated by **1** + $[Ag][Al(OR^F)_4]$ with $[rac\text{-LA}]_0$ = 1M (●,orange dot) and 1.5M (■, blue square) showing no catalyst deactivation.

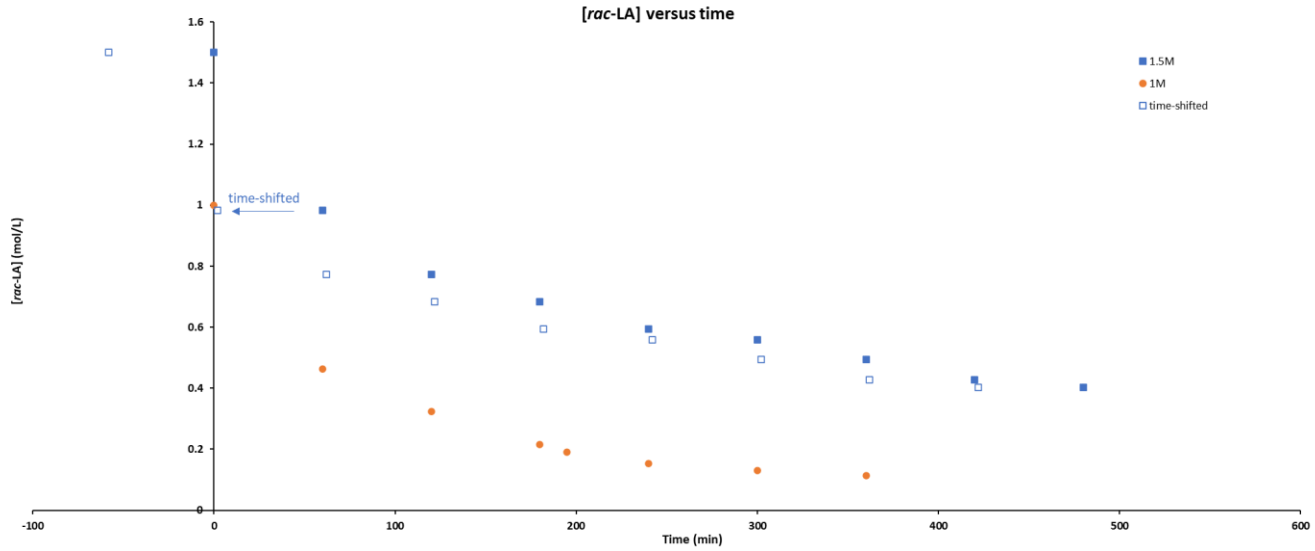

Figure S36: *rac*-LA polymerisation initiated by **1** + [Ag][SbF_6] with [*rac*-LA]$_0$ = 1M (●, orange dot) and [*rac*-LA]$_0$ = 1.5M (■, blue square) showing deactivation (time-shifted curve slower activity after [*rac*-LA] = 1M)

➢ **Effect of silver salt [Ag][Al(OR^F)$_4$] equivalents for *rac*-LA ROP initiated by 1.**

Table 2: Effect of silver salt **[Ag][Al(OR^F)$_4$]** concentration [R^F = C(CF$_3$)$_3$]

Entry	cat. / [Ag][X] /*rac*-LA (equiv.)	[X]$^-$ (1 equiv.)	Time (min)	Conversion (%)
2-60	1/1/100	[Al(OR^F)$_4$]$^-$	20	86.9
2-58	1/0.5/100	[Al(OR^F)$_4$]$^-$	60	61.8
2-60	1/2/100	[Al(OR^F)$_4$]$^-$	20	92.2

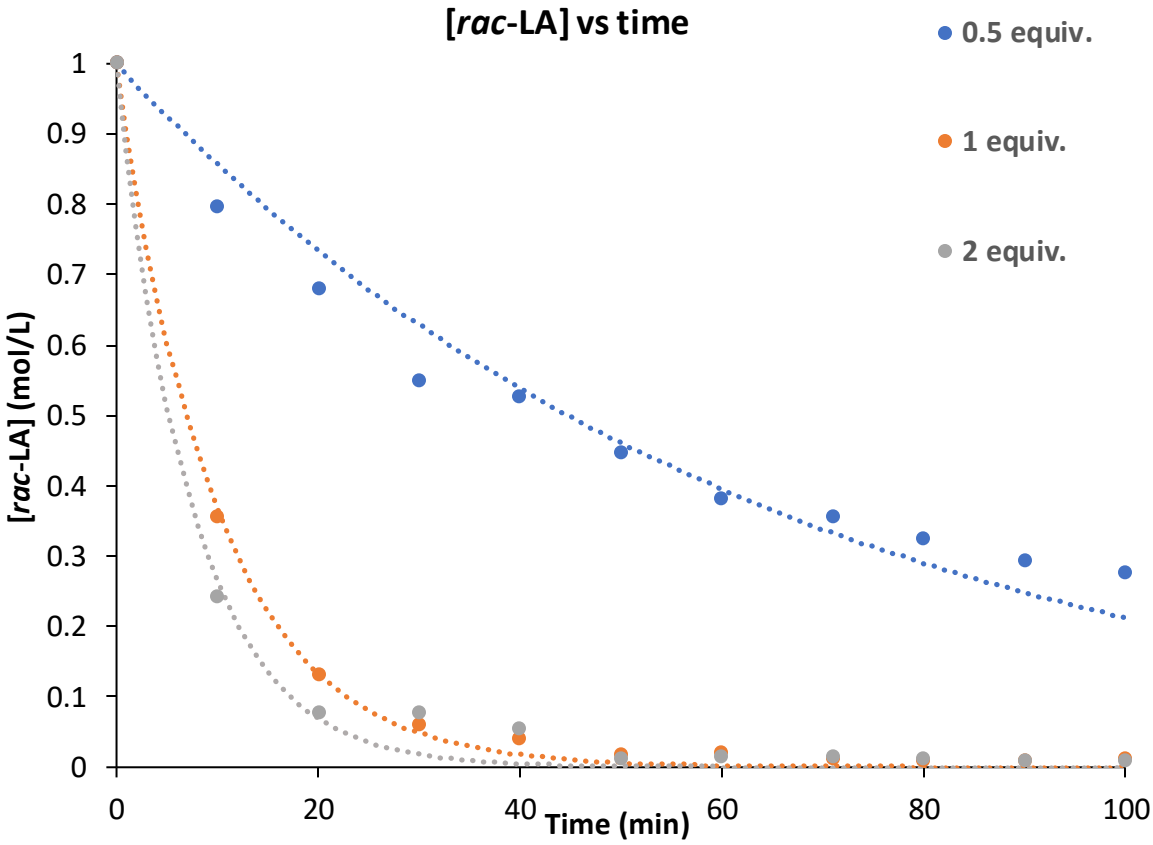

Figure S37: [*rac*-LA] versus time for polymerisation initiated with **1** in the presence of 0.5 (●, blue dot), 1 (●, orange dot) and 2 equivalents (●, grey dot) of [Ag][Al(OR^F)$_4$] as per Table S2.

➢ Data for *rac*-LA ROP initiated by **2** in the presence of [Ag][OTf]

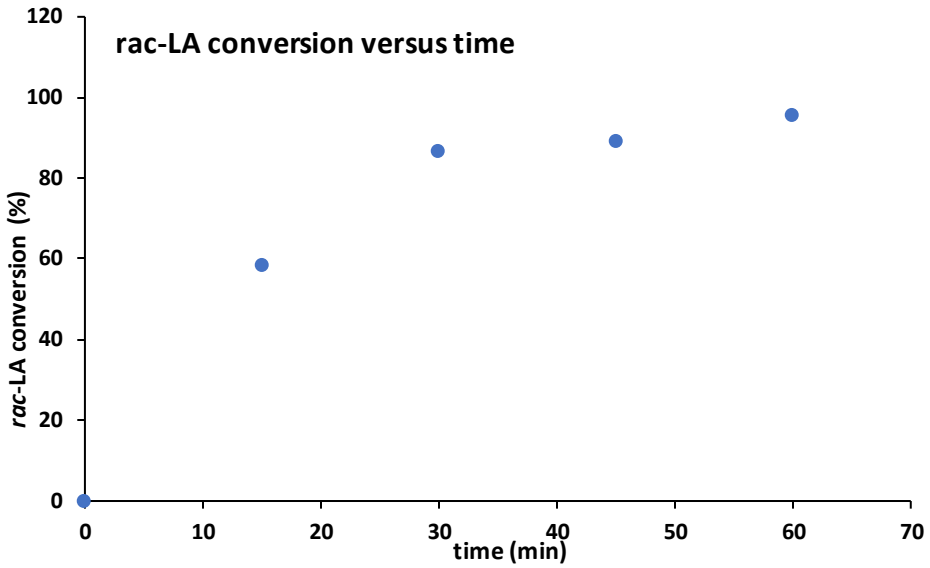

Figure S38: *rac*-LA conversion versus time for polymerisation initiated by **2** + [Ag][OTf] (Table 2, Entry 1).

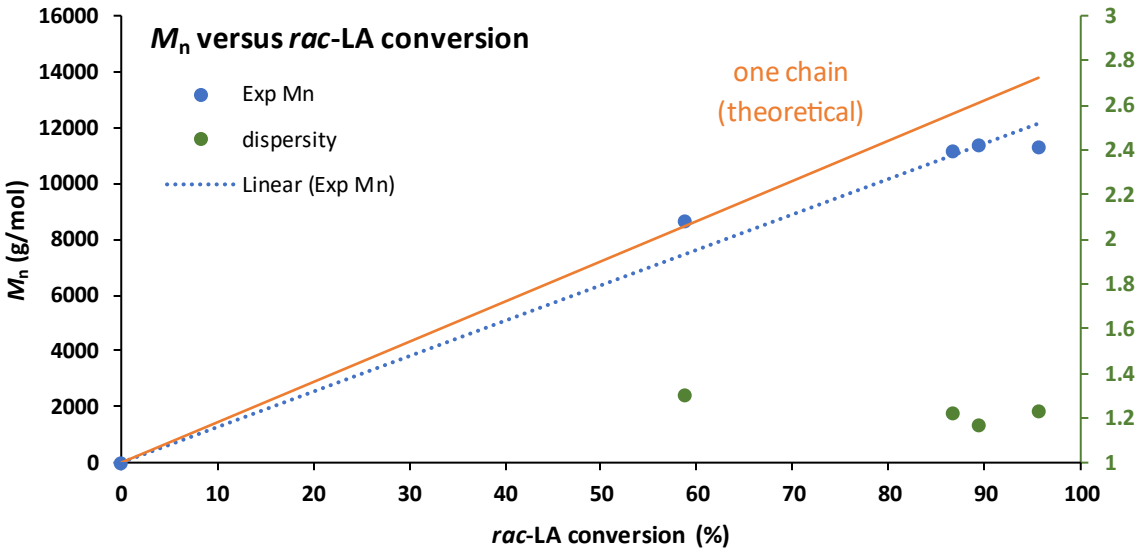

Figure S39: M_n versus *rac*-LA conversion for polymerisation initiated by **2** + [Ag][OTf] showing 1 chain per Ti complex suggesting only one O^{i}Pr initiating (orange line), (Table 2, Entry 1).

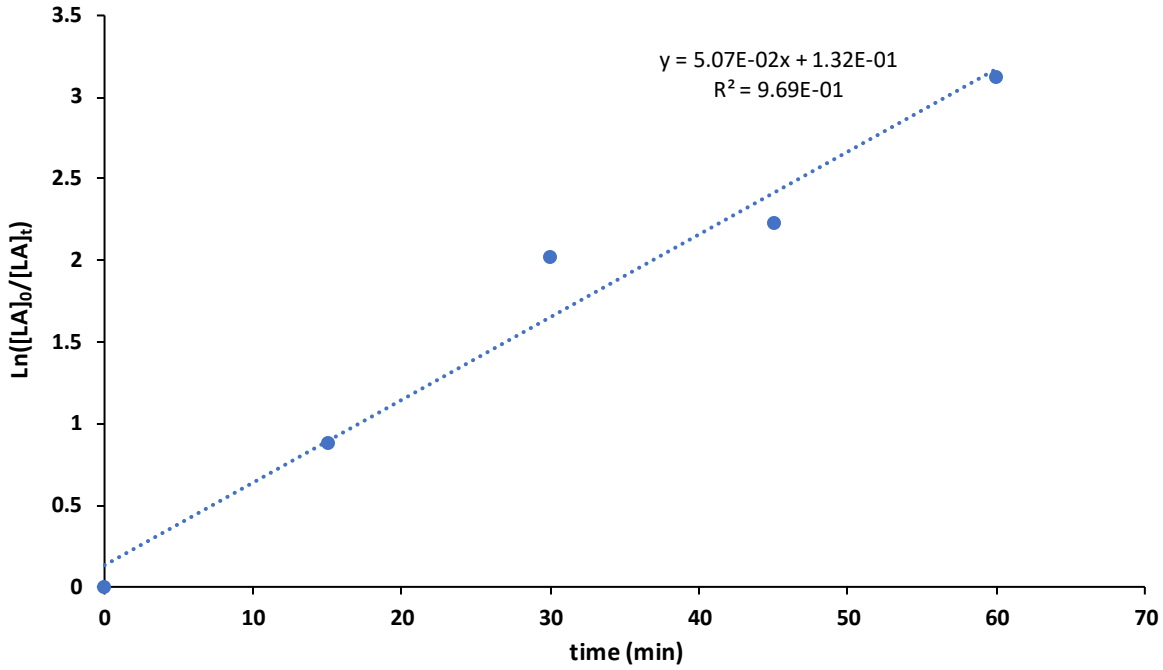

Figure S40: ln([*rac*-LA]$_0$ / [*rac*-LA]$_t$) vs time (min) for *rac*-LA ROP initiated by **2** + [Ag][OTf], (Table 2, Entry 1).

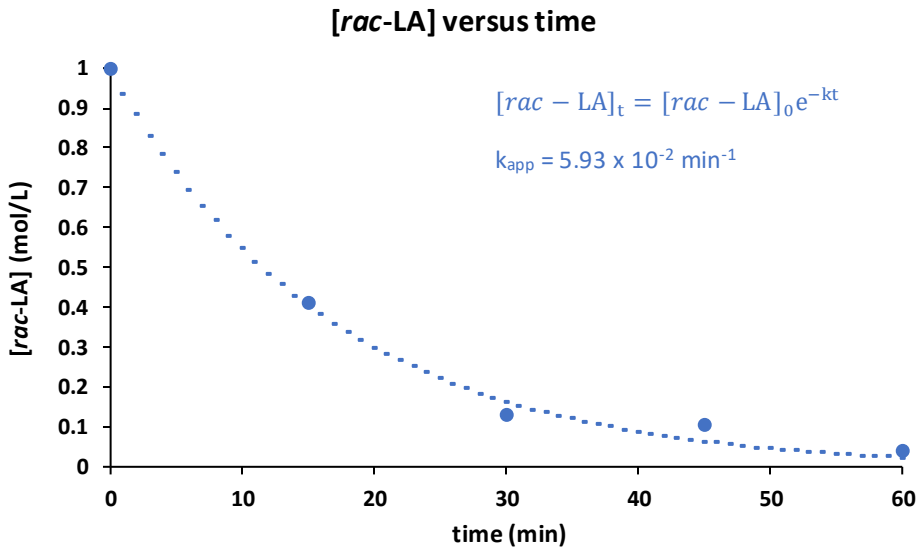

Figure S41: [*rac*-LA] versus time for reaction initiated by **2** + [Ag][OTf] (Table 2, Entry 1). (temporal least-square fit with k_{app} = 5.93 x 10^{-2} min^{-1})

➢ Data for *rac*-LA ROP initiated by **2** in the presence of [Ag][SbF_6]

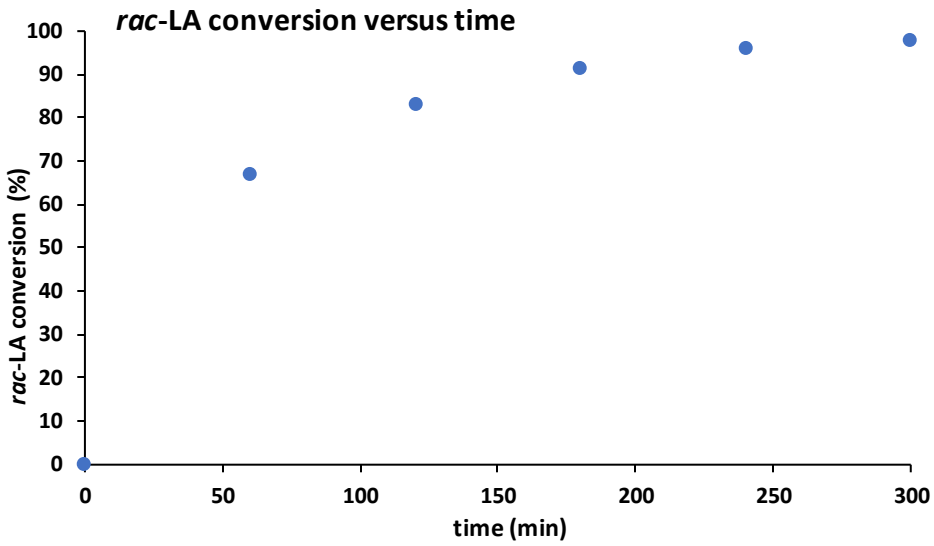

Figure S42: *rac*-LA conversion versus time for polymerisation initiated by **2** + [Ag][SbF_6] (Table 2, Entry 2).

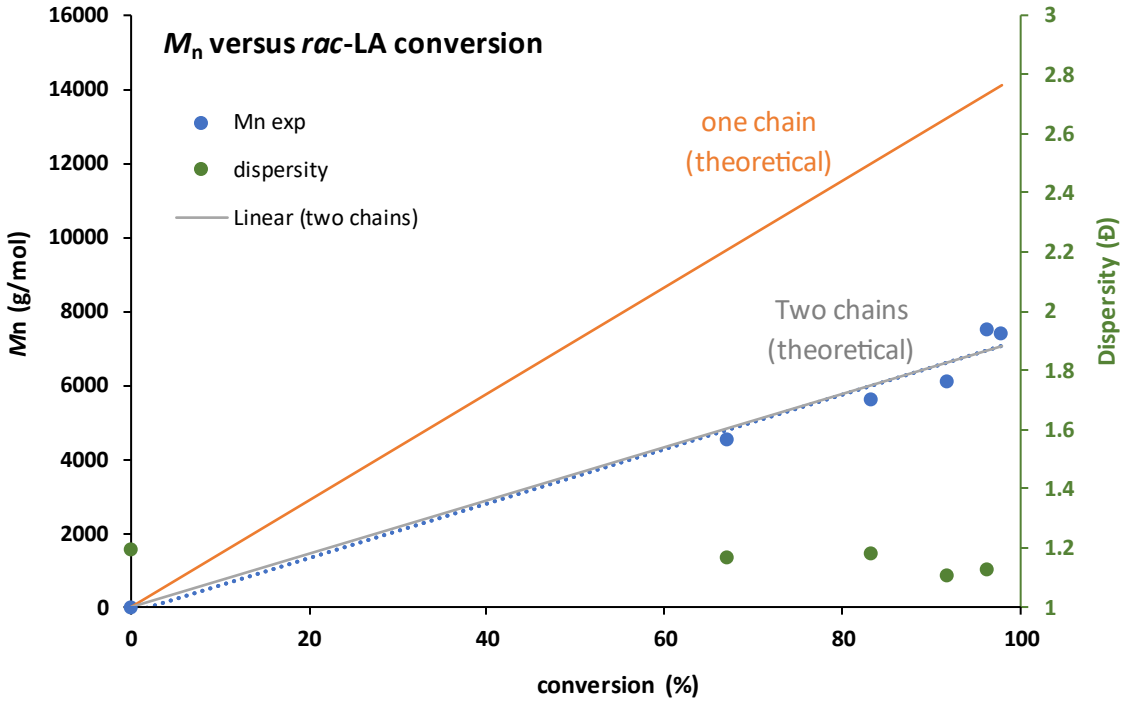

Figure S43: M_n (•) and dispersity (•) versus *rac*-LA conversion for polymerisation initiated by **2** + [Ag][SbF_6] showing 2 chains per Ti (both O^{i}Pr groups initiating) (Table 2, Entry 2).

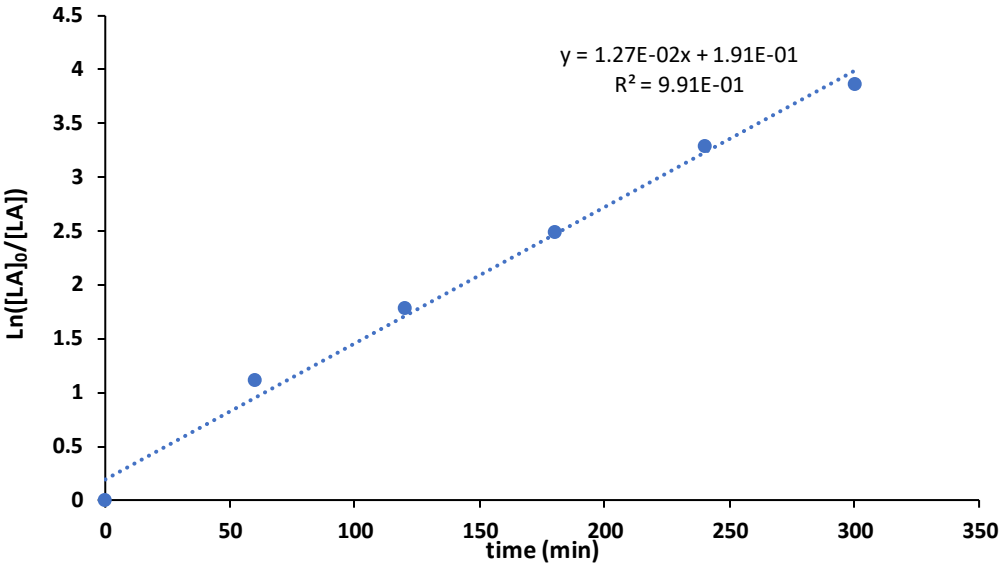

Figure S44: ln($[rac\text{-LA}]_0$ / $[rac\text{-LA}]_t$) vs time (min) for *rac*-LA ROP initiated by **2** + [Ag][SbF_6] (Table 2, Entry 2).

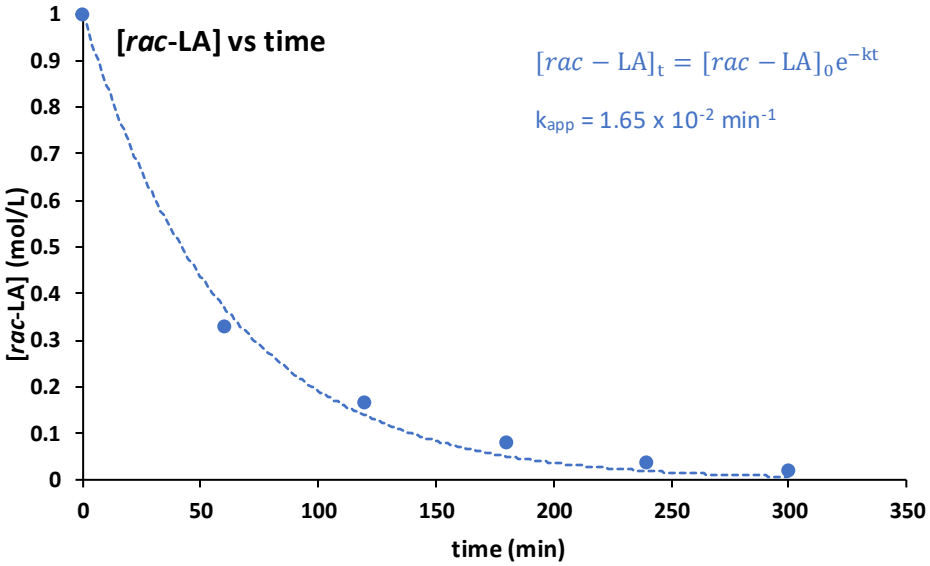

Figure S45: [*rac*-LA] versus time for reaction initiated by **2** + [Ag][SbF_6] (Table 2, Entry 2). (temporal least-square fit with k_{app} = 1.65 x 10^{-2} min^{-1})

➢ Data for *rac*-LA ROP initiated by **2** in the presence of [Ag][B(Ar^{CF3})$_4$]

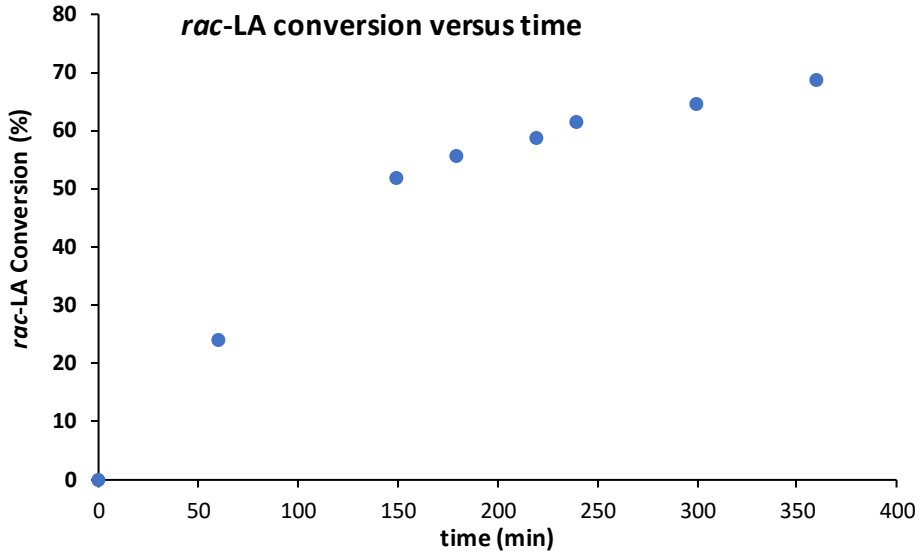

Figure S46: *rac*-LA conversion versus time for polymerisation initiated by **2** + [Ag][B(Ar^{CF3})$_4$] (Table 2, Entry 3).

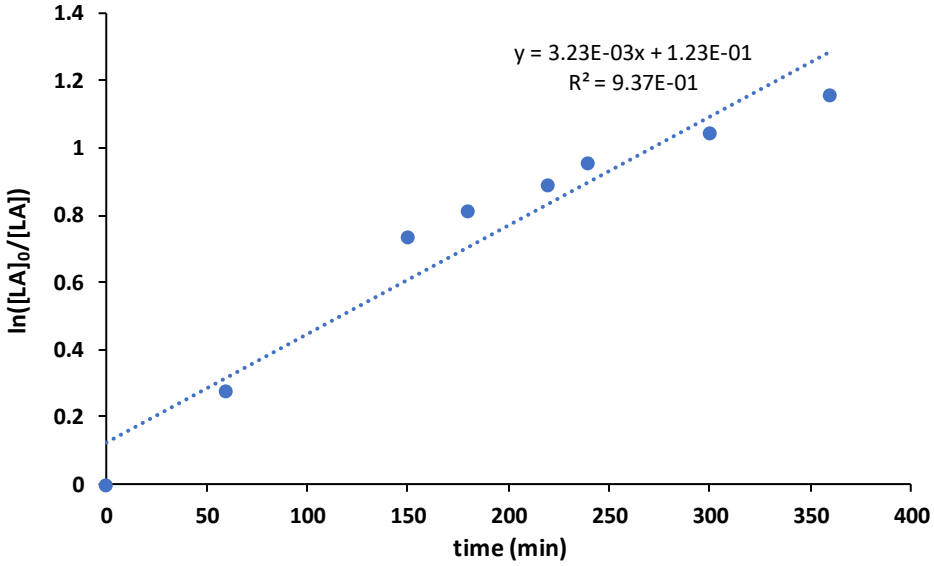

Figure S47: ln([*rac*-LA]$_0$ / [*rac*-LA]$_t$) vs time (min) for *rac*-LA ROP initiated by **2** + [Ag][B(Ar^{CF3})$_4$] (Table 2, Entry 3).

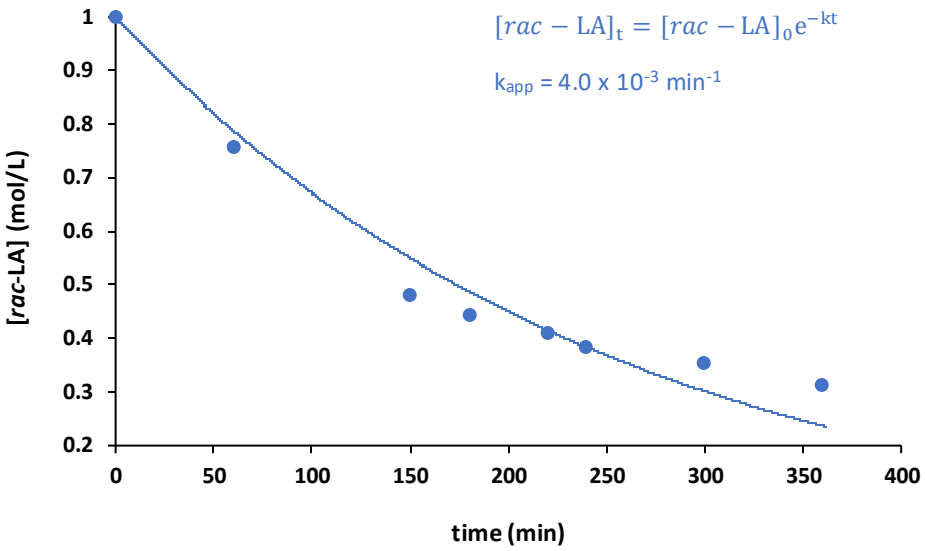

Figure S48: [*rac*-LA] versus time for reaction initiated by **2** + [Ag][B(Ar^{CF3})$_4$] (Table 2, Entry 3). (temporal least-square fit with k_{app} = 4.0 x 10^{-3} min^{-1}).

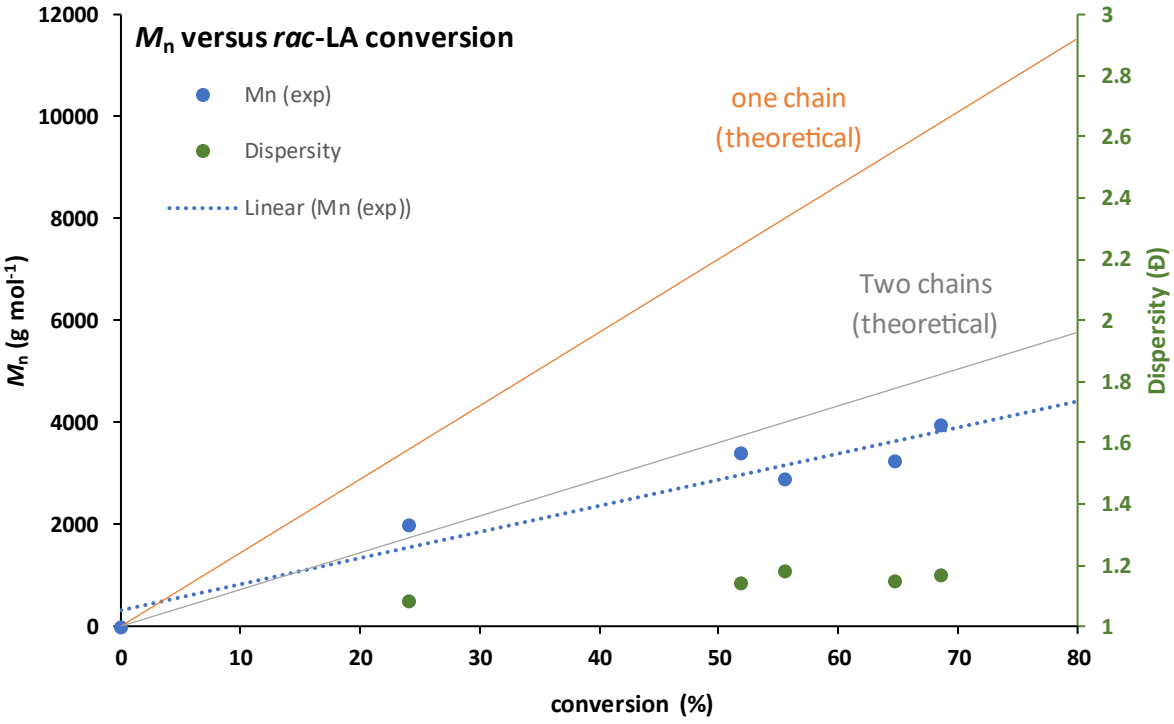

Figure S49: M_n (•) and dispersity (•) versus *rac*-LA conversion for polymerisation initiated by **2** + [Ag][B(Ar^{CF3})$_4$] showing 2 chains per Ti (both O^{i}Pr groups initiating) (Table 2, Entry 3).

➢ **Data for *rac*-LA ROP initiated by 2 + [Ag][Al(OR^F)$_4$]**

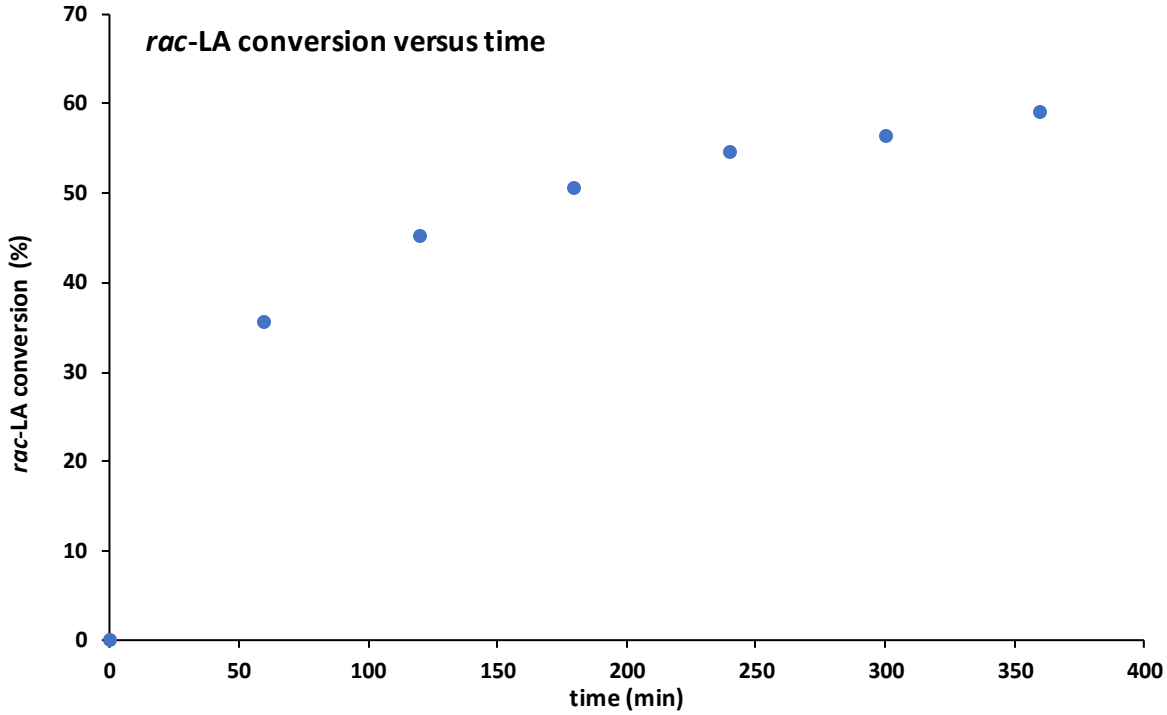

Figure S50: *rac*-LA conversion versus time for polymerisation initiated by **2** + [Ag][Al(OR^F)$_4$] (Table 2, Entry 4).

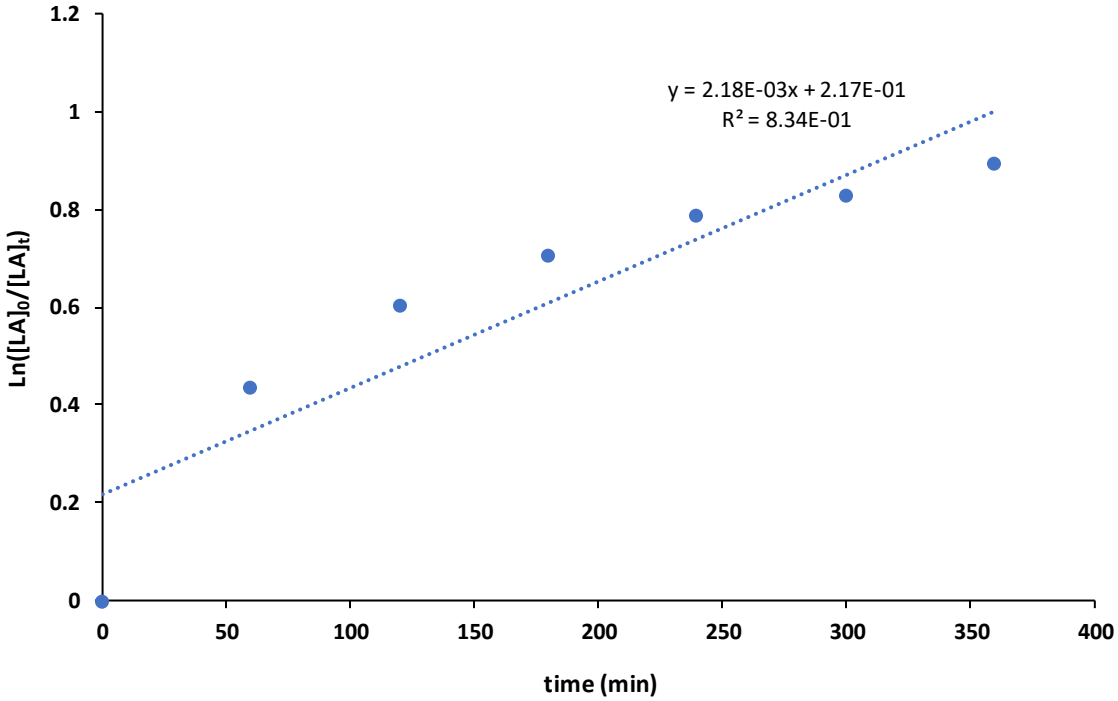

Figure S51: ln([*rac*-LA]$_0$ / [*rac*-LA]$_t$) vs time (min) for *rac*-LA ROP initiated by **2** + [Ag][Al(OR^F)$_4$] (Table 2, Entry 4) and a poor linear fit suggesting departure from the assumed first order in monomer.

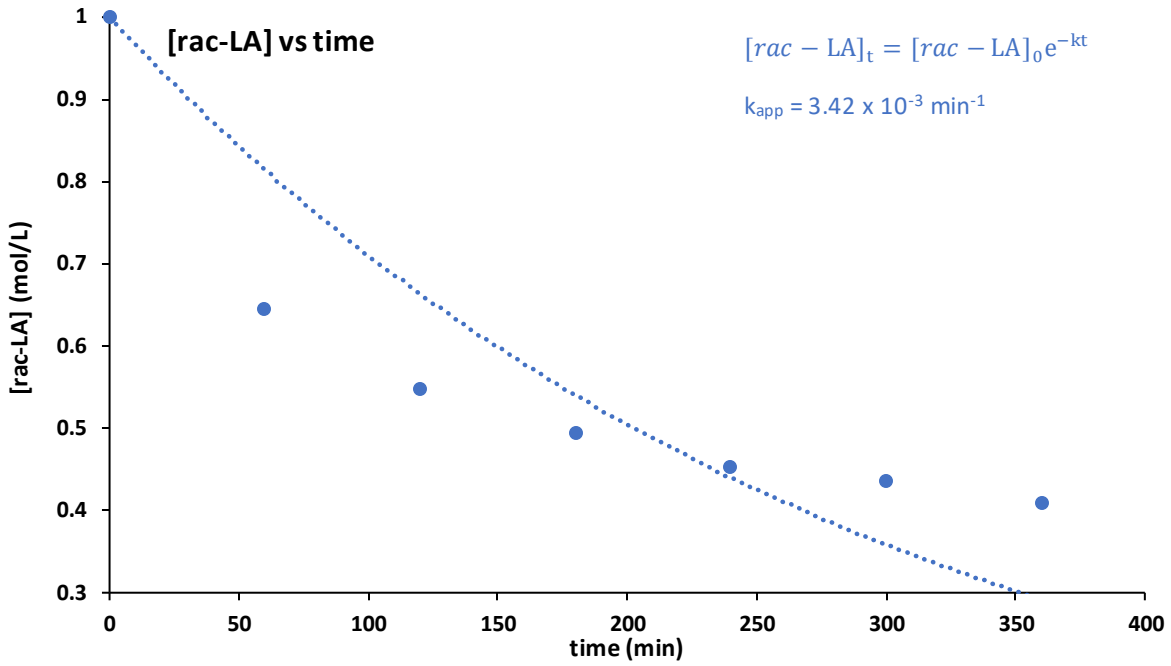

Figure S52: [*rac*-LA] versus time for reaction initiated by **2** + [Ag][Al(OR^F)$_4$] (Table 2, Entry 4). (the poor temporal least-square fit with k_{app} = 3.42 x 10^{-3} min^{-1} suggests departure from the assumed first order in monomer).

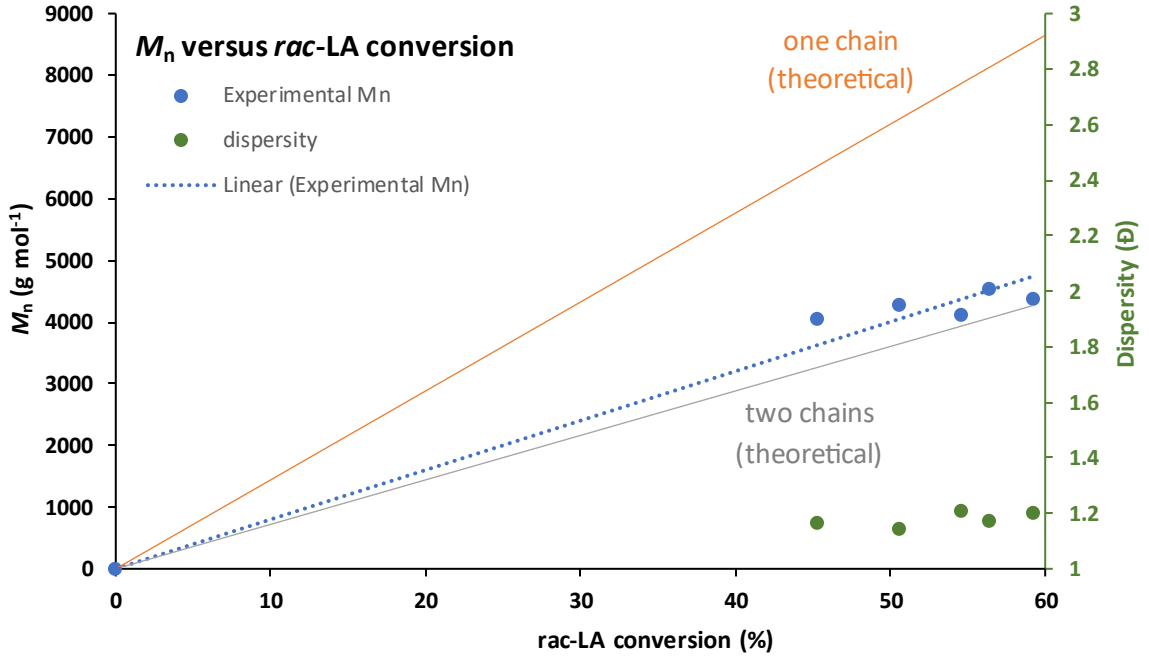

Figure S53: M_n (•) and dispersity (•) versus *rac*-LA conversion for polymerisation initiated by **2** + [Ag][Al(OR^F)$_4$] showing 2 chains per Ti (both O^{i}Pr groups are initiating) (Table 2, Entry 4).

➢ **Data for *rac*-LA ROP initiated by (S,S)-2 + [Ag][Al(OR^F)$_4$]**

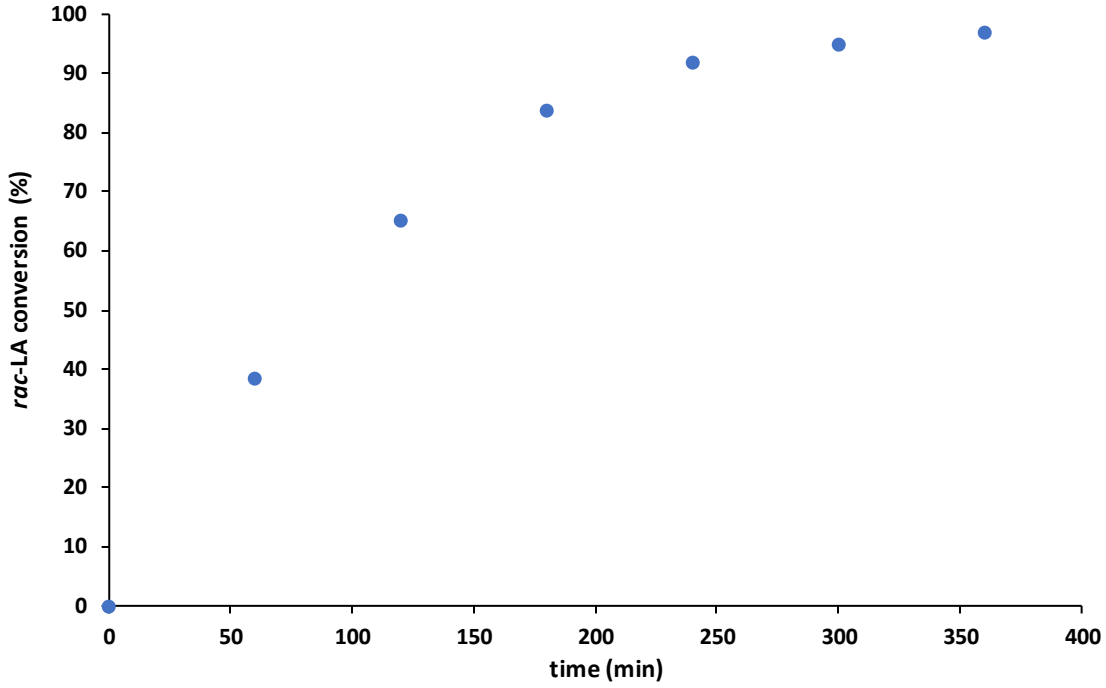

Figure S54: *rac*-LA conversion versus time for polymerisation initiated by **(S,S)-2** + [Ag][Al(OR^F)$_4$] (Table 2, Entry 5).

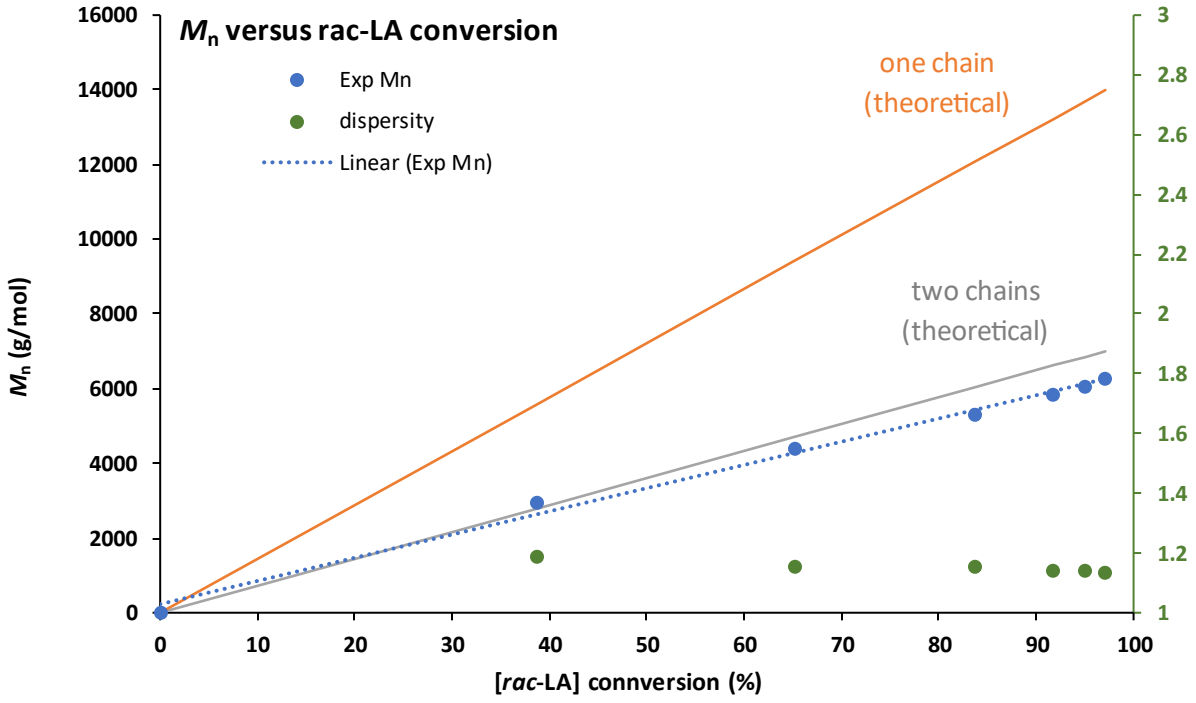

Figure S55: M_n (•) and dispersity (•) versus *rac*-LA conversion for polymerisation initiated by **(S,S)-2** + [Ag][Al(OR^F)$_4$] showing 2 chains per Ti (both O^{i}Pr groups are initiating), (Table 2, Entry 5).

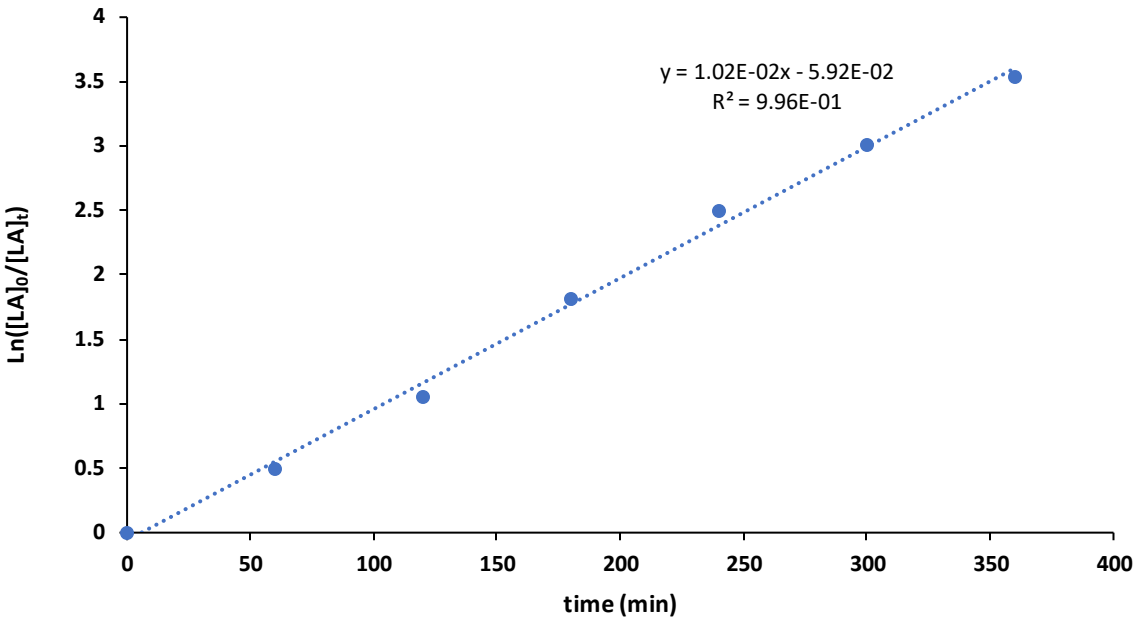

Figure S56: ln([*rac*-LA]$_0$ / [*rac*-LA]$_t$) vs time (min) for *rac*-LA ROP initiated by **(S,S)-2** + [Ag][Al(OR^F)$_4$] (Table 2, Entry 5)

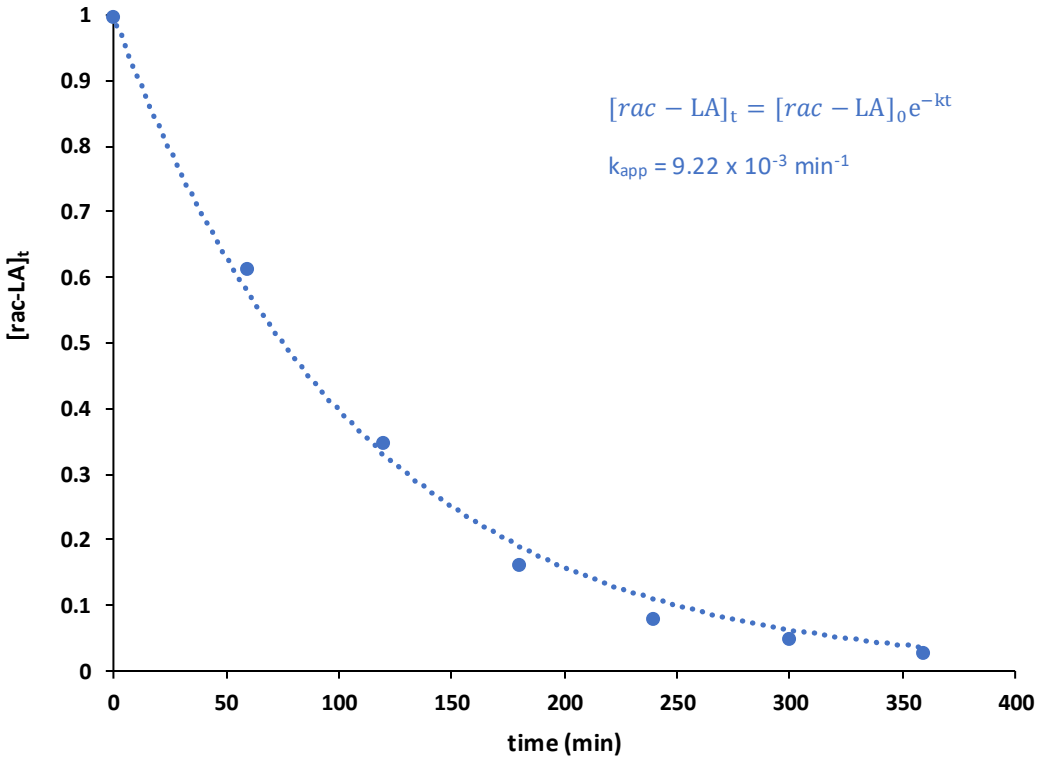

Figure S57: [*rac*-LA] versus time for reaction initiated by **(S,S)-2** + [Ag][Al(OR^F)$_4$] (Table 2, Entry 5). (temporal least-square fit with k_{app} = 9.22 x 10^{-3} min^{-1}.

➢ **Data for *L*-LA ROP initiated by (S,S)-2 + [Ag][Al(OR^F)$_4$]**

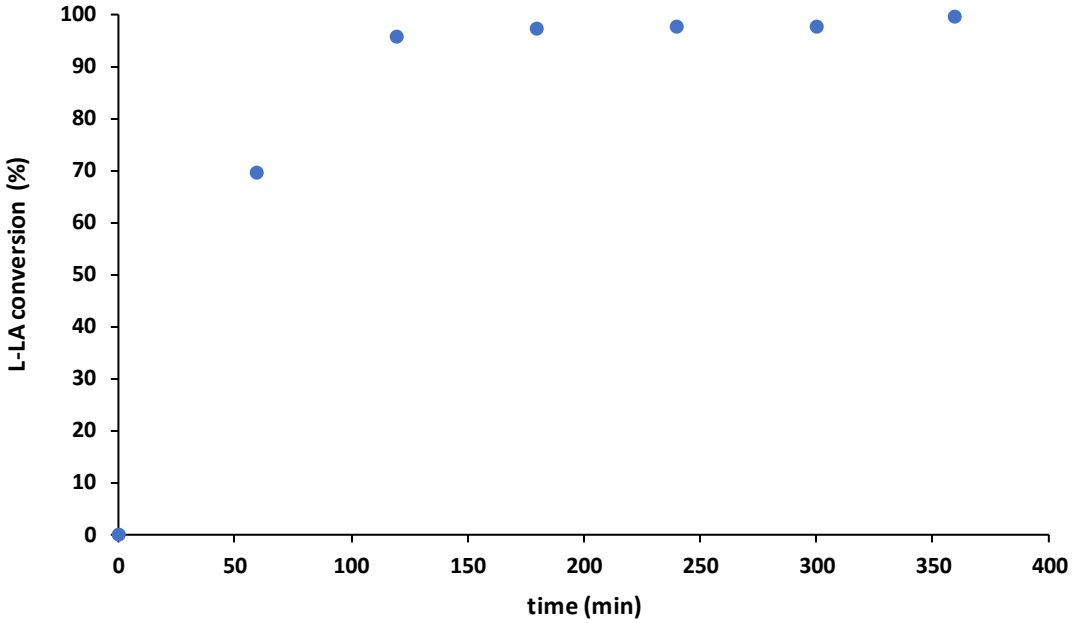

Figure S58: L-LA conversion versus time for polymerisation initiated by **(S,S)-2** + [Ag][Al(OR^F)$_4$], reaction conditions: cat = **(S,S)-2)**, [L-LA]$_0$ = 1M, [cat]/[AgAl(OR^F)$_4$]/[L-LA] = 1/1/100, DCM, 25°C.

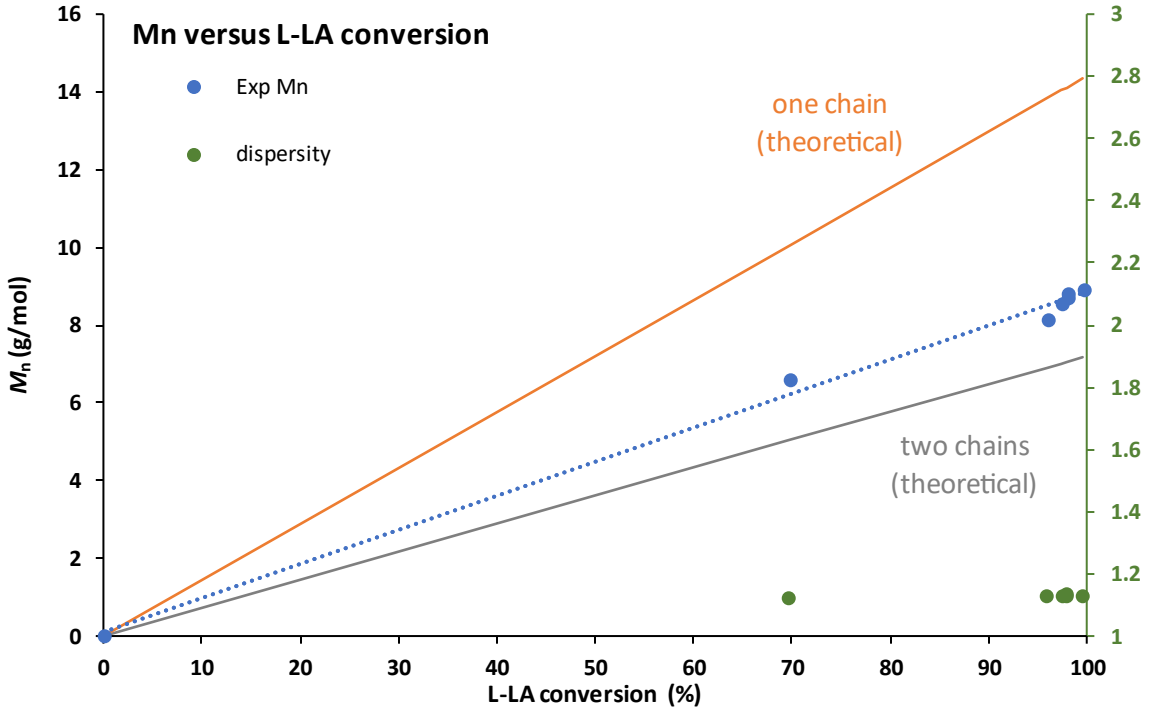

Figure S59: M_n (•) and dispersity (•) versus *L*-LA conversion for polymerisation initiated by **(S,S)-2** + [Ag][Al(OR^F)$_4$] showing 2 chains per Ti (both O^{i}Pr groups are initiating),], reaction conditions: cat = **(S,S)-2)**, [*L*-LA]$_0$ = 1M, [cat]/[AgAl(OR^F)$_4$]/[*L*-LA] = 1/1/100, DCM, 25°C.

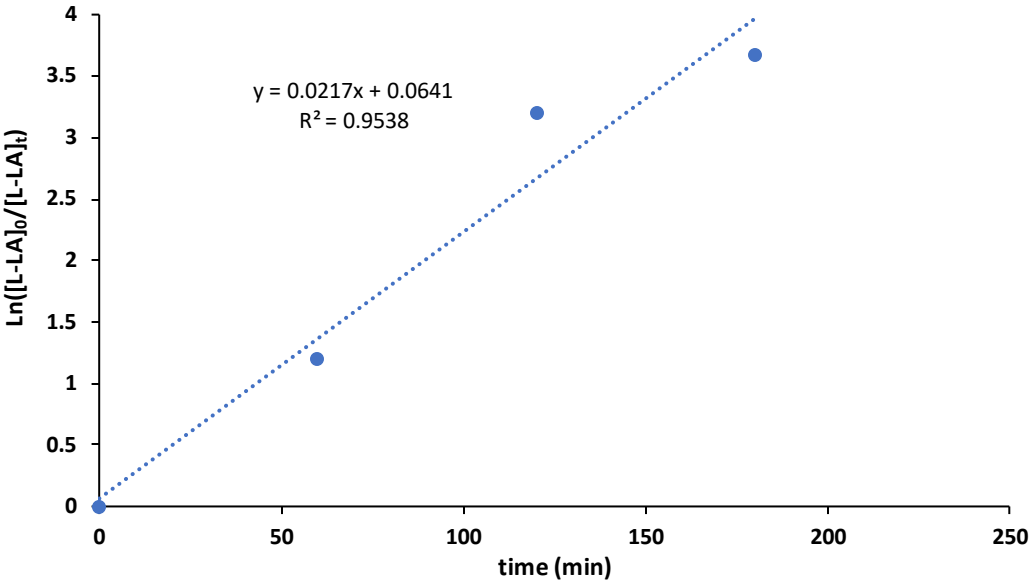

Figure S60: Ln($[\text{L-LA}]_0 / [\text{L-LA}]_t$) vs time (min) for *L*-LA ROP initiated by **(S,S)-2** + $[Ag][Al(OR^F)_4]$, reaction conditions: cat = **(S,S)-2)**, $[L\text{-LA}]_0$ = 1M, $[cat]/[AgAl(OR^F)_4]/[L\text{-LA}]$ = 1/1/100, DCM, 25°C.

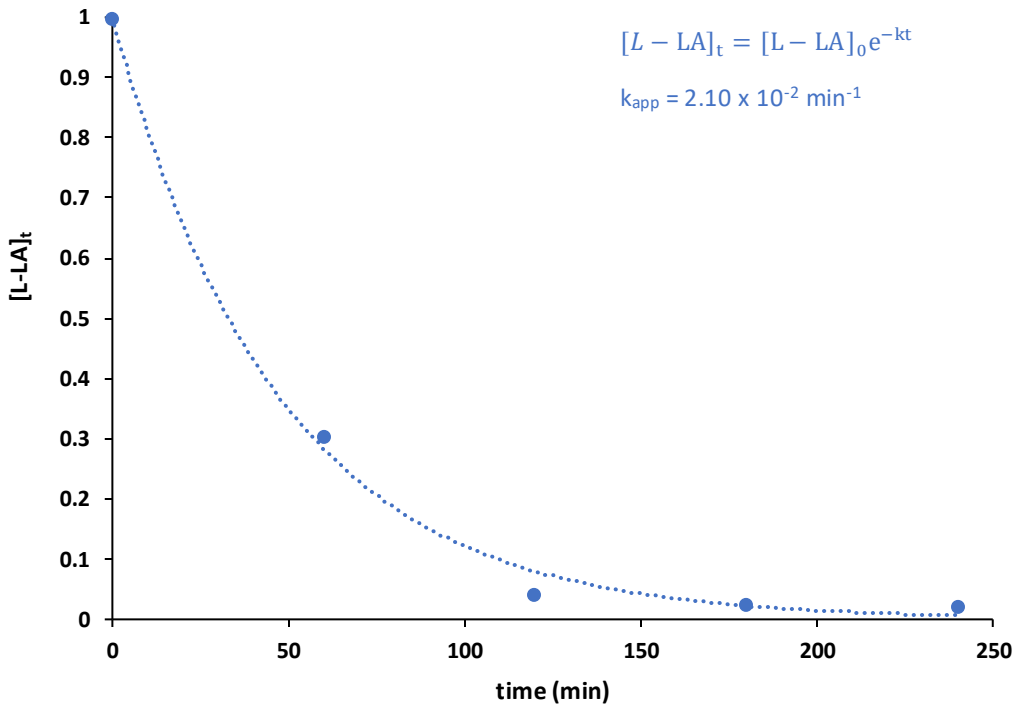

Figure S61: [*L*-LA] versus time for reaction initiated by **(S,S)-2** + $[Ag][Al(OR^F)_4]$ (Table 2, Entry 5). (temporal least-square fit with k_{app} = 2.10 x 10^{-2} min^{-1}.

➢ **Data for *D*-LA ROP initiated by (S,S)-2 + [Ag][Al(OR^F)$_4$]**

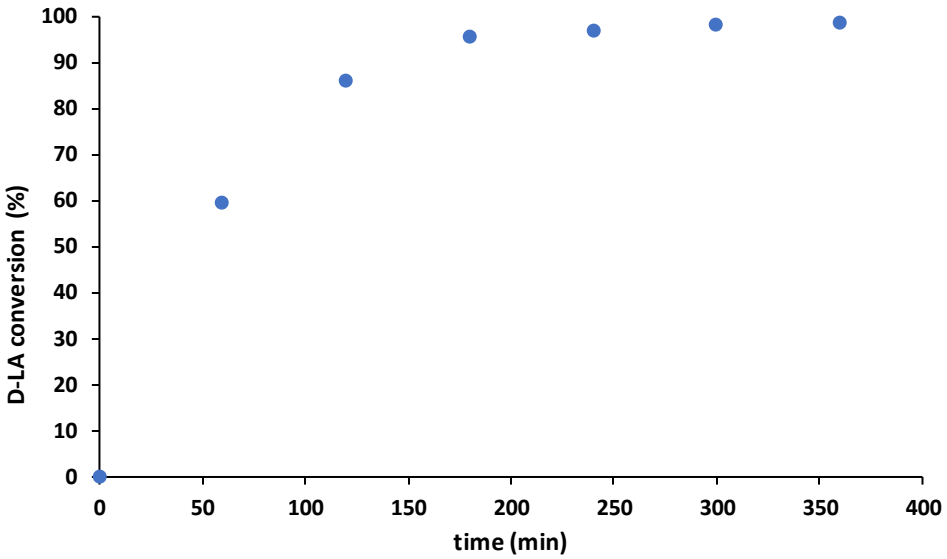

Figure S62: *D*-LA conversion versus time for polymerisation initiated by **(S,S)-2** + [Ag][Al(OR^F)$_4$], reaction conditions: cat = **(S,S)-2)**, [*D*-LA]$_0$ = 1M, [cat]/[AgAl(OR^F)$_4$]/[D-LA] = 1/1/100, DCM, 25°C.

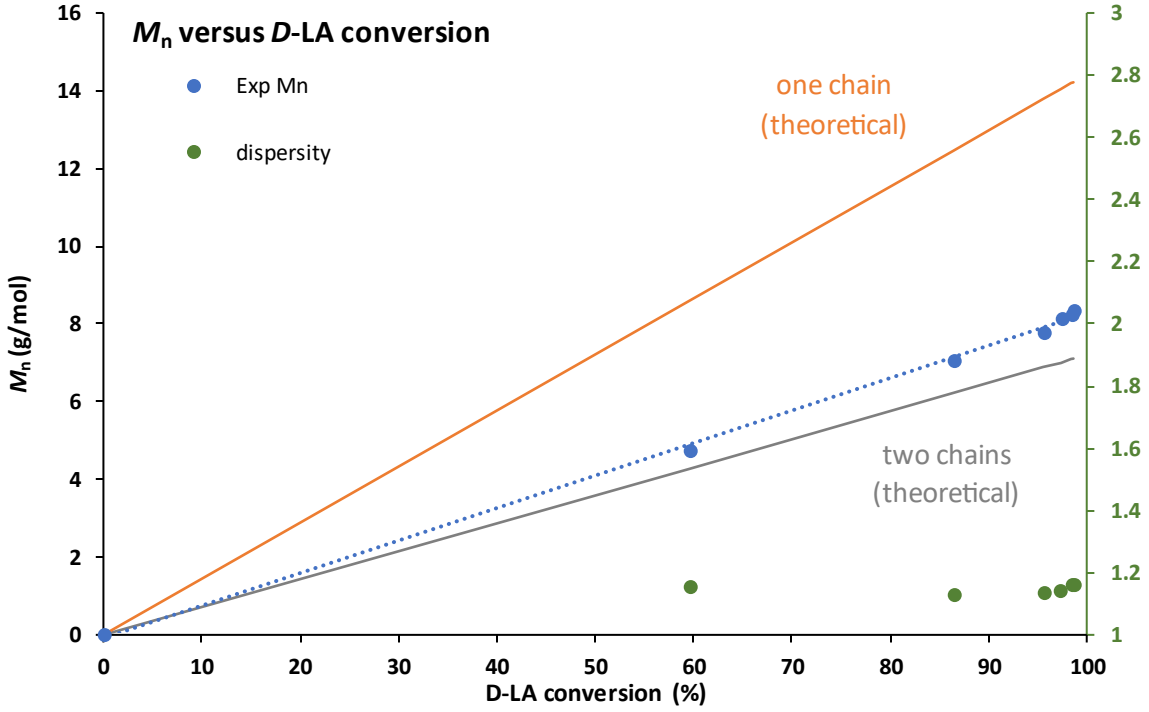

Figure S63: M_n (•) and dispersity (•) versus *D*-LA conversion for polymerisation initiated by **(S,S)-2** + [Ag][Al(OR^F)$_4$] showing 2 chains per Ti (both O^{i}Pr groups are initiating),], reaction conditions: cat = **(S,S)-2)**, [*D*-LA]$_0$ = 1M, [cat]/[AgAl(OR^F)$_4$]/[D-LA] = 1/1/100, DCM, 25°C.

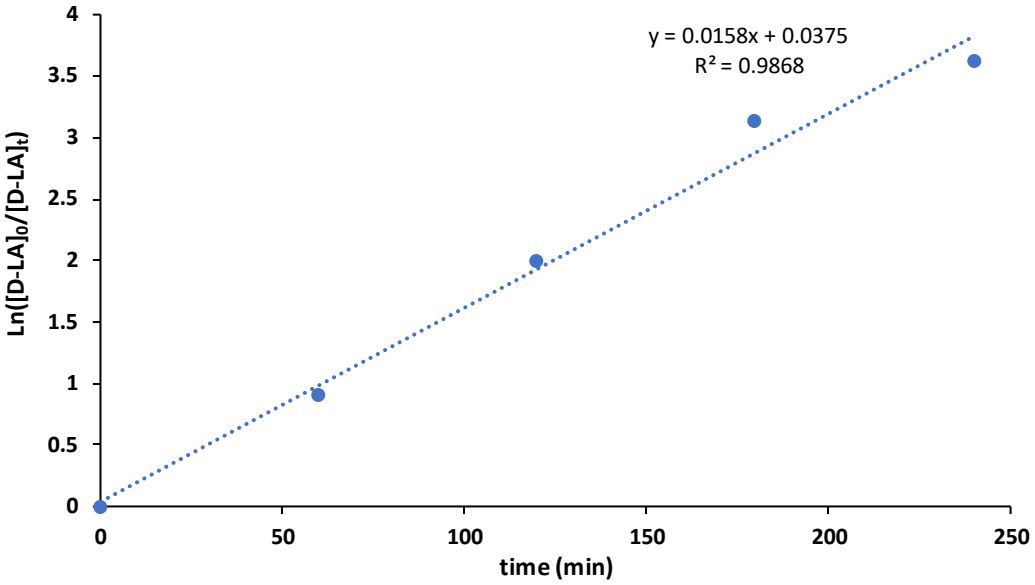

Figure S64: Ln([*D*-LA]$_0$ / [*D*-LA]$_t$) vs time (min) for *D*-LA ROP initiated by **(S,S)-2** + [Ag][Al(OR^F)$_4$], reaction conditions: cat = **(S,S)-2)**, [*D*-LA]$_0$ = 1M, [cat]/[AgAl(OR^F)$_4$]/[*D*-LA] = 1/1/100, DCM, 25°C.

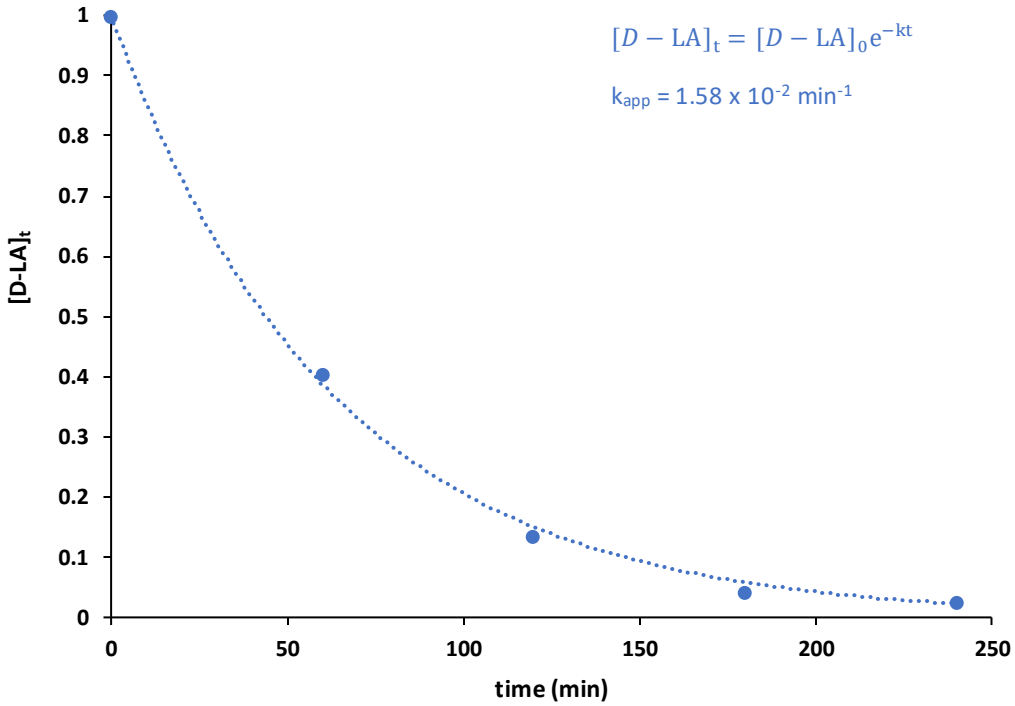

Figure S65: [*D*-LA] versus time for reaction initiated by **(S,S)-2** + [Ag][Al(OR^F)$_4$] with temporal least-square fit with k_{app} = 1.58 x 10^{-2} min^{-1}, reaction conditions: cat = **(S,S)-2)**, [*D*-LA]$_0$ = 1M, [cat]/[AgAl(OR^F)$_4$]/[*D*-LA] = 1/1/100, DCM, 25°C.

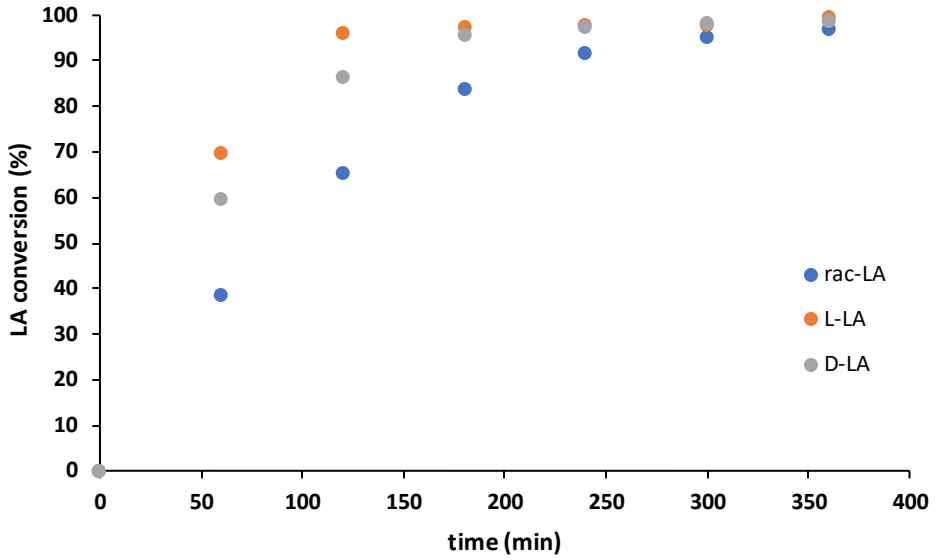

Figure S66: Overlay of *L*-LA (•), *D*-LA (•) and *rac*-LA (•) conversion (%) versus time for polymerisation initiated by **(S,S)-2**, reaction conditions: cat = **(S,S)-2)**, $[LA]_0$ = 1M, [cat]/[$AgAl(OR^F)_4$]/[LA] = 1/1/100, DCM, 25°C.

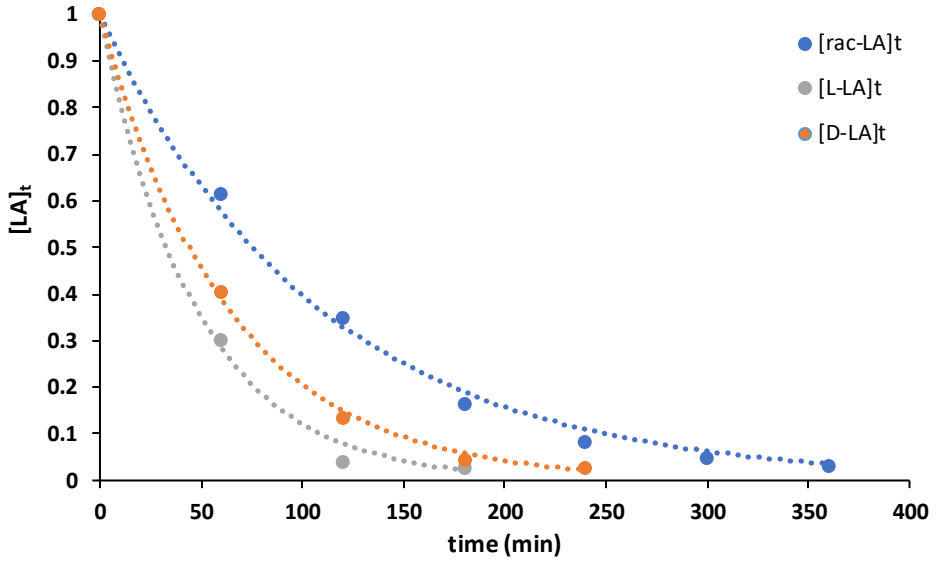

Figure S67: Overlay of [L-LA], [D-LA] and [rac-LA] versus time for reaction initiated by **(S,S)-2** + [Ag][$Al(OR^F)_4$] (temporal least-square fit with $k_{app,}$ $[LA]_t = [LA]_0.exp-(k_{app}.t)$

Table S3: reaction rate for L-LA, D-La and rac-LA polymerisation initiated using **(S,S)-2** + [Ag][$Al(OR^F)_4$]

Complex (1 equiv.)	**Lactide (LA)** (100 equiv.)	k_{app}[a] (min^{-1})
(S,S)-2	*L*-LA	2.1 x 10^{-2}
(S,S)-2	*D*-LA	1.6 x 10^{-2}
(S,S)-2	*rac*-LA	9.2 x 10^{-3}

Reaction conditions: **(S,S)-2**/[Ag.$Al(OR^F)_4$]/[LA] = 1/1/100, $[LA]_0$ = 1 M, dichloromethane, room temperature; a) k_{app} determined using temporal least-square fit for an exponential decay, $[LA]_t = [LA]_0.exp(-k_{app}.t)$.

➢ Tacticity measurements for polymer obtained using complex 2 and (S,S)-2

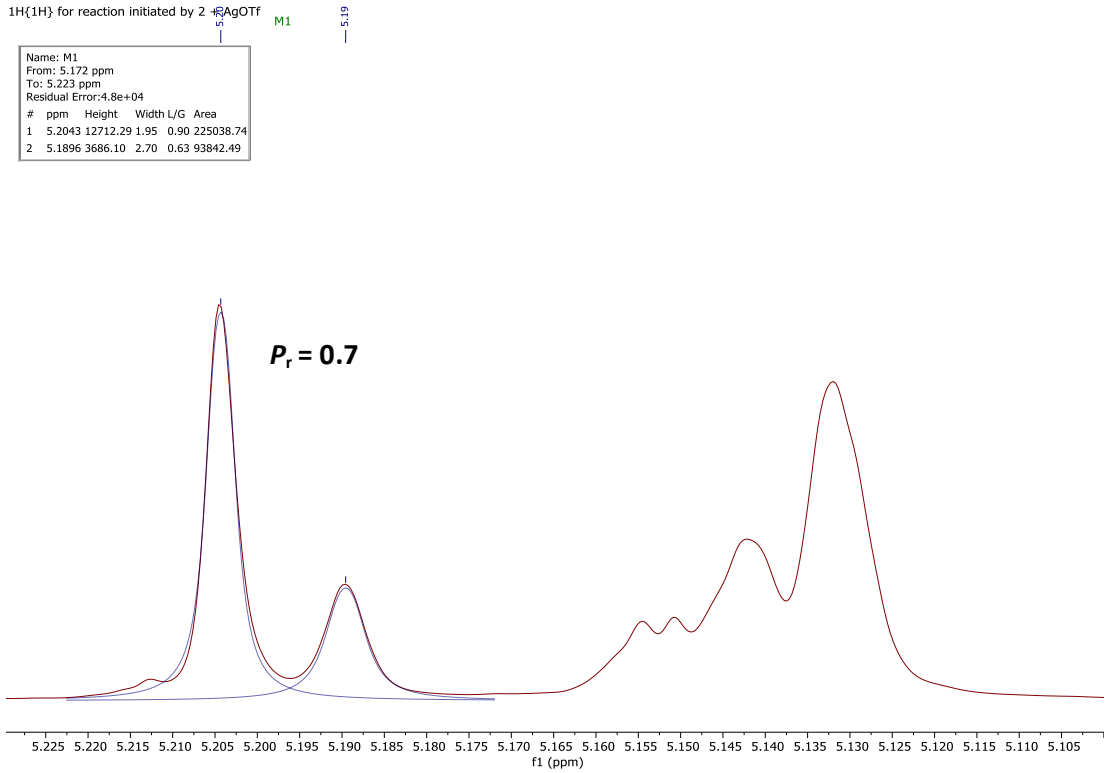

Figure S68: ^{1}H-{^{1}H}[7] for *rac*-LA ROP initiated by **2** + [Ag][OTf] showing slightly heterotactic PLA with P_r = 0.7, calculated using the first two tetrad rmr and rmm.

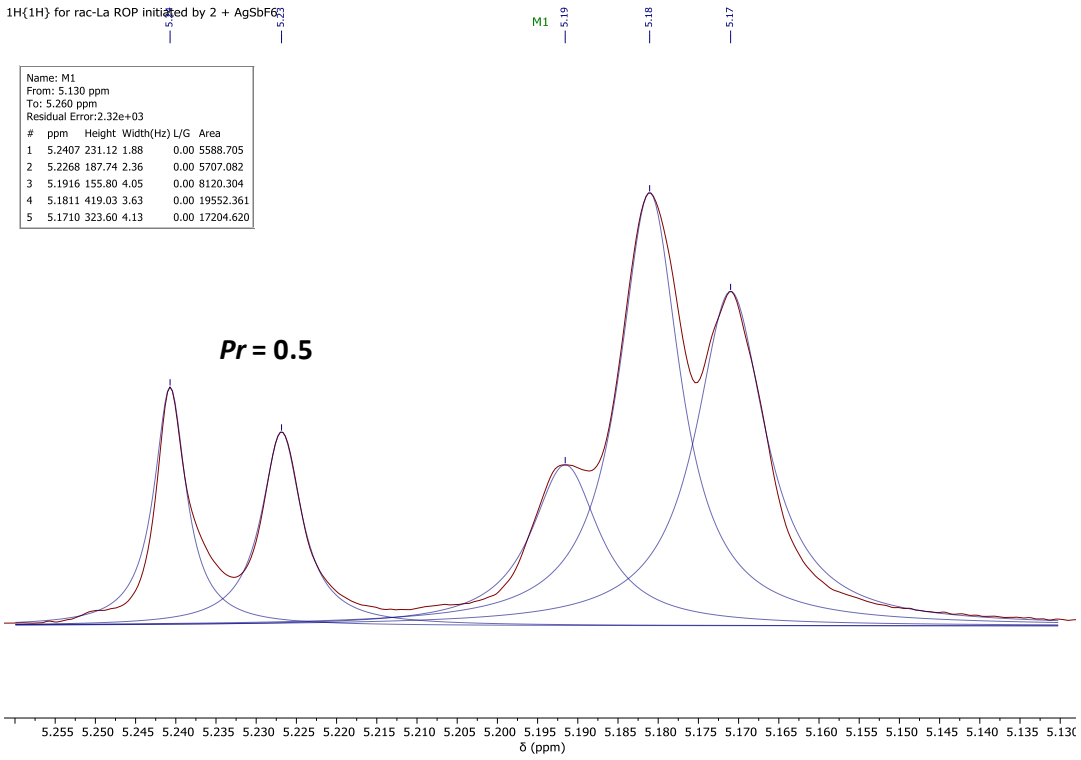

Figure S69: ^{1}H-{^{1}H} for rac-LA ROP initiated by **2** + [Ag][SbF_6] showing atactic PLA with P_r = 0.49, calculated using the first two tetrad rmr and rmm (P_r = 0.53 using all five tetrads).

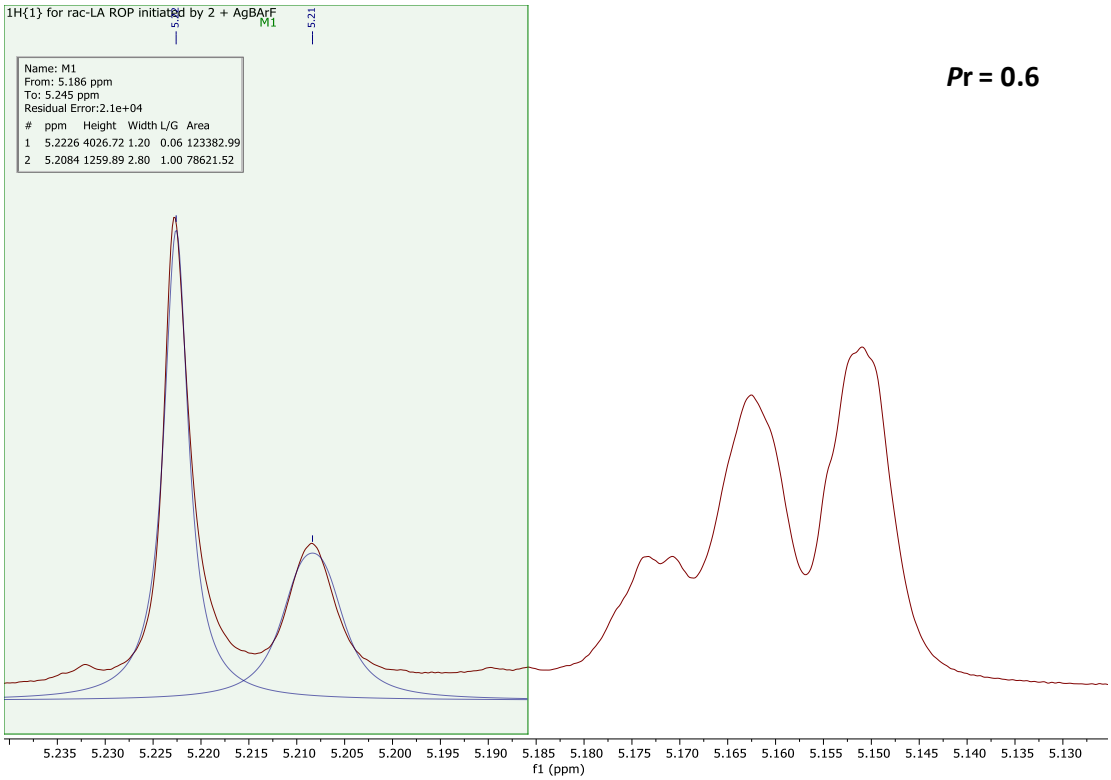

Figure S70: ^{1}H-{^{1}H} for *rac*-LA ROP initiated by **2** + [Ag][B(Ar^{CF3})$_4$] showing an heterotactic bias with P_r = 0.61, calculated using the first two tetrad rmr and rmm.

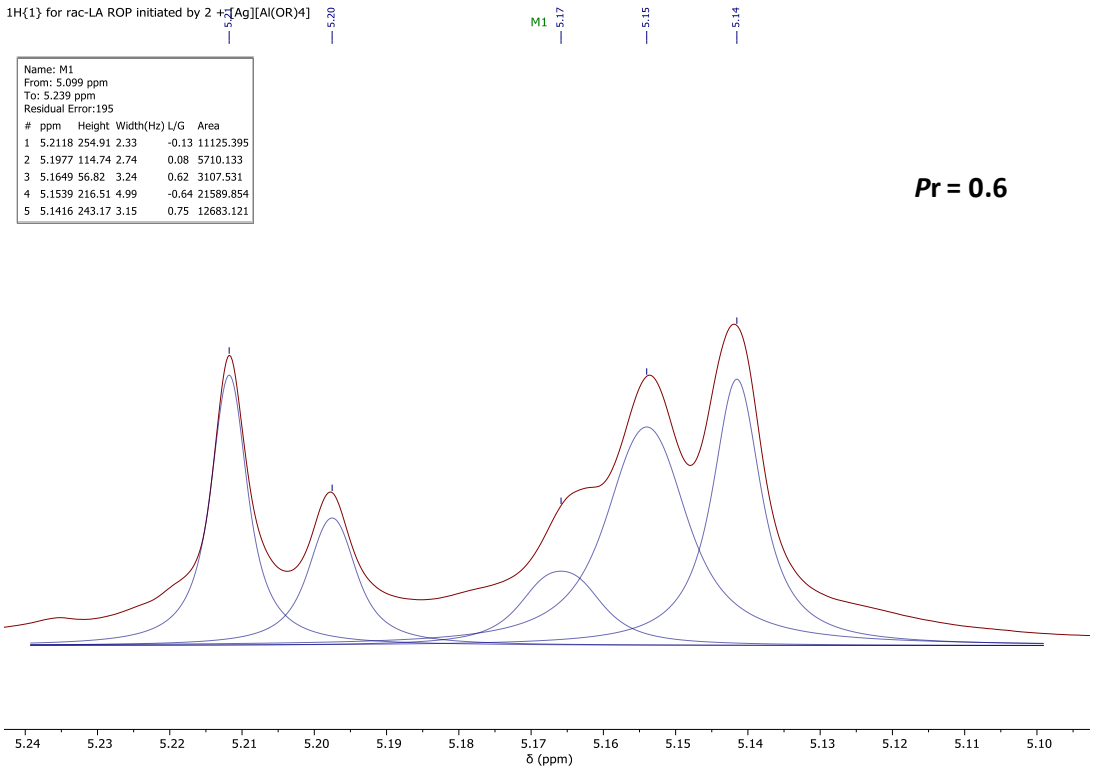

Figure S71: ^{1}H-{^{1}H} for *rac*-LA ROP initiated by **2** + [Ag][Al(OR^{F})$_4$] showing an heterotactic bias with P_r = 0.60, calculated using the first two tetrad rmr and rmm.

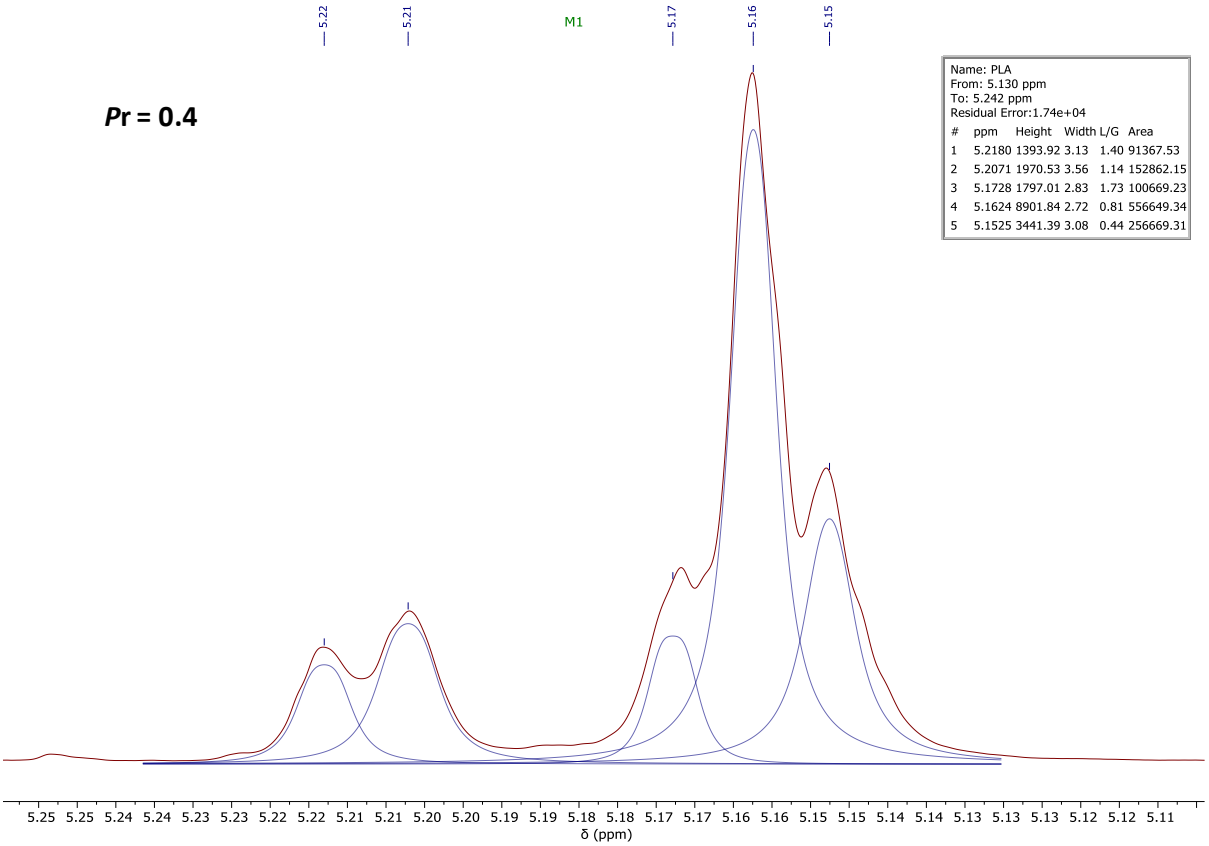

Figure S72: ^{1}H-{^{1}H} for *rac*-LA ROP initiated by **(S,S)-2** + [Ag][Al(OR^{F})$_4$] showing an isotactic bias with P_m = 0.60 (P_r = 0.40), calculated using the five tetrads (P_m = 0.63 using the first two tetrads).

➢ **Polymerisation data using complex 3**

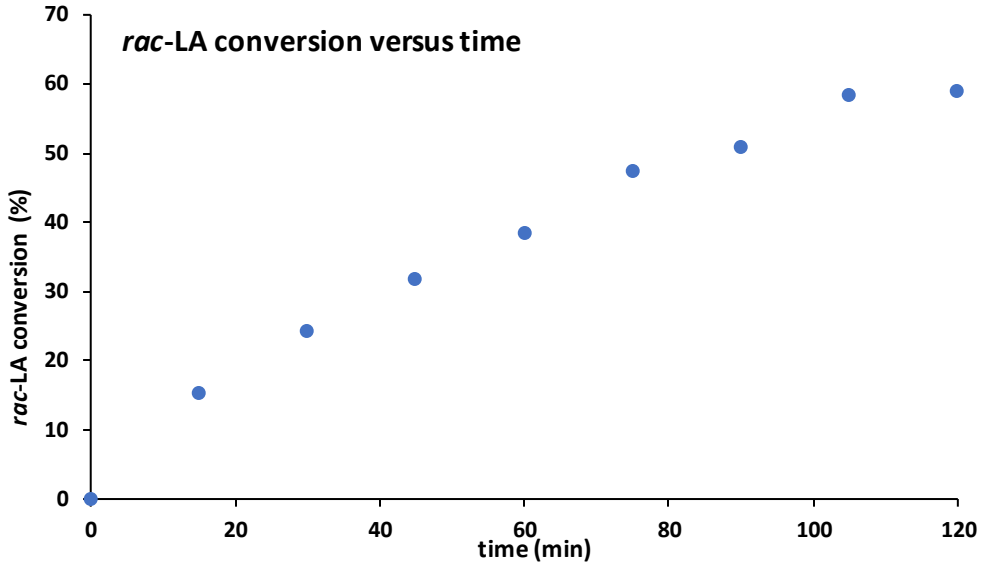

Figure S73: *rac*-LA conversion versus time for polymerisation initiated by **3** + [Ag][OTf] (Table 2, Entry 6).

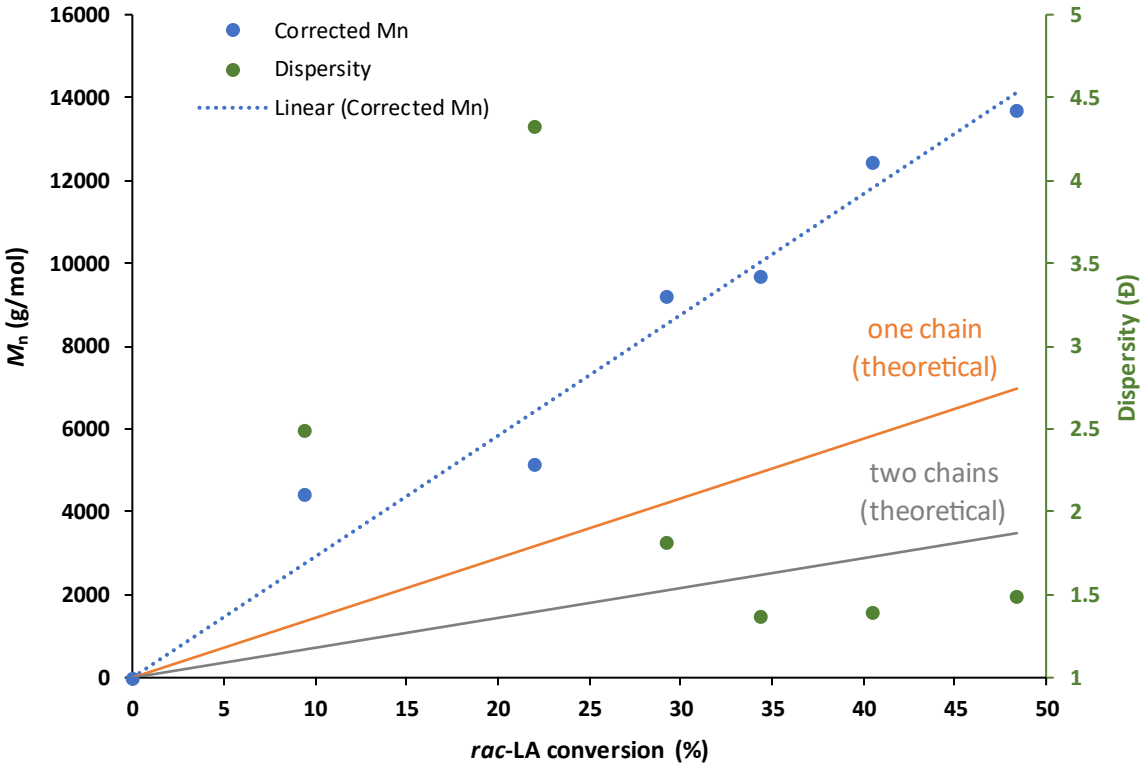

Figure S74: M_n (•) and dispersity (•) versus *rac*-LA conversion for polymerisation initiated by **3** + [Ag][OTf], showing experimental M_n higher than expected with one or two chains per Ti (Table 2, Entry 6).

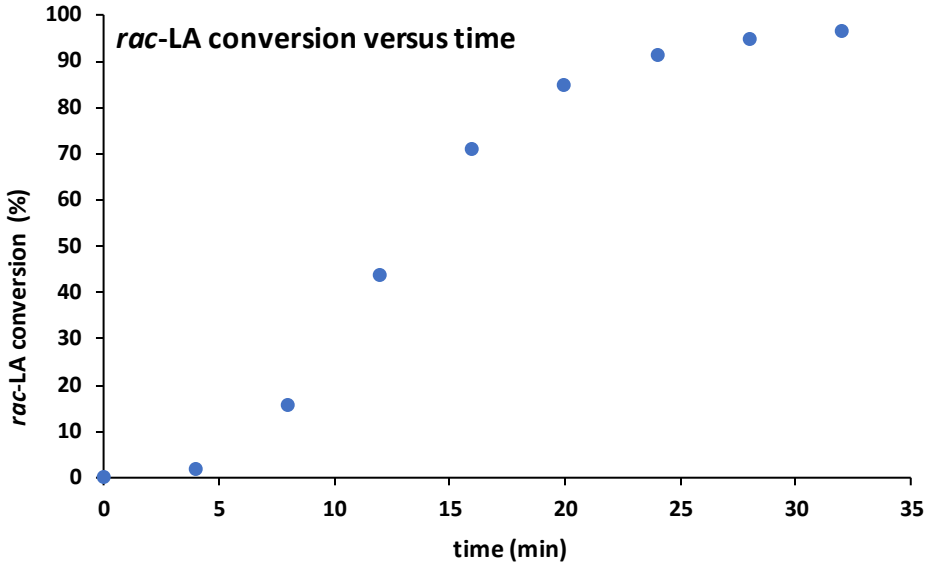

Figure S75: *rac*-LA conversion versus time for polymerisation initiated by **3** + [Ag][SbF_6] (Table 2, Entry 6).

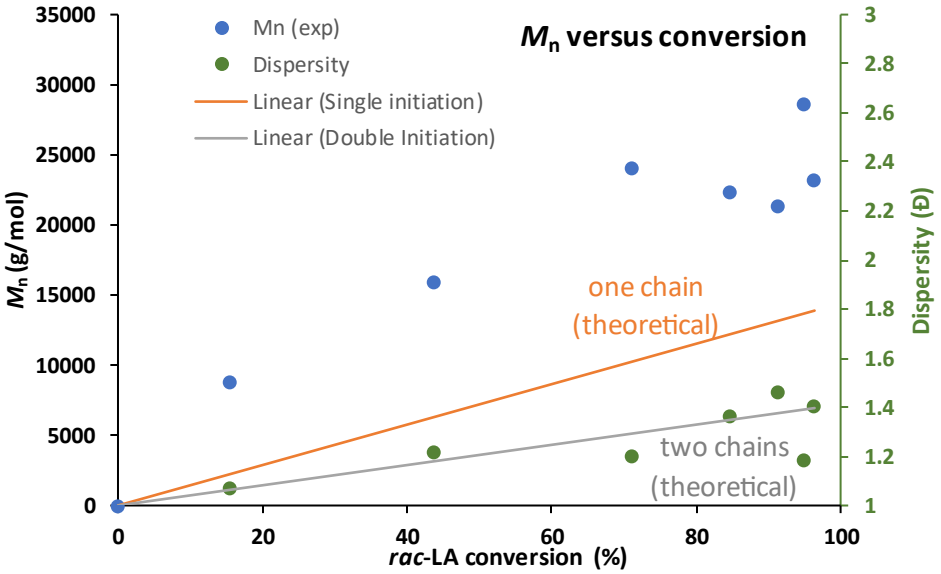

Figure S76: M_n (•) and dispersity (•) versus *rac*-LA conversion for polymerisation initiated by **3** + [Ag][SbF_6] showing higher than expected molar masses (Table 2, Entry 7).

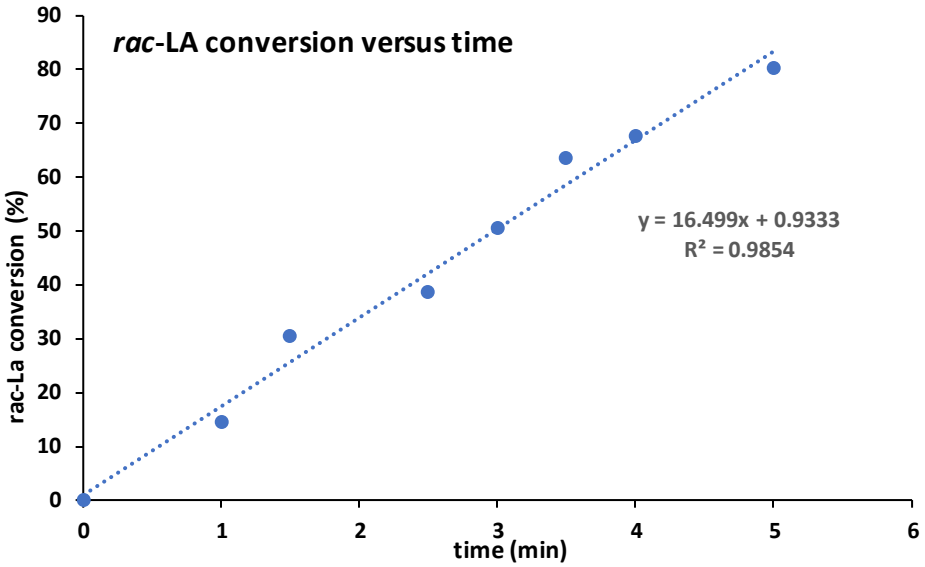

Figure S77: *rac*-LA conversion versus time for polymerisation initiated by **3** + [Ag][Al(OR^F)$_4$] (Table 2, Entry 8).

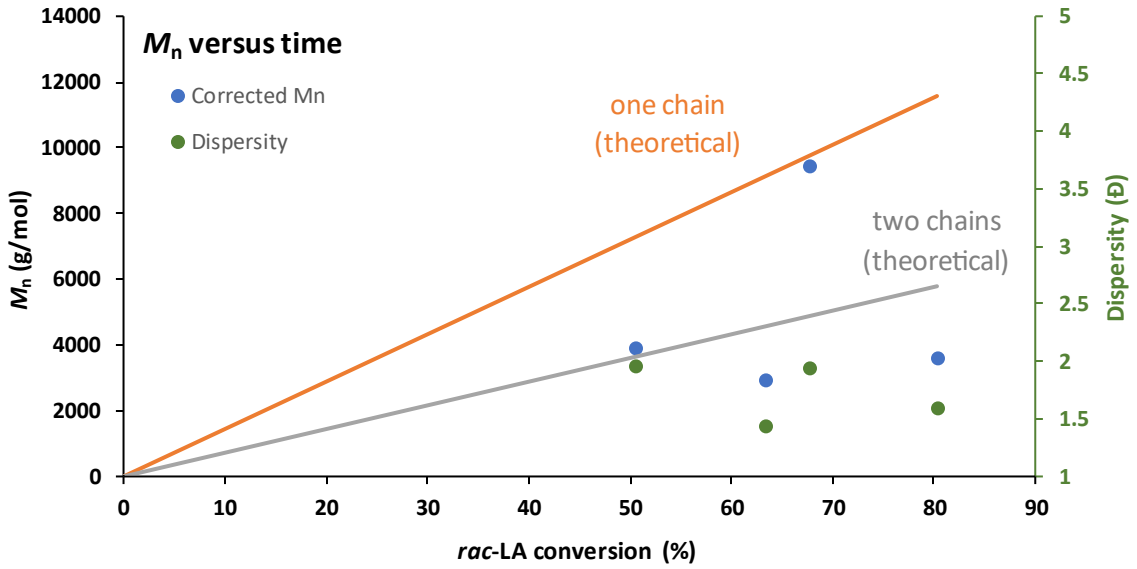

Figure S78: M_n (•) and dispersity (•) versus *rac*-LA conversion for polymerisation initiated by **3** + [Ag][Al(OR^F)$_4$] showing poorly controlled molar masses (Table 2, Entry 8).

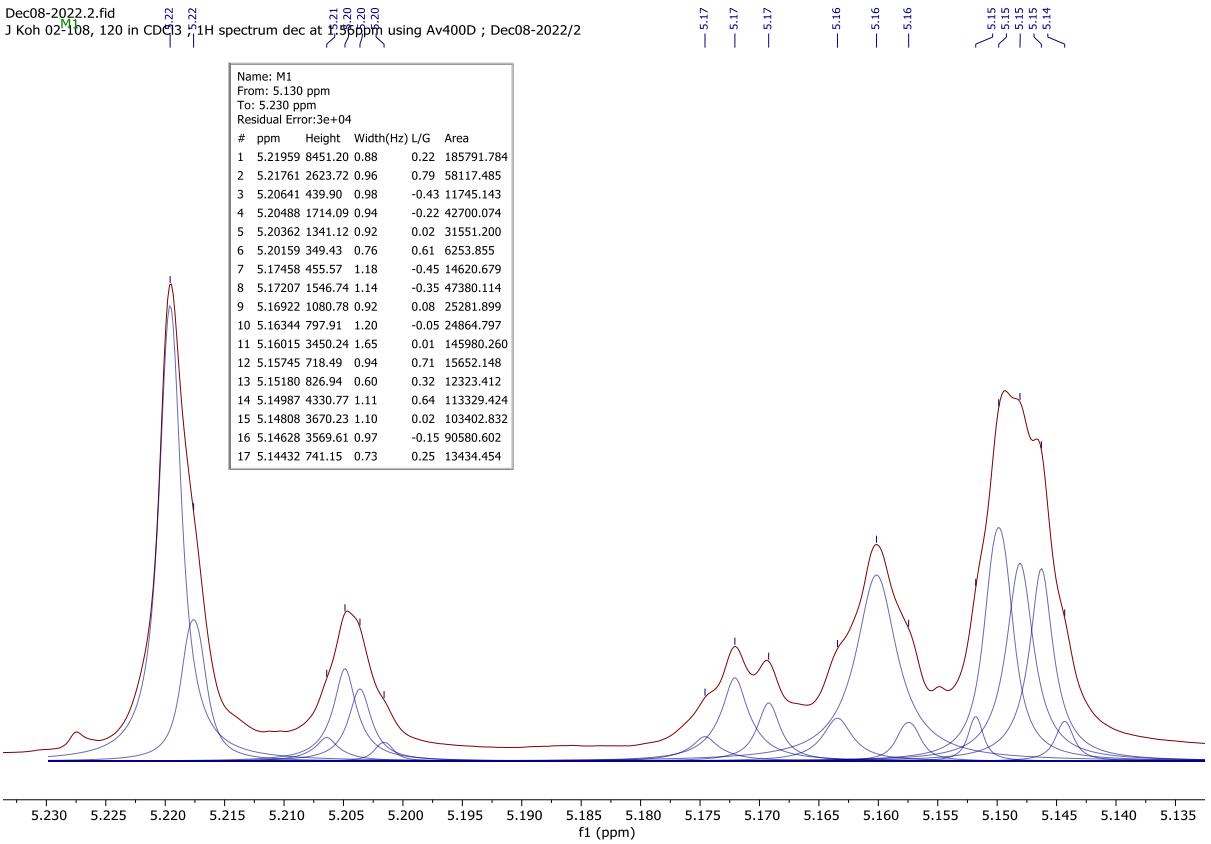

Figure S79: ^{1}H-{^{1}H} spectrum for *rac*-LA ROP initiated by **3** + [Ag][OTf] showing heterotactic PLA with P_r = 0.71, calculated using the first two tetrad rmr and rmm (P_r = 0.73 using all five tetrads) (Table 2, Entry 6).

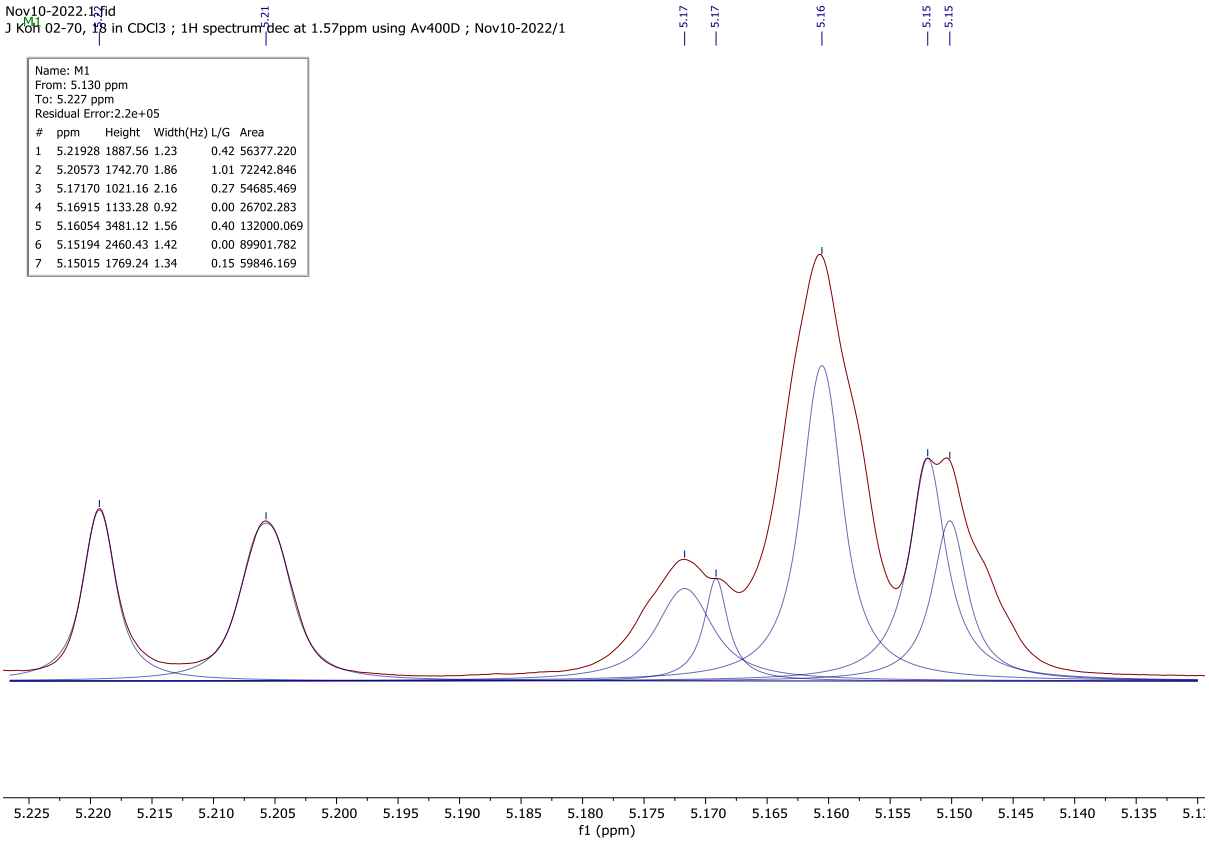

Figure S80: ^{1}H-{^{1}H} for rac-LA ROP initiated by **3** + [Ag][SbF_6] showing isotactic biased PLA with P_r = 0.44, calculated using the first two tetrad rmr and rmm (Table 2, Entry 7).

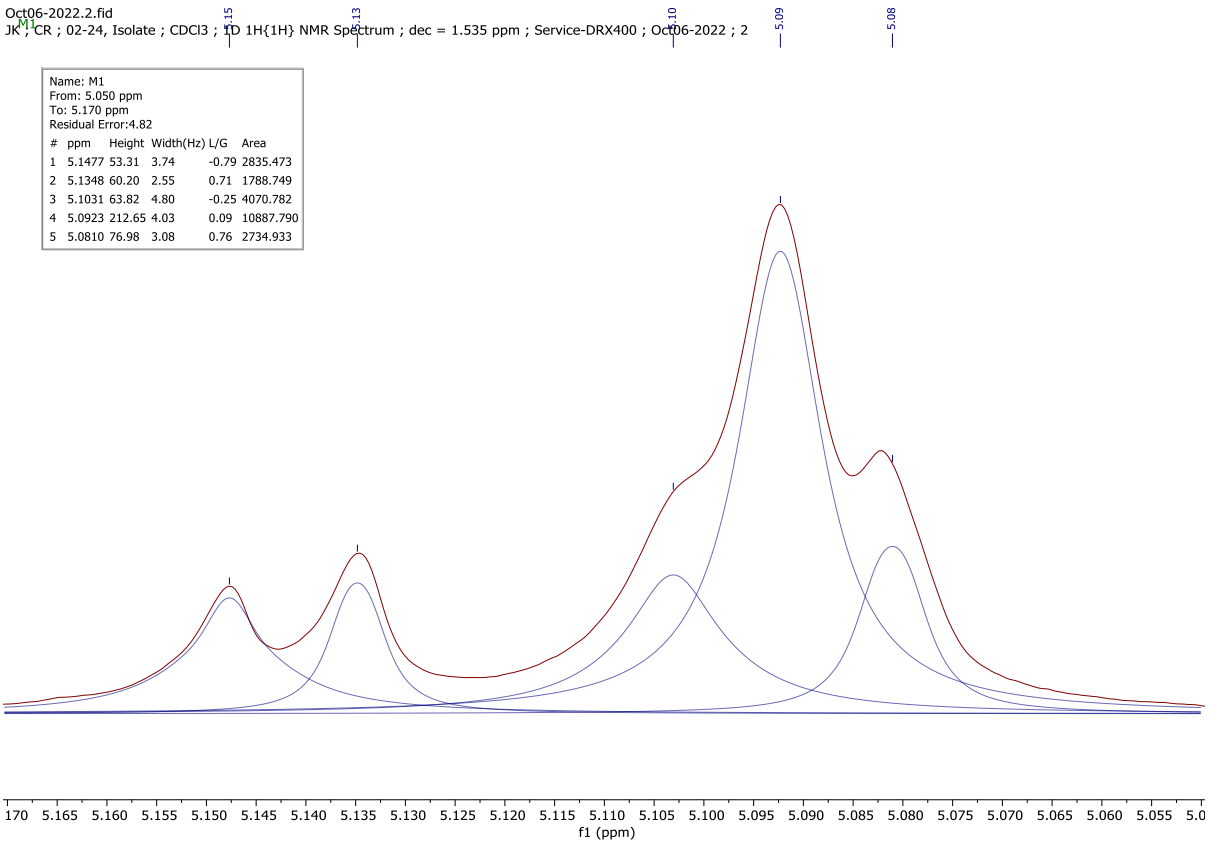

Figure S81: ^{1}H-{^{1}H} spectrum for *rac*-LA ROP initiated by **3** + [Ag][Al(OR^{F})$_4$] showing slightly isotactic PLA with P_r = 0.38, calculated using using all five tetrads (Table 2, Entry 8).

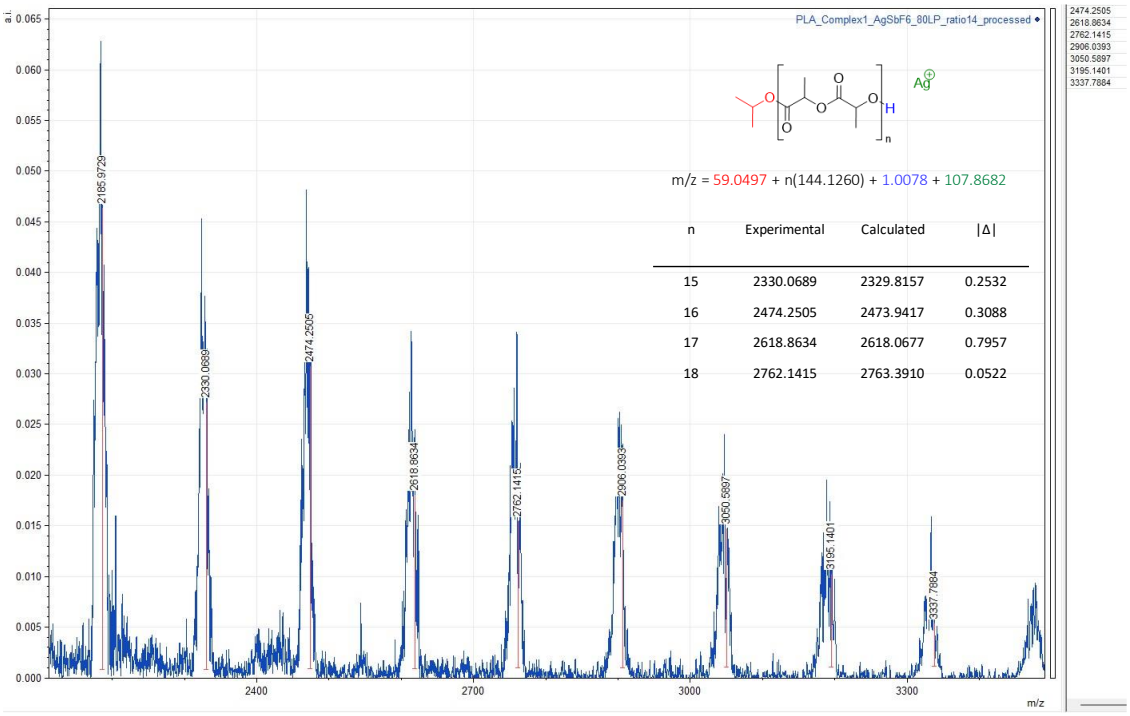

Figure 82: MALDI-ToF spectrum of PLA obtained via rac-LA ROP initiated by complex **1** in the presence of 1 equiv of [Ag][SbF_6] showing peaks spaced by 144 and O^{i}Pr terminated polymeric chains. Polymer sample obtained from polymerisation with conditions **1**/1/30 = cat./ [Al(OR^F)$_4$]$^-$/*rac*-LA

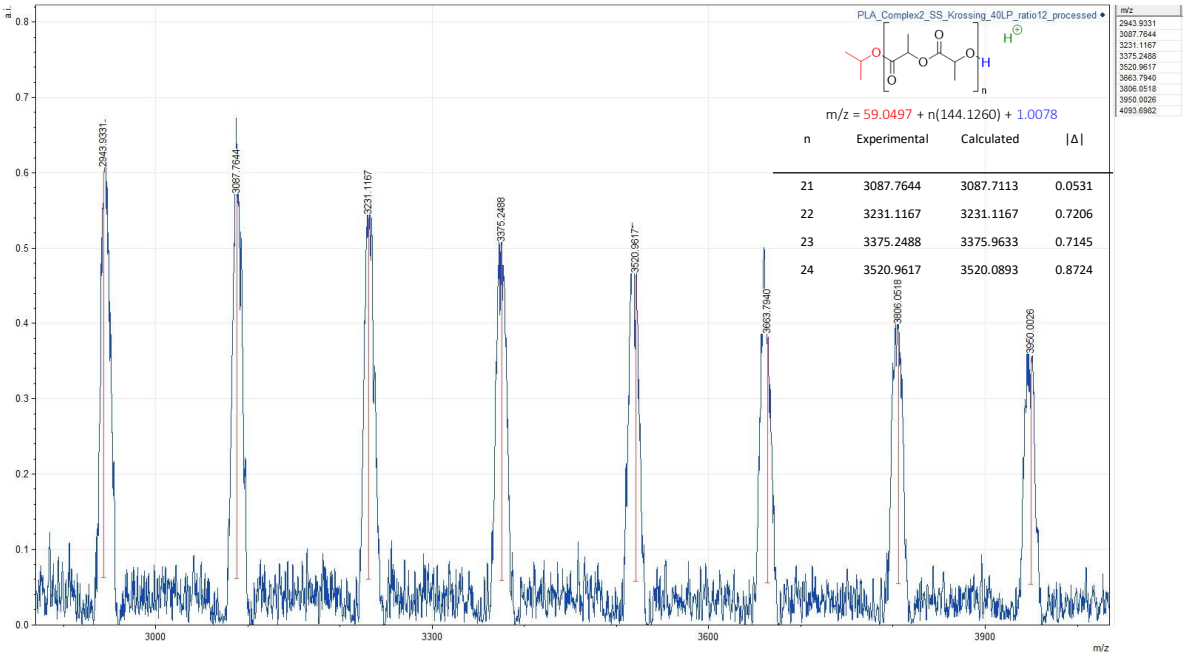

Figure S83: MALDI-ToF spectrum of PLA obtained via rac-LA ROP initiated by complex (S,S)-**2** in the presence of 1 equiv of [Ag][Al(OR^F)$_4$] showing peaks spaced by 144 and O^{i}Pr terminated polymeric chains. Polymer sample obtained from t=60 min aliquot (Table 2, Entry 5).

References:

1. C. K. Gregson, I. J. Blackmore, V. C. Gibson, N. J. Long, E. L. Marshall and A. J. White, *Dalton Trans.*, 2006, DOI: 10.1039/b518266b, 3134-3140.
2. B. Gao, X. Li, R. L. Duan and X. Pang, *New J. Chem.*, 2015, **39**, 2404-2408.
3. a) A. J. Martinez-Martinez and A. S. Weller, *Dalton Trans.*, 2019, **48**, 3551-3554; b) X. Wang, O. Shyshov, M. Hanzevacki, C. M. Jager and M. von Delius, *J. Am. Chem. Soc.*, 2019, **141**, 8868-8876.
4. Y. M. Zhang, A. M. Santos, E. Herdtweck, J. Mink and F. E. Kühn, *New J. Chem.*, 2005, **29**, 366-370.
5. K. J. Miller, T. T. Kitagawa and M. M. Abu-Omar, *Organometallics*, 2001, **20**, 4403-4412.
6. T. J. Herrington, A. J. Thom, A. J. White and A. E. Ashley, *Dalton Trans.*, 2012, **41**, 9019-9022.
7. C. A. Baker, C. Romain and N. J. Long, *Chem Commun (Camb)*, 2021, **57**, 12524-12527.